

REPUBLIQUE DU CAMEROUN

Paix-Travail-Patrie

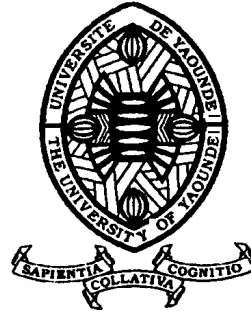
UNIVERSITE DE YAOUNDE I

CENTRE DE RECHERCHE ET DE
FORMATION DOCTORALE EN SCIENCES,
TECHNOLOGIES ET GEOSCIENCES

UNITE DE RECHERCHE ET DE
FORMATION DOCTORALE PHYSIQUES ET
APPLICATIONS

P.O Box : 812, Yaoundé

Email : crfd_stg@uy1.uninet.cm



REPUBLIC OF CAMEROON

Peace-Work-Fatherland

UNIVERSITY OF YAOUNDE I

POSTGRADUATE SCHOOL FOR
SCIENCE, TECHNOLOGY AND
GEOSCIENCE

RESEARCH AND POSTGRADUATE
TRAINING UNIT FOR PHYSICS
AND APPLICATIONS

P.O Box : 812, Yaoundé

Email : crfd_stg@uy1.uninet.cm

MODULATION INSTABILITY AND INTERACTION OF NON PARAXIAL BEAMS IN SELF FOCUSING KERR MEDIA MEDIA

Thesis

Submitted and defended publicly in fulfillment of the requirements for the degree of

Doctor of Philosophy in Physics

Speciality: **Mechanics, Materials and Structures**

Option: **Mechanics and complex systems**

Written and Presented by:

AMBASSA OTSOBO Jenny Alban

Registration number: **11W1220**

M. Sc. in Physics



Under the supervision of

KOFANE Timoléon Crépin

Professor,

University of Yaoundé I

University of Yaoundé I

Faculty of Sciences

Department of Physics

**MODULATION INSTABILITY AND INTERACTION OF
NONPARAXIALITY BEAMS IN SELF-FOCUSING KERR
MEDIA**

Submitted and defended in Fulfillment of the Requirements for the Degree of Doctor of
Philosophy/PhD in Physics
Option: Fundamental Mechanics and Complex Systems

By

AMBASSA OTSOBO JENNY ALBAN

Registration number: 11W1220

Master in Physics

Director

Prof. KOFANE Timoleon Crepin

Senior Lecturer, University of Yaoundé I (Cameroon)

Supervisor

Professor, University of Yaoundé I (Cameroon)

Laboratory of Mechanics, Materials and Structures

Copyright ©AMBASSA OTSOBO, jennyambassa1@gmail.com
Year 2022

Dedication

- ✠ To almighty God for all he has done for me.*
- ✠ To the soul of my father from where you are, know that I will always make you proud.*
- ✠ To my mother for her unconditional love and support.*

Acknowledgements

The accomplishment of this thesis would not be possible without the assistance and the help of numerous individuals and institutions.

★ First of all, I would like to express my full gratitude to my Supervisor, Professor **Kofane Timoleon Crepin**, who has supported me scientifically since the beginning of this thesis by giving me the means of my ambitions. He gave me a much appreciated confidence that few students are lucky enough to have. I would also like to thank him for the precious time he has given me on a daily basis throughout my academic career. for his advice and his help during all the duration of this work. His great physical insight and his unreserved willingness to share his understanding of physics with others made this project very enjoyable and informative. I owe him a debt of gratitude and respect.

★ A very special acknowledgment goes out to professor **Tabi Bertrand Conrad** for your relentless support and patience throughout this work I have not always been the best student but you have been very tolerant of me I thank you professor

★ Professor **Bouetou Bouetou Thomas** I would like to thank you for all the advice you gave me during my university career, you were like a father to me. Thank you for the time you gave me, your encouragement in this work allowed me to set the bar very high and to believe that it is not impossible that I too can be the winner at the end of this thesis. I thank you from the bottom of my heart professor

★ I would like to acknowledge Professor **Ben Bolie**, for your relentless support and patience throughout this work .

★ I would like to acknowledge Professor **Jean-Marie Bienvenu Ndjaka**, the Head of Department of Physics at the Faculty of Science at the University of Yaoundé I, for receiving me in his Department.

★ I am grateful to Professor **Woafu Paul**, Chairman of the Cameroon Physical Society for his teaching specially in numerical methods.

★ It would be very pleasing to recognize trade and constructive discussions combined with great moments of sharing with all the teachers of the Department of Physics in general and of the laboratory of Mechanics, Materials and Structures in particular. I

have named Professor **Zekeng Serge**, Professor **Tchawoua Clement**, Professor **Djuidje Germaine**, Professor **Nana Nbandjo Blaise Roméo**, Professor **Fewo Serge**, Professor **Vondou Derbetini**.

★ Special thanks to **Megne Tiam Laure**, **Ganyou Stephanie**, **Dr Zanga Dieudonnee**, **GNINZANLONG Carlos**,

★ I express my eternal gratefulness to my parents, **Ambassa Bissimbi** and **Bobiono Marie**, without whose support and love throughout my entire life, I would not have started and finished this thesis. I also thank the permanent support provided by my dears aunt: **Abatchong Chantal**, **Amatalita Martine**, **Moudio Rebecca**, **Aliga alicie**.

★ I would like to thank my uncle **Bouyantchan** for his presence, his attention and all the help he gave me so that I would always be the best. Thank you uncle for believing in me and I will always be grateful to you.

★ I would like to thank my uncle Professor **Kofana** for his big heart, and for all the help he gave me during my first steps in this university.

★ My sincere thanks to Professor **Nkeng Elambo Goerge**, ENSTP Director

★ I hope to thank the one who lived this experience from beginning to end to with me in the last minutes of this thesis **Efouba Joseph Marie Flaubert**, he accompanied me in all the plans for my development in order to carry out my work you are really a love

★ I would like to express my great gratitude to **Colonel MAHI JEAN** for the support, both psychological and financial, that he has so often shown.

★ A huge thank you to my family especially my brothers and sisters **Ambassa (Ndeme Rose, Madiama Paule, Abiaga Claudia, Bissimbi Yacinthe, Abagouda Marcelle, Bobiono Alexandra, Ambassa Ben, Elime Raymond)** for their love and all the confiances they have granted me

★ Special thank goes to my grandmother **Abiaga Barbine** who accompanied and protected me as best she could thank you for your prayers

• My sincere thanks go to the official editors and referees of **Chaos Soliton and Fractals**, for their detailed review, constructive criticism and excellent advice during the preparation of my publication.

• I express my apologies and sincere thanks to all those I might have forgotten; it is even more difficult to find the right words to thank everyone as much as they deserve.

Contents

Dedication	i
Acknowledgements	ii
Table of Contents	iv
List of Figures	vi
Abstract	ix
Résumé	x
Chapter I Literature Review	7
I.1 Introduction	7
I.2 General information on optical fibers	7
I.2.1 Optical losses	8
I.2.2 Chromatic dispersion	10
I.2.3 Optical Kerr effect	12
I.3 Linear and nonlinear responses of the medium	14
I.4 Historical reminder (Bragg gratings)	18
I.4.1 Types of short step right Bragg gratings	20
I.4.2 Modeling of fiber Bragg gratings (coupled mode theory)	22
I.5 Application of Bragg gratings to telecommunication	24
I.6 Filtering and multiplexing	24
I.6.1 Optical filter	24
I.7 Observation of a solitary wave and its consequences	25
I.7.1 The optical solitons	26
I.8 Different types of optical solitons according to their physical origin	33
I.8.1 Kerr solitons	34
I.8.2 Solitons in liquid crystals	35
I.8.3 Solitons in fiber Bragg gratings	35
I.9 Conclusion	36

Chapter II Model and Methodology	37
II.1 Introduction	37
II.2 The nonlinear nonparaxial coupled mode equation	38
II.2.1 Propagation of light pulses in fiber Bragg gratings	38
II.2.2 Paraxial coupled mode theory	40
II.2.3 Relation of linear dispersion	42
II.2.4 Theory of nonlinear coupled modes	46
II.2.5 On the Townes soliton	47
II.3 Analytical method	48
II.3.1 The Method of Multiple Scales	49
II.3.2 Modulational instability phenomenon	51
II.4 Numerical method	53
II.4.1 Split-step Fourier method	54
II.4.2 Fourth-order Runge-Kutta method	57
II.5 Conclusion	59
Chapter III Results and discussions	60
III.1 Introduction	60
III.2 Derivation a 2D NLS equation with higher-order correction terms in the nonparaxial regimes.	60
III.3 Asymptotic study of the dynamics of gap-soliton bullet in the nonparaxial regime	63
III.3.1 Numerical gap-soliton bullet stability under nonparaxiality effects	68
III.4 Modulational instability growth rates in a 2D NLS equation in nonparaxial regime	73
III.4.1 The study of the linear stability analysis	76
III.4.2 Numerical solution of the 2D NLS equation in nonparaxial regime	78
III.5 Conclusion	83
General Conclusion and Perspectives	86
Bibliography	88
List of Publications	103

List of Figures

Figure 1	Optical fiber	8
Figure 2	Multimode fiber: here the light can follow paths inside the core .	9
Figure 3	Single-mode fiber: in this case, there is only one mode of light propagation	9
Figure 4	Diagram of a Bragg grating and their spectra	20
Figure 5	: Index modulations of different types of networks. (a): Uniform network, (b): Variable pitch network, (c): Variable amplitude network, (d): apodized network, (e): Phase jump network, (f): Sampled network	21
Figure 6	: Propagation of the fields through the Bragg grating	23
Figure 7	: Schematic diagram of soliton propagation in fibers. The non-linearity of the fiber produces a frequency drift that exactly compensates the one produced by the dispersion. The soliton pulse propagates without deformation	29
Figure 8	: Modeling of soliton propagation in a nonlinear medium	31
Figure 9	Dispersion relationship showing a periodic Bragg grating band .	44
Figure 10	Intensity reflectivity of a fibered Bragg grating, whose parameters are: length $L = 8mm$ and $\kappa = 5cm^{-1}$ or $\delta_n \approx 10^{-6}$ if the length of Bragg $\lambda_\beta = 1550nm$. The maximum reflectivity $\max R$ can reach values higher than 95, when $\kappa L \geq 2$, and is ≈ 100 ($\kappa L = 4$)	45
Figure 11	Schematic illustration of the split-step Fourier method	58
Figure 12	Dispersion relationship showing a periodic Bragg grating band .	64
Figure 13	Panels (a1), (b1), (c1) and (d1) show the intensity profiles for the propagation of the initial gap-soliton bullet at the respective instants $t=0, t=2, t=3, t=4$ and $t=5$, with panels (a2), (b2), (c2) and (d2) corresponding to their contour plots. The third column, with index 3, from left displays the phase distribution at the respective instants, with the other parameters being $\epsilon = 0.01, \kappa = -1$ and $c_g = 0.5$	71

- Figure 14** Panels (a1), (b1), (c1) and (d1) show the intensity profiles for the propagation of the initial gap-soliton bullet at the respective instants $t=0, t=2, t=3, t=4$ and $t=5$, with panels (a2), (b2), (c2) and (d2) corresponding to their contour plots. The third column, with index 3, from left displays the phase distribution at the respective instants, with the other parameters being $\epsilon = 0.01, \kappa = -1$ and $c_g = 0.5$ 72
- Figure 15** Panels (a1), (b1) and (c1) show the intensity profiles for the propagation of the initial light bullet at the respective instants $t=0, t=2, t=3$, and $t=5$, with panels (a2), (b2) and (c2) corresponding to their contour plots. The third column, with index 3, from left displays the phase distribution at the respective instants, with the other parameters being $\epsilon = 0.032, \kappa = -2.3$, and $c_g = 0.64$ 74
- Figure 16** Panels (a1), (b1) and (c1) show the intensity profiles for the propagation of the initial light bullet at the respective instants $t=0, t=2, t=3$, and $t=5$, with panels (a2), (b2) and (c2) corresponding to their contour plots. The third column, with index 3, from left displays the phase distribution at the respective instants, with the other parameters being $\epsilon = 0.04, \kappa = -2.9$, and $c_g = 0.69$ 75
- Figure 17** Growth rate of the modulational instability associated with solutions G_+ of Eq (III.29). Graph (a) shows the 3D representation of the gain G_+ as functions of K_x and $\kappa * 10^5$. Graph (b) shows the MI gain for different values of G_+ as a function of K_x in 2D. Graph (c) shows the 2D representation of the gain G_+ as a function of $\kappa = 1 \times 10^5$. The other parameters used are: $c_g = 5, \epsilon = 1.3, P_0 = 5.2, K_y = 0.1$. It is obvious that by increasing the value of kappa, the instability zone expands; this means that the nonparaxiality parameter increases the MI in the FBG. It is shown that the growth rate of instability G_+ can be dramatically affected by the nonparaxiality parameter κ 80
- Figure 18** Modulational instability gain associated with solutions G_+ of Eq. (III.29). Graph (a) shows k_x as a function of K_y , and Graph (b) shows the gain spectrum G_+ as a function of K_x . Graph (c) shows the gain spectrum G_+ as a function of K_y , for a fixed $\epsilon = -1.3$ value. The other parameters used are: $c_g = 5, p_0 = 5.2, \kappa = 1 \times \epsilon^{-4}$ 81

- Figure 19** Modulational instability gain associated with solutions G_+ , of Eq. (III.29). Graph (a) shows K_x as a function of K_y , Graph (b) shows the gain spectrum G_+ as a function of K_x . Graph (c) shows the gain spectrum G_+ as a function of K_y , for a fixed $\epsilon = -1.3$ value . The other parameters used are: $c_g = 5, p_0 = 5.2, \kappa = 1 \times \epsilon^{-4}$. 82
- Figure 20** Effect of p_0 on the gain of modulational instability. Here, p_0 takes high values. The graph shows a curve of K_x versus p_0 . The other parameters used are: $c_g = 5, p_0 = 6, \kappa = 1 \times \epsilon^{-4}$ 83
- Figure 21** 2D representation of the evolution of solitons in an instability medium in the nonparaxial regime. $Z= 0$ in Fig. 20(a), $Z= 20$ in Fig.20(b), and $Z= 30$ in Fig. 20(c). Other parameters are: $p_0 = 1.0, k = -1, c_g = 5, v_g = 5, \epsilon = 1.3, \epsilon = -1.3, \kappa = 2 \times 10^{-4}$, Initial: input is $U = \sqrt{p_0}(1 + 10^{-4}(\cos(1.1 \times 2\pi x) + \cos(1.5 \times 2.p_0 y)))$ 84
- Figure 22** 2D representation of the evolution of solitons in an instability medium in the non-paraxial regime for $Z=48$, Z is considered here as a counter. 85

Abstract

We investigate the formation and propagation of gap-soliton bullets in fiber-Bragg-gratings at frequencies close to the gap for Bragg reflection beyond the paraxial approximation. With the help of the Maxwell's equations, using a multiple-scales analysis, we derive a two-dimensional (2D) nonlinear Schrödinger (NLS) equation with higher-order correction terms that consider the nonparaxial regimes in the slowly-varying envelope approximation. In addition, a fully numerical simulation of the newly derived model equation is carried out based on the split-step Fourier method, with the initial condition being a Townes soliton. We demonstrate that the mutual balancing Kerr effect, dimensionality, higher-order dispersions and nonparaxiality allows shape-preserving propagation of gap-soliton bullets in nonlinear periodic waveguides. Next, the modulational instability of continuous-wave (CW) solutions of the 2D NLS equation with higher-order correction terms is studied. The standard linear stability analysis is used to investigate the stability of CW and to obtain the criterion for modulational instability. The analytical predictions for plane wave stability are confirmed by exhaustive numerical simulations.

Keywords: Gap-soliton bullets, Fiber-Bragg-grating, 2D Nonlinear Schrödinger equation, Nonparaxial regime, Higher-order dispersion, Townes soliton, Modulational Instability, split-step Fourier method.

Résumé

Nous étudions la formation et la propagation des balles de lumière de type solitons de gap dans des réseaux de Bragg fibrés, à des fréquences proches du seuil de réflexion de Bragg, au-delà de l'approximation paraxiale. A l'aide des équations de Maxwell, en utilisant une analyse à plusieurs échelles, nous dérivons une équation de Schrödinger non linéaire bidimensionnelle, avec des termes de correction d'ordre supérieur, qui considèrent les régimes non-paraxiaux dans l'approximation de l'enveloppe à variation lente. De plus, une simulation entièrement numérique de l'équation modèle, nouvellement dérivée, est effectuée sur la base de la méthode de Fourier à pas divisés, la condition initiale étant un soliton de Townes. Nous démontrons que l'équilibrage mutuel entre l'effet Kerr, la dimensionalité, les dispersions d'ordre supérieur et la non-paraxialité permettent la propagation, en préservant la forme, des balles de lumière de type solitons de gap, dans des guides d'ondes périodiques non linéaires. Ensuite, l'instabilité modulationnelle des solutions d'ondes continues de l'équation de Schrödinger non linéaire bidimensionnelle avec des termes de correction d'ordre supérieur est étudiée. L'analyse de stabilité linéaire standard est utilisée pour étudier la stabilité de l'onde continue et pour obtenir le critère d'instabilité modulationnelle. Les prédictions analytiques de la stabilité des ondes planes sont confirmées par des simulations numériques exhaustives.

Mots clés: Balles de lumière de type soliton de gap, réseaux de Bragg fibrés, équation de Schrödinger non linéaire bidimensionnelle, régime non paraxial, dispersion d'ordre supérieur, soliton de Townes, instabilité modulationnelle, méthode de Fourier à pas divisés.

General Introduction

The generation of solitons in optical fibers, predicted by Hasegawa and Tappert [1, 2], has enabled the generation of stable picosecond and subpicosecond pulses in the near-infrared. Verification of many of the predicted soliton pulse characteristics was carried out in a series of experiments by Mollenauer et al. [4, 3, 5]. The field of temporal, spatial, and spatiotemporal optical solitons emerged from the fundamental studies of the interaction of intense laser beams with matter. Furthermore, various types of soliton phenomena have been studied extensively in more nonlinear media, including electrical transmission line [6], optical fibers [7, 8], Bose-Einstein condensation [9, 10], deep water waves [11], Langmuir waves [12], DNA [13, 14], metamaterials [15, 16], spatial and vortex solitons in photorefractive materials or waveguides, and cavity solitons in resonators [17]. It has also been well-known that fiber Bragg gratings (FBGs) [18, 19, 20, 21, 22] with Kerr nonlinearity can exhibit optical-soliton-like phenomena [23, 24, 25]. FBGs, which are produced by periodically varying the refractive index along with an optical fiber, have a large effective dispersion, resulting from the resonant coupling between the forward- and backward-propagating waves due to the Bragg resonance, with magnitude more significant than the underlying chromatic dispersion of the fiber [26, 27]. Considerable improvement in grating performance has shown that thermal annealing of the gratings can reduce the loss coefficient smaller than the intrinsic diffraction loss in the cavity gap required to accommodate the atom [28]. At sufficiently high intensities, the FBG-induced dispersion may be counterbalanced by nonlinearity resulting in the formation of Bragg grating temporal [29] and spatiotemporal [30, 31] solitons, created in second-harmonic-generating crystals. Indeed, analytical soliton solutions of the standard FBG model, including exact periodic solutions expressed in terms of Jacobi's

elliptic functions sn and cn [32], standing and moving pulses, were reported [23, 24, 33]. A general quantum theory applied to the case of FBG has been developed [34]. The first experimental demonstration of the optical pulse compression has been presented in a Bragg grating [35]. In a model of a lossy nonlinear fiber grating which combines a local gain and an attractive perturbation of the refractive index, it has been demonstrated that stable pinned pulses show persistent internal vibrations and emission of radiation [36]. Exact solutions, expressed in terms of products of modified Bessel functions with algebraic functions, describing bidirectional pulses propagating in FBGs have been found [37]. It has been predicted that gratings permit robust signal amplification for large wave vector mismatches between pump, signal, and idler [38]. Wavelength selective amplification and single-mode lasing have been discussed in chirped and apodized FBGs influenced by parity and time-reversal symmetry [39]. Solitary-wave propagation in Bragg gratings with a fast saturable absorber [40] and in a FBG that is written in a slow saturable fiber amplifier, such as an erbium-doped fiber amplifier [41], were studied. The mean photon number, the second-order photon correlation function, and the atomic excited-state population have been calculated in a weakly driven FBG cavity [42]. The force, the friction coefficients, and the momentum diffusion of an atom moving in a weakly driven FBG cavity have been obtained numerically and analytically [43]. A gain controlled transition from superluminal to subluminal pulse reflection in pumped asymmetric FBG below lasing threshold has been investigated analytically [44]. Modulational instability conditions have been identified in a FBG that is uniformly doped with two-level resonant atoms [45]. The simultaneous presence of Raman gain, Kerr nonlinearity, grating dispersion, and Bragg reflection leads to the formation of Raman gap solitons in FBGs [46]. Moreover, the interplay between gain and loss and higher-order nonlinearities tailors the formation of gap solitons in a highly nonlinear FBG with cubic-quintic-septimal nonlinearities [47]. In the presence of the mismatch, the symmetry breaking bifurcation of gap solitons was investigated in a model including two linearly coupled Bragg gratings [48]. The possibility to capture a moving Bragg soliton that performs persistent oscillations in the cavity bounded by two repulsive defects has been

revealed [49]. Multifunctional capabilities such as the multiplexing, filtering, and lasing in a short length of the FBG depending on the different operating regimes have been described [50]. The effect and interplay of dispersive reflectivity, group velocity difference, and the grating-induced coupling on the stability and interactions between quiescent Bragg grating solitons with dispersive reflectivity have been systematically investigated in a dual-core fiber [51, 52, 53, 54, 55]. In addition, 2D gap solitons in a Kerr nonlinear 2D waveguide with a Bragg grating in the propagation direction and homogeneous in the transverse direction have been considered, where the mechanism of trapping at a special class of nonlinear localized defect modes has been predicted [56]. In quasi-one-dimensional (1D) case, the evolution of envelope waves in nonlinear dispersive media can be modeled, in the paraxial approximation, by a 1D nonlinear Schrödinger (NLS) equation with cubic nonlinearity, leading to bright and dark stable soliton solutions, when the dispersion and nonlinearity effects can effectively balance each other. Solutions to the NLS equation with attractive or focusing nonlinearity, in contrast to repulsive, or defocusing nonlinearity, are unstable in three dimensions (3D) and are stable in 1D. The critical dimensionality for the 2D NLS equation [57] has been derived. For instance, in optics, propagation of a laser beam through a transparent medium is governed by the 2D NLS equation, and wave collapse occurs when nonlinear focusing, due to the intensity-dependent refractive index, overcomes linear diffraction. It has been shown experimentally that the spatial profile of a collapsing optical wave evolves into a universal, self similar, circularly symmetric shape, known as the Townes profile, regardless of the shape of the initial profile [58, 59]. Thus, the Townes soliton is fundamental to understanding the self-similar collapse of solutions to the 2D NLS [60] equation. A great effort has been devoted to searching for systems with stable solitary waves due to this well-known collapse property in multidimensional configurations. Some ideas to prevent collapse have been proposed such as using a spatial modulation of the Kerr coefficient [61, 62], time-dependent nonlinearity [63, 64, 65], modulation of dispersion [66, 67, 68], addition of mutually incoherent fractions of Townes solitons that are stabilized under the effect of a periodic modulation of the nonlinearity [69], saturation of the

Kerr response [70], cubic-quintic [71, 72, 73, 74], cubic-quintic-septic [75, 76, 77, 78], and quadratic [79, 80, 81] nonlinear media, self-induced transparency [82, 83, 84], confined geometries [85, 86, 87], dipole-dipole interactions [88, 89, 90], feedback control of the interatomic interactions [91], inclusion of the nonlinear dissipative term [92], gauge potential [93], the Lee-Hung-Yang quartic term [94], magneto-optical control [95], orbital angular momentum [96], thermal effects [97, 98], polarization coupling [99], parametric coupling to a weakly radiating harmonic field [100], nonparaxiality. In the following, we note that so far we have witnessed several research on the propagation of optical beams in non-linear media which can be described by the parabolic scalar equation [101]. This equation is derived from the Helmholtz equation in slowly varying amplitude approximations and paraxial approximations. However, the paraxial model has many limitations in realistic applications [102, 103], for example the paraxial approximation overestimates the change in nonlinear phase shift for waveguides [102]. Collapses into a singularity (self-focusing point) over a finite distance, which is finite distance, which is in contradiction with many practical problems [104], diffraction can generally occur in the transverse and longitudinal directions in 2D media. Therefore, the assumption of a paraxial beam is not valid. The non-paraxiality is particularly important when there is miniaturization of the devices. This shows the importance of including the non-paraxial term in the NLS equation by considering the light propagations in nanophotonic waveguide devices. Recently, there has been much interest in the context of the Lax et al. [103], especially on ultra-narrow beams [105] where the non-paraxial NLS equation term is considered. Blair studied scalar and vector nonparaxial nonlinear evolution equations for propagation in two dimensions. Temgoua and Kofane studied nonparaxial scattering waves in optical Kerr media [106], where they demonstrated that the non-paraxiality increases the intensity of scattering waves by increasing the length and reducing the width of the peak simultaneously. They also shown that the non-paraxial scattering waves are faster than those obtained from the standard NLS equation, with non-paraxiality shifting the highest peak of the scelerate waves from the center to the periphery. At the same time, non-paraxiality results in the reduction of

the interaction of spurious waves. Chen, and Shi [107] studied one-dimensional spatial optical solitons with nonlinearity. Then, they show how the degree of non-locality can affect the width of the non-local soliton beams, but have no effect on their stability. Chamorro-Posada et al. [108] studied non-paraxial spatial solitons, which could be used in miniaturized nonlinear photonic devices. They found an exact solution of the nonparaxial soliton from which the paraxial soliton is recovered with appropriate limits. The studies of soliton in the non-paraxial limit continues to attract increased interest from research in recent times, due to its fundamental and applied interest, particularly in miniaturized photocells. The soliton being a structure that appears everywhere in nonlinear physics, it could be a subject of great importance for advanced research, intervening in several fields such as nonlinear fiber optics [109, 110, 111], matter waves in Bose-Einstein condensates, shallow waves [112, 113], molecular biology [114], nonlinear optics of ultrashort pulses [115, 116, 117]. Temporal, spatial and space-time solitons, have applications in near all-optical routing, and transparencies, and the massive integration of optical operations in a fully 3D system. So far, we have recorded two different types of envelope solitons, bright and dark, which can propagate in nonlinear dispersive media. In contrast to the bright soliton, which is a pulse on a background of zero intensity, the dark soliton appears as a trough of intensity in a constant infinitely extended background. When linear effects (such as scattering, diffraction or diffusion) are exactly balanced by non-linearity (automatic phase modulation, autofocusing or kinetic properties, respectively), robust and self-trapped structures solitons can emerge as dominant modes of the system dynamics [118]. We will focus on the process of modulation instability (MI). The first experimental demonstrations of the implementation of MI in an optical fiber date from the early 1980s [119]. This phenomenon is at the basis of many complex nonlinear effects such as the generation of pulse trains [120].

The main objective:

By means of the multiple-scales analysis, we derive a new 2D nonlinear Schrödinger equation with higher-order correction terms that consider the nonparaxial regimes in the slowly varying envelope approximation at frequency close to the gap for Bragg re-

flection. **Specific objectives:** – Investigating the formation and propagation of gap-soliton bullets in nonlinear periodic waveguides at frequencies close to the gap for Bragg reflection beyond the paraxial approximation.

– The standard linear stability analysis is used to investigate theoretically the stability of continuous-wave solution and to obtain an expression for the modulational instability gain spectrum.

– Direct numerical simulation of the new 2D nonlinear Schrödinger equation with higher-order correction terms are performed to support the analytical predictions.

To reach the above to mentioned aims, the remainder of this thesis is organized as follows: Chapter 1 is devoted to the review of the literature on generalities related to the propagation of light in an optical fiber. The following concepts will thus be discussed: different types of soliton and their importance, Bragg gratings, optical fiber, the optical fiber in optical communication systems, linear and nonlinear effects, chromatic dispersion.

Chapter 2 is devoted to the models describing the wave dynamics in the fiber Bragg gratings in the nonparaxial regime. We also present some analytical and numerical methods used in our studies.

Chapter 3 presents the main results of this thesis. These results concern the self-organization of the gap-soliton bullets in nonlinear periodic waveguides, modeled by the 2D nonlinear Schrödinger equation beyond the paraxial approximation. Then, we relate the formation of the gap-soliton bullets to the modulation instability of a uniform state beyond the paraxial approximation. Direct numerical simulations of the 2D nonlinear Schrödinger equation beyond the paraxial approximation are performed and the space-time evolution of wave amplitude is displayed, showing the generation of gap-soliton bullets for modes predicted to be unstable. The present thesis ends with a general conclusion. We summarize our results and give some future directions that could be investigated.

LITERATURE REVIEW

I.1 Introduction

In this chapter, we describe the characteristic of the nonlinear optical fiber. In particular, we present results about optical losses, chromatic dispersion, optical Kerr effect, temporal, spatial and spatiotemporal solitons. We focus on the propagation of light in fiber Bragg gratings.

I.2 General information on optical fibers

The optical fiber is a dielectric waveguide, made primarily of fused silica (SiO_2). Generally and schematically, an optical fiber is a very thin glass or plastic wire that has the properties of being a conductor of light and is used in data transmission. It offer a much higher information rate than coaxial cables, and can be used to support a network through which television, telephone, video conferencing or computer data can be transmitted. The principle of the optical fiber was developed during the 1970s in the laboratories of the American company Corning Glass Works (now Corning incorporated). An optical fiber is made up of 3 concentric elements, represented on the Figure(1.1) a cylindrical core of a few meter, diameter (a) and optical index n_c . It is in this area, made of glass, that the light is guided and propagates along the optical fiber; an outer cladding of larger diameter (b); and index n_g , which is a layer of glass that surrounds the core, while a protective plastic cladding wraps the whole. Light guidance into the fiber core is provided by total reflexion at the core-cladding interface and obtained when the refractive index is higher than that of the optical cladding. Since the core and cladding are essentially fused silica, the difference in index between these two parts is achieved by

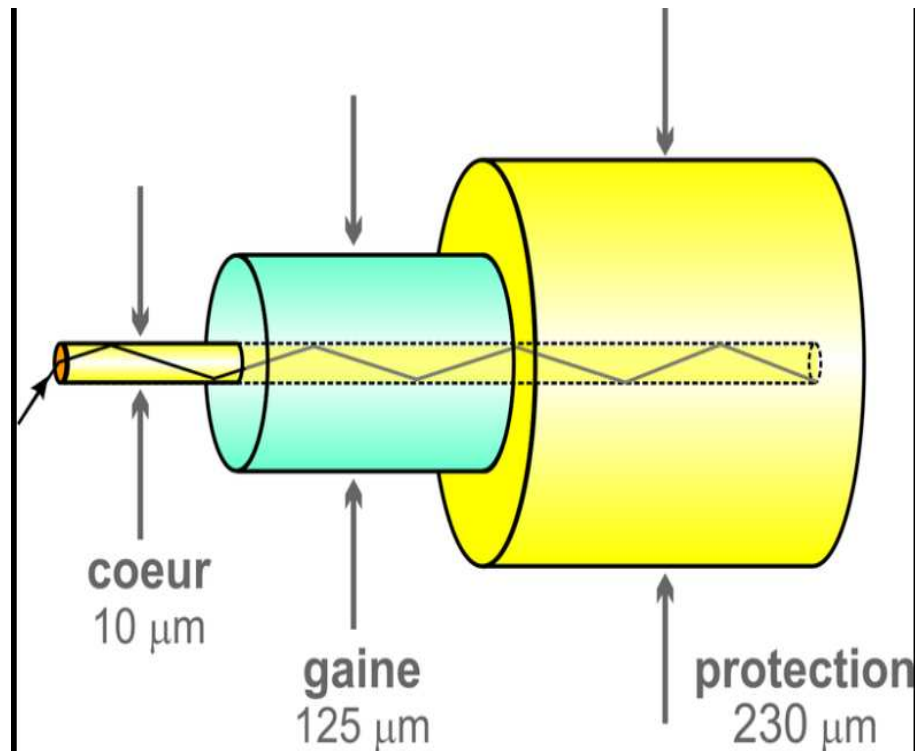


Figure 1: Optical fiber [121].

adding dopants. There are two types of optical fiber, among which the multimode fiber. This type of fiber is said to be multimode because light propagates according to several modes, i.e., it can follow several paths inside the core, then we have the single-mode fiber; in this case, the optical fiber is said to be single-mode because, due to the very small size of the core ($9\mu\text{m}$), there is only one mode of light propagation.

I.2.1 Optical losses

Light transmission through optical fibers uses the principle of total reflexion at the core-cladding interface. Although today new technologies have greatly improved the minimization of guiding losses, there are inevitably intrinsic losses due to Rayleigh diffusion of light by silica [123], due to localized variations in the refractive index, created by changes in density or composition that appeared at the time of solidification of the material. This diffusion results in the propagation of part of the incident energy in all directions of space, this at any point of the optical fiber. If a power P_0 is injected within

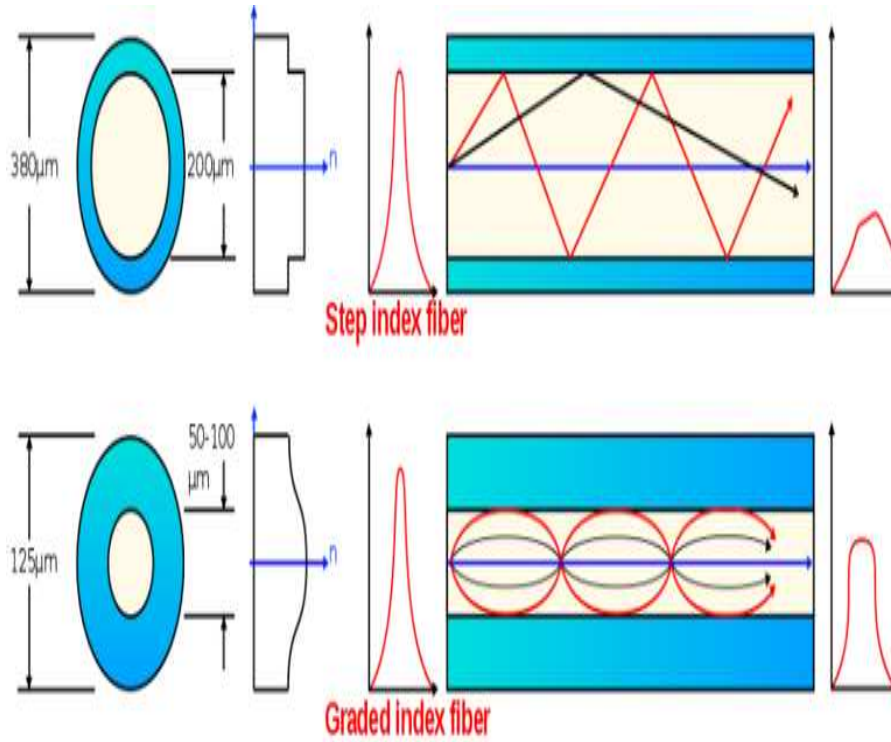


Figure 2: Multimode fiber: here the light can follow paths inside the core [122].

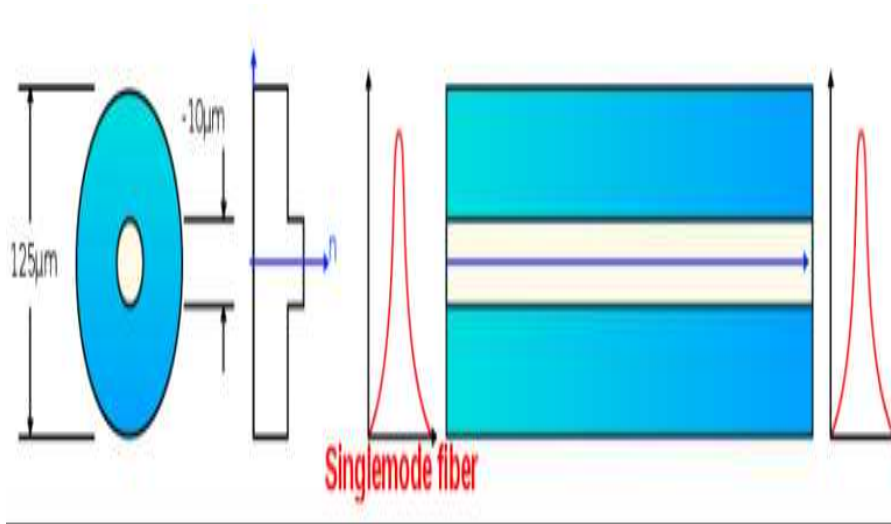


Figure 3: Single-mode fiber: in this case, there is only one mode of light propagation [122].

an optical fiber of length l , the power effectively transmitted P_T will be expressed by [124] :

$$P_T = P_0 \exp(-\alpha_L L), \quad (\text{I.1})$$

where α_L denotes the linear loss coefficient of the fiber. The α_L coefficient is usually expressed in decibels per kilometer (dB/km), and is given by [125] :

$$\alpha_{dB} = -\frac{10}{L} \log \left(\frac{P_T}{P_0} \right) \approx 4,343 \alpha_L. \quad (\text{I.2})$$

Fiber losses depend on the wavelength of light. Silica fiber exhibits a minimum loss of about 0.2 dB/km near $1,55 \mu\text{m}$. It is found that the Rayleigh diffusion decreases with wavelength in $\frac{1}{\lambda^4}$. This imposes a fundamental limit on optical losses. Other factors of optical losses can be the cause of intrinsic losses in the fiber, such as the presence of OH^- ions, due to the manufacturing process of impurities, which are responsible for an absorption peak around 1400 nm . The curvature of the fiber or various resonances can also cause an increase of the losses in the fiber.

I.2.2 Chromatic dispersion

When an electromagnetic wave propagates in a dielectric material, it interacts with the electrons bound to this material. The chromatic dispersion expresses the fact that the response of this medium, and in particular, its refractive index $n(\omega)$, depends on the frequency of the incident wave. Far from the resonance frequencies of the material, the dependence of the refractive index on the pulsation can be evaluated with a good approximation thanks to the Sellmeier equations given by

$$n^2(\omega) = 1 + \sum_{j=1}^m \frac{\beta_j \omega_j^2}{\omega_j^2 - \omega^2} = 1 - \sum \frac{\beta_j \lambda^2}{\lambda^2 - \lambda_j^2}, \quad (\text{I.3})$$

where ω_j , λ_j and β_j represent the pulsation, the wavelength in vacuum, and the amplitude of the j^{th} resonance, respectively. As the speed of propagation of a monochromatic

wave in a medium of index $n(\omega)$ is given by $\frac{c}{n(\omega)}$ (with c : celerity of light in vacuum), a light pulse composed of several spectral components and traveling within an optical fiber will see its spectral components propagate at different speeds, to finally generate a spread of the pulse. We see here the dramatic consequences that chromatic dispersion can have on a system of transmission of information by optical fibers and the immediate interest for the Telecom to find a way to overcome it. Traditionally, the scientific community accounts for the effects of dispersion by developing the constant of propagation $\beta(\omega)$ in Taylor series around the frequency of the carrier $\omega(0)$, as follows

$$\begin{aligned} \beta(\omega) = \frac{\omega}{c}n(\omega) = \beta_0 + \beta_1(\omega - \omega_0) + \\ \frac{1}{2}\beta_2(\omega - \omega_0)^2 + \frac{1}{6}\beta_3(\omega - \omega_0)^3 + \dots, \end{aligned} \quad (\text{I.4})$$

where $\beta_0 = \beta(\omega_0)$ and $\beta_m = \left(\frac{\partial^m \beta}{\partial \omega^m}\right)_{\omega=\omega_0}$ for $m = 1, 2$. We may notice that the parameters β_1 and β_2 are intuitive physical quantities in the sense that β_1 simply reflects the speed at which the pulse energy propagates. Indeed β_1 parameter has the inverse of the group velocity v_g and is expressed as:

$$\beta_1 = \frac{1}{v_g} = \frac{1}{c} \left(n + \omega \frac{\partial n}{\partial \omega} \right). \quad (\text{I.5})$$

The coefficient β_2 represents the dependence of the speed of energy propagation on the frequency of the wave. It is the chromatic dispersion parameter of order 2, essential data for the characterization of optical fibers and essential for engineers designing telecom systems. β_2 is expressed in $ps/km.nm$ and is given by:

$$\beta_2 = \frac{\partial \beta}{\partial \omega} = -\frac{1}{v_g^2} \frac{\partial v_g}{\partial \omega}. \quad (\text{I.6})$$

β_2 , also represents the variation of the group velocity with respect to frequency. It is commonly called the group velocity dispersion coefficient (GVD). However, the telecom scientific community prefers the parameter D which is expressed in $ps/km.nm$ and

replaces β_2 in the literature. The two parameters are related by:

$$D = -\frac{2\pi c}{\lambda^2} \beta_2. \quad (I.7)$$

In general, D is the sum of two contributions: the chromatic dispersion of the material D_m and the dispersion of the guide D_g [126]. For pure silica, the D_m dispersion cancels out near a wavelength of $1.27\mu\text{m}$, while D_g depends essentially on the geometric characteristics of the optical fiber. However, the contribution of the guide only slightly shifts the zero dispersion wavelength λ_0 which is generally around $1.3\mu\text{m}$ for standard index hopping fibers. The zero dispersion wavelength then allows to define two propagation regimes separated by λ_0 . The first dispersion regime is qualified as abnormal ($D > 0$). The spectral components of lower frequency then propagate faster than the high frequency components and this conversely for the second regime, qualified as normal and for which $D < 0$. This value of λ_0 can easily be modified by changing the nature and quantity of the dopants (*e.g.* GeO_2 or P_2O_5) introduced into the fiber during its manufacture, but also by changing the fiber index profile. As a consequence, the current scientific and technological knowledge allows manufacturers to have a very complete range of optical fibers which allows them to design telecom systems with zero, positive or negative dispersion fibers, but also to choose the sign of the dispersion slope.

I.2.3 Optical Kerr effect

The incident field induces a displacement of the charges and consequently a polarization occurs within the material [127]. If this field is of low intensity compared to the atomic field of the material and sufficiently far from its resonance frequencies, the response of the medium is proportional to the incident field. We are then in the presence of a linear response. That is to say that the polarization induced by the external field has the same frequency as the field that gave rise to it, with an amplitude that is proportional to it. As nature loves complexity, most observable phenomena can be qualified as nonlinear if their origin is sufficiently important. In the case of a light wave, if the amplitude of the

incident field becomes too large, the response of the material is no longer simply proportional to the initial field but involves different harmonics and will therefore be qualified as nonlinear. Assuming that the fiber is isotropic and that the initial electric field \vec{E} is rectilinearly polarized, the polarization resulting from the wave-matter interaction can then be expressed as a power series expansion of \vec{E} . This series is generally seen as the sum of two contributions: a first term called linear \vec{P}_L , because it is proportional to the incident field, and a second term called nonlinear \vec{P}_{NL} , because it is proportional to higher orders of \vec{E} . The polarization finally takes the following form:

$$\vec{P} = \vec{P}_L + \vec{P}_{NL} = \epsilon_0 \chi^{(1)} \vec{E} + \frac{3\epsilon_0}{4} \chi^{(3)} |E|^2 \vec{E} + \dots, \quad (\text{I.8})$$

where $\chi^{(1)}$ and $\chi^{(3)}$ are the first- and third-order susceptibility tensors of fused silica, respectively. We notice the absence of the second-order susceptibility tensor $\chi^{(2)}$ in Eq. (I.8) indeed, the optical fiber being composed of fused silica in the form of an amorphous glass, there is no preferred direction of orientation of the molecules. Therefore, the microscopic susceptibility tensors of order 2 are randomly directed and compensated on average, which cancels the macroscopic susceptibility tensor $\chi^{(2)}$. Finally, in a homogeneous optical fiber, the third-order susceptibility tensor $\chi^{(3)}$ will be the source of the smaller-order nonlinear effects. In order to highlight the linear and nonlinear effect, we rewrite Eq. (I.8) as follows.

$$\vec{P} = \epsilon_0 [\chi^{(1)} + \epsilon_{NL}] \vec{E}, \quad (\text{I.9})$$

with

$$\epsilon_{NL} = \frac{3}{4} \chi^{(3)} |E|^2. \quad (\text{I.10})$$

Knowing that the polarization and the refractive index are closely related by the following Maxwell relation:

$$\vec{D} = n^2 \vec{E} = \epsilon_0 \vec{E} + \vec{P}, \quad (\text{I.11})$$

we deduce that, at a given pulsation, the refractive index n is given by :

$$n^2 = 1 + \chi^{(1)} + \epsilon_{NL} = (n_0 + \Delta n_{NL})^2 \cong n^2 + 2n_0\Delta n_{NL}. \quad (\text{I.12})$$

By using $n_0 = \sqrt{1 + \chi^{(1)}}$, it finally comes that, at a given pulse ω [128] :

$$n(\omega, |E|^2) = n_0(\omega) + n_2|E|^2, \quad (\text{I.13})$$

where n_2 represents the nonlinear refractive index coefficient given by :

$$n_2 = \frac{3}{8n_0}\chi^{(3)}. \quad (\text{I.14})$$

We can clearly see in Eq. (I.13) that the linear part of the polarization is responsible for the dependence of the refractive index on frequency, while the nonlinear part generates a dependence of the index on the intensity I , a phenomenon known as the optical Kerr effect [129]. Knowing that $I = aE^2$, with $a = 1/2cn_0\epsilon_0$, the refractive index can be rewritten as follows:

$$n(\omega, I) = n_0(\omega) + n_2^I I, \quad (\text{I.15})$$

with $n_2^I = n_2/a$; For a standard Telecom fiber, n_2^I is typically worth to $2.7 \times 10^{20} \text{m}^2/\omega$ [130]. For an incident intensity of $1 \text{GW}/\text{cm}^2$, Δn_{NL} will therefore be worth about 2.5×10^{-7} , which is still much lower in front of $n_0 = 1.45$, for fused silica. The optical Kerr effect or intensity dependence of the refractive index is ultimately responsible for many of the effects that we will detail later, such as self-phase modulation, cross-phase modulation, mixing at modulation instability or the existence of pulses.

I.3 Linear and nonlinear responses of the medium

A light wave is composed of an electric field and a magnetic field which vary sinusoidally at high frequency. When light propagates in a material medium, it will induce

charge displacements within the material. In a dielectric medium, the charged particles, which in this case are electrons, will oscillate in the applied electric field. They form electric dipoles. The contributions of the magnetic field component of the wave and of the quadrupoles are much smaller and are usually neglected. This is the electric dipole approximation. The responses of the oscillating dipoles add up to the macroscopic polarization \vec{P} , which describes the light-matter interaction. In a non-magnetic medium, this vector can be written as functional $\vec{P} = \vec{P}(\vec{E})$. To account for this explicitly in the development, the constitutive equations of the medium are introduced :

$$\begin{aligned}\vec{D} &= \epsilon_0 \vec{E} + \vec{P}, \\ \vec{B} &= \mu_0 \vec{H}.\end{aligned}\tag{I.16}$$

When the wave is not very intense, i.e. for small amplitudes of the applied electric field, the charges can follow almost exactly the oscillations of the field, and the relation between the field \vec{E} and the polarization \vec{P} is essentially linear. In other words, the effects are proportional to the causes. When the amplitude increases, the motion of the charges will no longer be a replica of the applied field, and the nonlinear contributions become important. As long as these new terms remain small compared to the linear term, the polarization \vec{P} can be developed as a power series of the electric field \vec{E} . In silica optical fibers, this expansion is given by:

$$\vec{P}(\vec{r}, t) = \vec{P}^1(\vec{r}, t) + \vec{P}^3(\vec{r}, t),\tag{I.17}$$

$$\vec{P}^1(r, t) = \epsilon_0 \chi^1 \vec{E},\tag{I.18a}$$

$$\vec{P}^3(r, t) = \epsilon_0 \chi^3 : \vec{E} \vec{E} \vec{E}.\tag{I.18b}$$

This is indeed the case when each higher order term is much smaller than the lower order terms preceding it. In the range of wavelengths of interest (typically $0.5\mu m$ to $0.2\mu m$), this assumption is verified because we are far from the resonances of the medium.

We can better understand the importance of polarization in the medium if we remember that any oscillating dipole also emits radiation, at its oscillation frequency. It thus modifies the optical field which induces the polarization. Thus, the first term takes into account the linear response of the medium, at the frequency of the applied field. The quadratic term is zero here, because the silica has an inversion symmetry. The second term of the development is therefore cubic in field. It represents the nonlinear response of silica, responsible in optical fibers for the four-wave mixing process and the Kerr effect. These two effects are of primary importance at any level in our thesis work. Finally, higher order nonlinear terms are usually neglected because their effects are very small far from the resonances. To account for causality (the response at time t affects the field at time $(t + \tau)$) and the possible nonlocality of the response \vec{P} (the response at a point \vec{r} affects points in $\vec{r} + \vec{\rho}$), each term in the series (I.8) is in fact a double integral over time (from $-\infty$ to t) and over the spatial coordinate r (over a volume V around the point under consideration). The response function of the medium is thus contained in the dielectric susceptibility tensors $\chi^{(1)}$ and $\chi^{(3)}$. A number of symmetries exists within the susceptibility tensors, which lead to their simplification. The most important symmetry is that of the medium because it imposes a specific symmetry on the optical response. In particular, we have already pointed out that the nonlinear quadratic response ($\chi^{(2)}$) is zero, since silica is a symmetric center medium. We will see later Eq. (I.5), the other symmetries to be considered in optical fibers, and maintain for now the generality of the tensor. We still assume that the light waves treated here can be considered as quasi-monochromatic. In practice, this approximation is valid as long as the envelope of the waves varies in a time of the order of 100fs at least [131]. The electric field of an electromagnetic wave whose spectrum is centered around the frequency ω and the linear optical response can be written in terms of their complex spectral amplitudes $\vec{E}(\vec{r}, \omega)$ and $\vec{P}^{(1)}(\vec{r}, \omega)$:

$$\vec{E}(\vec{r}, t) = \frac{1}{2} \left[\vec{E}(\vec{r}, \omega) \right] e^{-i\omega t} + \frac{1}{2} \left[\vec{E}(\vec{r}, \omega) \right]^* e^{i\omega t}, \quad (\text{I.19})$$

$$\vec{P}(\vec{r}, t) = \frac{1}{2} \left[\vec{P}^{(1)}(\vec{r}, \omega) \right] e^{-i\omega t} + \frac{1}{2} \left[\vec{P}^{(1)}(\vec{r}, \omega) \right]^* e^{i\omega t}. \quad (\text{I.20})$$

In this form, it immediately appears that the electric field $\vec{E}(\vec{r}, \omega)$ and the linear polarization $\vec{P}^{(1)}(\vec{r}, \omega)$ remain real quantities. In the spectral domain, we can then show that [132] the spectral amplitude of the linear polarization becomes

$$\vec{P}_i^{(1)}(\vec{r}, \omega) = \left[\chi_{ij}^{(1)}(\omega) \right] \vec{E}_j(\vec{r}, \omega) + \Gamma_{ijz}^{(1)}(\omega) \nabla_{\perp} \vec{E}_j(\vec{r}, \omega), \quad (\text{I.21})$$

with $\chi_{ij}^{(1)}(\omega) = \epsilon_{ij}(\omega) - \delta_{ij}$; δ_{ij} is the Kronecker symbol and ∇_{\perp} defines a gradient in the direction orthogonal to the propagation direction z . In this equation, the indices refer to the spatial coordinates (x, y, z) ; repeated summation over all successive indices is in order although it is not explicit here, in order to lighten the notations. We will keep this notation in the following. In the linear constitutive equation (I.21), we have separated the local response $\chi_{ij}^{(1)}(\omega)$ from the nonlocal optical response $\Gamma_{ijz}^{(1)}$ of the medium. In silica, the local response results in temporal dispersive effects-chromatic dispersion- and spatial dispersive effects-linear birefringence-, while the nonlocal response of the medium is the cause of the optical activity or circular birefringence of the fiber, pose the following equation:

$$\vec{P}(\vec{r}, t) = \frac{1}{2} \left[\vec{P}^{(3)}(\vec{r}, \omega) \right] e^{-i\omega t} + \frac{1}{2} \left[\vec{P}^{(3)}(\vec{r}, \omega) \right]^* e^{i\omega t}. \quad (\text{I.22})$$

Similarly, it can be shown that the constitutive equations for the complex amplitude components of the nonlinear polarization take the following form:

$$\vec{P}_i^{(3)}(\vec{r}, \omega) = \left[\epsilon_0 \chi_{ijk}^{(3)}(\omega) \right] \vec{E}_j(\vec{r}, \omega) \vec{E}_j(\vec{r}, \omega) \vec{E}_k(\vec{r}, \omega) \vec{E}_l(\vec{r}, -\omega) \quad (\text{I.23})$$

To obtain Equations (I.9) and (I.18), we made a number of assumptions. First, we retained only the electric field components of the same frequency (unsigned). Only ω terms and third harmonics in 3ω then remain. In Equation (I.21), we further assumed that the latter terms oscillate rapidly and are therefore negligible (away from the phase

tuning conditions, $\vec{P}_i^{(3)}(\vec{r}, 3\omega) = 0$. We performed a previously implicit summation over all permutations of the frequencies ω and $-\omega$ of the components \vec{E}_j, \vec{E}_k and \vec{E}_l as long as they produce a response at frequency ω . Finally, we considered the nonlinear response as instantaneous. The electronic contribution to the nonlinearity indeed has an estimated response time of a few femtoseconds at most, while the delayed molecular contribution that we neglect here has a time on the order of 60-70 fs in silica [133]. Finally, we have omitted the non-local contribution of the cubic nonlinear response, which can be perfectly neglected in the present context. Then, using the constitutive equations for the linear and nonlinear polarizations, the propagation equation of the light waves in the silica fibers can be rewritten for each component \vec{E}_i of the complex amplitude of the electric field as follows:

$$\Delta \vec{E}_i(\vec{r}, \omega) + \frac{\omega^2}{c^2} \vec{E}_i(\vec{r}, \omega) = -\mu_0 \omega^2 \vec{P}_i^{(n)}(\vec{r}, \omega). \quad (\text{I.24})$$

I.4 Historical reminder (Bragg gratings)

The Bragg grating is a passive photo-induced filter in the core of an optical fiber, allowing the selective reflection of wavelengths. It consists of a periodic longitudinal perturbation of the refractive index of the fiber core. When the light propagates in the optical fiber, the network reflects wavelengths that verify the relationship:

$$\lambda = 2n_{ef} \Lambda. \quad (\text{I.25})$$

Λ : is the period of the index modulation. This index modulation is obtained by exposing the core of the fiber to an intense interference pattern, created from an ultraviolet laser, which excites defects in the core of the optical fiber and modifies the glass. This exposure has the effect of increasing the refractive index of the regions exposed to high intensities. The first gratings inscribed inside an optical fiber were produced in 1978 in Ottawa at the Communications Research Center by Hill et al; [134, 135]. These re-

searchers observed that the injection of a high power single mode argon ion laser into a germanium doped fiber led, after a certain exposure time, to the partial reflection of the injected light. By performing spectral measurements, they noticed that the reflection of the grating was very selective and that the maximum reflection corresponded to the wavelength of the injected laser. The inscribed grating was formed due to the presence of a standing wave created by the injected light and the light reflected from the fiber tip. This type of guided injection network has been called "Hill's network". Further work on the training of photo-induced structures in the fiber, using lasers emitting in the visible range, demonstrated that the change in the refractive index was caused by the formation of defects and that this process was based on two-photon absorption. Over time, several other grating methods have been developed to increase the efficiency and to offer more flexibility in the choice of the spectral response of the gratings. Indeed, Hill's gratings only allowed to reflect the wavelength corresponding to the wavelength of the laser used for the inscription. These methods use the ultraviolet transparency of the fiber cladding to inscribe the grating by transverse exposure of the core. Thus, an ultraviolet laser can be used for writing while still obtaining gratings that reflect wavelengths in the infrared spectrum. It should also be noted that the use of the ultraviolet laser, with a wavelength of 244 nm, allows the formation of defects in the glass matrix with a single photon absorption. In this way, the defects no longer depend on the probability of interaction between two photons to form the defects, which accentuates the number of defects produced and consequently the change induced in the refractive index. These types of gratings are called type 1 photo Bragg gratings. Typically, the interference pattern used to write Bragg gratings is obtained with a diffractive element called a phase mask. The use of this element offers the possibility to modify the period of the inscribed grating without modifying the wavelength of the writing laser. This manufacturing method has allowed the Bragg gratings to build a niche in the field of optical telecommunications, as they are very selective in wavelength. Different applications of these filters have emerged such as: optical channel selector, external laser diode stabilizer, chromatic dispersion compensator, gain equalizer external stabilizer of erbium optical

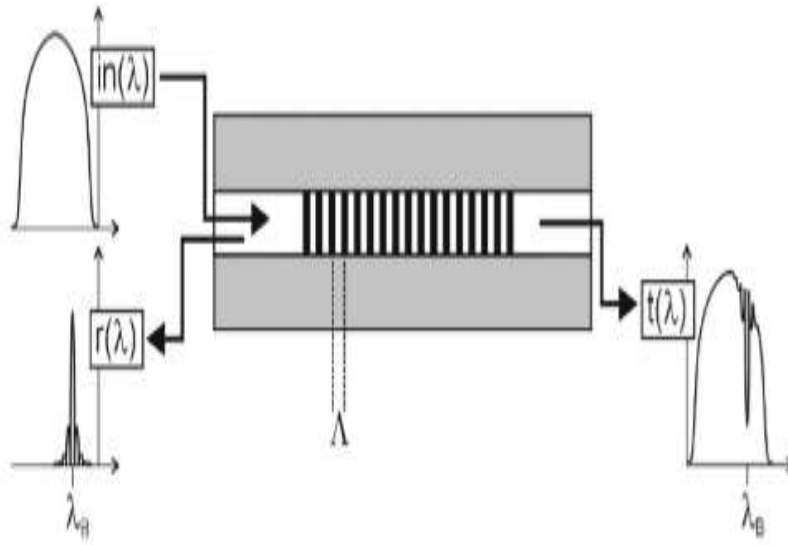


Figure 4: Diagram of a Bragg grating and their spectra [136].

amplifiers and different types of optical sensors.

I.4.1 Types of short step right Bragg gratings

Generally speaking, a Bragg grating is a periodic modulation of the index $\Delta n_{eff}(z)$ of the fiber core. This index perturbation can be formulated as follows [137]:

$$\Delta n_{eff}(z) = \Delta \bar{n}_{eff}(z) \left(1 + v(z) \cos\left(\frac{2\pi}{\Lambda}(z) + \theta(z)\right) \right). \quad (I.26)$$

$\Delta \bar{n}_{eff}(z)$ is the average change in the visible refractive index, $v(z)$ is the apodization of the modulation, Λ is the period of the modulation, $\theta(z)$ is its phase. In this way, we can identify simulations of different types of gratings whose index modulation is shown in Figure 5.

- a) Uniform gratings: $\Delta \bar{n}_{eff}(z)$, $\theta(z)$ and $v(z)$ are constants and do not vary with z .
- b) Variable pitch (chirped) gratings: $\theta(z)$ is non-zero, the pitch of the grating varies with z .
- c) Variable amplitude gratings: $\Delta \bar{n}_{eff}(z)$ varies as a function of z in a Gaussian fashion.

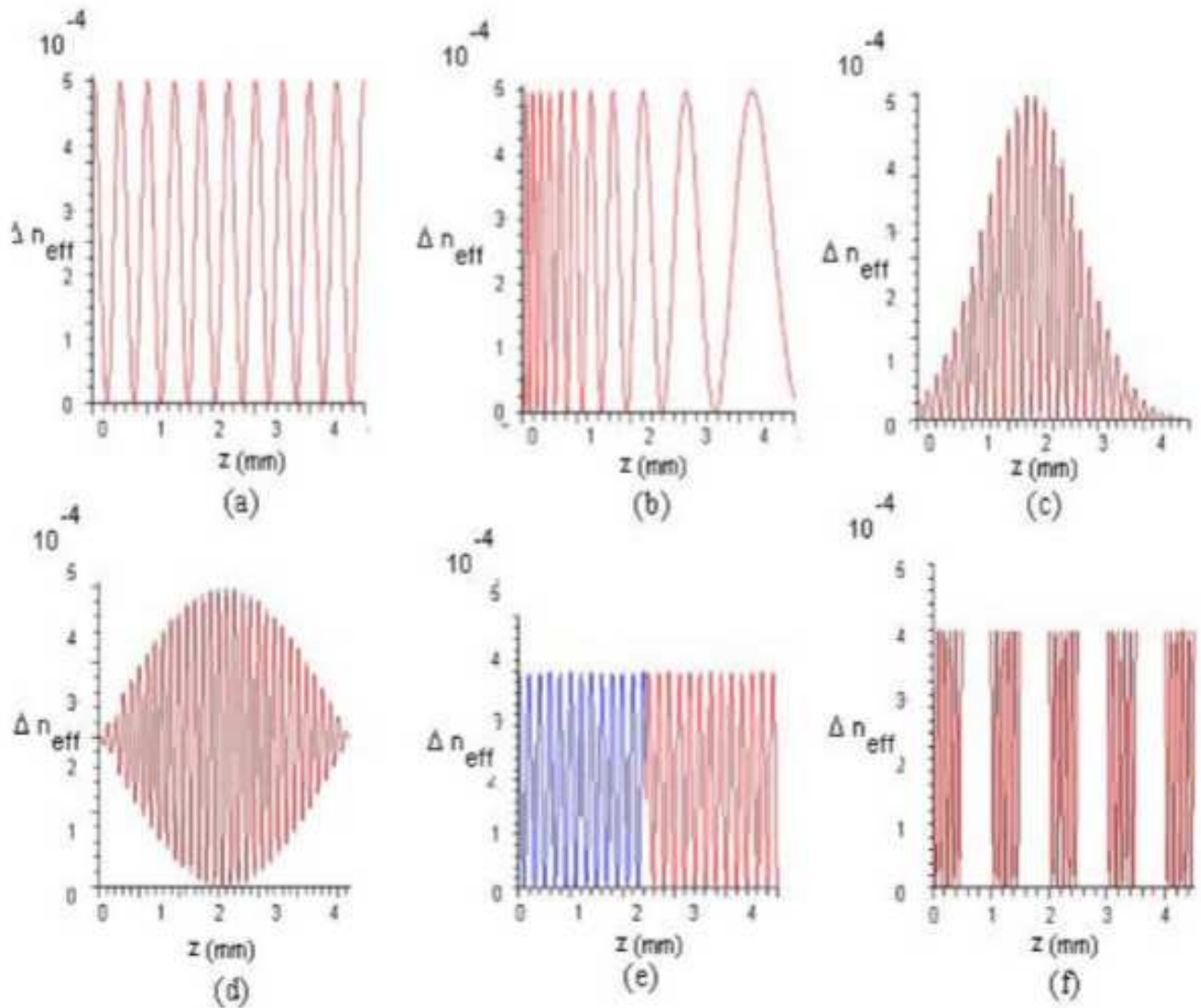


Figure 5: : Index modulations of different types of networks. (a): Uniform network, (b): Variable pitch network, (c): Variable amplitude network, (d): apodized network, (e): Phase jump network, (f): Sampled network

[138].

d) Apodized gratings: $v(z)$ varies in a sinusoidal fashion and $\Delta\bar{n}_{eff}(z)$ is constant.

e) Phase-skipped gratings: the phase $\theta(z)$ varies discontinuously in places, in bursts.

f) Sampled gratings : $v(z)$ varies in a periodic manner. Several methods exist to describe the behavior of Bragg gratings in order to characterize them and to calculate the reflectivity of the Bragg grating fiber. Among them, we can cite:

★ Rouard's method in which the grating is divided into several uniform planes (thin layers) in order to calculate the reflectivity, even for complex shapes. Its main disadvantage being the very long computation time [139].

★ Gel'Fand-Levitan-Marchenko's inverse scattering method, based on the coupled mode theory, and which aims to design optical filters with specific properties [140].

★ The Bloch theory method which consists in finding the exact eigenmodes of the Bragg grating [141],

★ The method of coupled modes associated with Marcuse [142], Snyder [143], Yariv [144] and Kogelnik [145], which has been chosen for this work thanks to its index.

I.4.2 Modeling of fiber Bragg gratings (coupled mode theory)

To apply this theory in the case of Bragg gratings, it is necessary to consider that the fiber is single mode, lossless and that the interaction takes place only between contra-propagating modes. The difference between the refractive indices of the core and the cladding being very small, we consider that the electric and magnetic fields propagate in the optical axis of the fiber. The difference between the refractive indices of the core and the cladding being very small, we consider that the electric and magnetic fields propagate in the optical axis of the fiber, which allows us to neglect the polarization effects due to the structure of the fiber [146]. Thus, we consider a Bragg grating with L , the length of the grating, Λ , its pitch, n_{eff} , the refractive index of the guided mode, and λ_β the Bragg wavelength, schematically shown in Figure 6. They propagate in the optical axis of the fiber, allowing polarization effects due to the fiber structure to be neglected [147]. From the theory of coupled modes, we can derive the well-known

system of equations describing the evolution of the amplitudes of the $U(z)$ and $V(z)$ fields propagating in the Bragg grating given by :

$$\frac{dU}{dz} = i\sigma(z)U(z) + ik(z)V(z), \quad (I.27)$$

$$\frac{dV}{dz} = -i\sigma(z)V(z) - ik(z)U(z), \quad (I.28)$$

where $k(z) = \frac{\Pi}{\lambda}v(z)\Delta\bar{n}_{eff}(z)$ represents the general coefficient of the alternating cou-

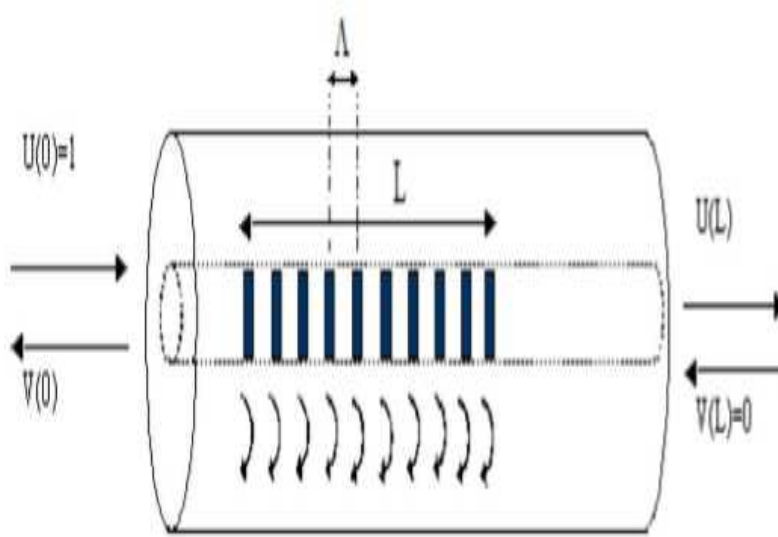


Figure 6: : Propagation of the fields through the Bragg grating [148].

pling (AC), which determines the energy exchange between the modes such that: $\sigma = 2\pi n_{eff} \left(\frac{1}{\lambda} + \frac{1}{\lambda\beta} \right) + \frac{2\Pi\Delta\bar{n}_{eff}(z)}{\lambda} - \frac{1}{2} \frac{d\theta}{dz}$, which represents the general coefficient of the mean coupling (DC). The first term gives the initial tuning (detuning wave vector) of the two modes independent of z . The second term describes the absorption loss in the grating. The third term is a possible chirp in the case of variable pitch gratings. The confinement factor is considered to be 0.8 (case of a single mode optical fiber).

I.5 Application of Bragg gratings to telecommunication

Photo inscribed Bragg gratings in optical fibers have become indispensable for amplifier gain equalization, pump or source wavelength stabilization, and fiber lasers. Their major advantages are low insertion loss, very low polarization sensitivity and extremely flexible design. These advantages also make them very attractive candidates for complex filtering or fine chromatic compensation applications.

I.6 Filtering and multiplexing

The reflection coefficient is proportional to the Fourier transform of the longitudinal profile of the refractive index. The filtering spectrum can then be obtained, by adjusting the grating period and the refractive index variation, for high adjacent channel rejects, rectangular shape. Today, advanced FBG writing techniques allow the realization of almost any desired spectral shape by controlling the phase response. FBGs are therefore excellent candidates for future complex WDM systems, but with inexpensive filters to adapt to this design. An example of a previously demonstrated filter containing 25 or 12.5 GHz channel spacing simultaneously showing rectangular shapes and zero dispersion has been reported [149]. The short period Bragg grating reflects light near the Bragg wavelength and remains transparent to others. To be used in a grating, the Bragg grating must be associated with another component with multiple inputs and outputs to extract the useful signal. Generally, this component is a circulator. However, circulators are expensive and it is possible to replace them by fiber devices like a Mach-Zhender interferometer, where the same Bragg grating is printed on both arms [150].

I.6.1 Optical filter

An example of the application of the Bragg grating as an optical filter, in association with a Fabry-Perot, is described in this example:

Filter composed of a Bragg grating

A filter is based on a Bragg network printed on fiber, on an optical circulator and on a Fabry-Perot : the input signal is reflected by the FBG and directed through the circulator to the Fabry-Perot. So, the global filter consists of the cascading of two independent filters. Each is characterized by its own transfer function $T_{FBG}(f)$ and $T_{FFP}(f)$. The global transfer function is: $T(f) = T_{FBG}(f)T_{FFP}(f)$.

I.7 Observation of a solitary wave and its consequences

John Scott Russell is mainly a mathematical engineer and naval architect. But his name is well-known today to mathematicians for his experimental discovery of the solitary wave. He noted the propagation in a narrow and shallow channel of this "translation wave" over several kilometers. Following this observation, Russell carried out several experiments using an artificial channel, testifying to his conviction of the unknown character of this phenomenon. He was able to determine the typical hyperbolic secant shape of the solitary wave as well as the relationship between its speed and amplitude. Russell's experimental work helped stimulate a renaissance in theoretical hydrodynamics in Great Britain. George Green, George Airy, Philip Kelland and Samuel Earnshaw all tried to describe the solitary wave theoretically, but without success. Airy objected to Russell's emphasis on his "great primary wave", arguing that it was neither great nor primary, but just a consequence of the shallowness of the water. G. G. Stokes was more cautious, but also doubted that a solitary wave could propagate without a change of form. An approximate but nevertheless correct theory was finally given by Boussinesq (1871) and Rayleigh (1876). But, it was not until the work of Korteweg and de Vries [151] in (1895), who discovered the nonlinear equation describing the propagation of long wavelength waves on the surface of a narrow, shallow channel, that this quarrel came to an end. The full meaning of the solitary wave and its generalization were first established in 1965 by Zabusky and Kruskal [152], who managed to show that the equation

known as the Korteweg-de Vries equation admits soliton solutions which were the one of Russell. Beyond this first and formidable observation of the hydrodynamic soliton, many researchers turned to this new era of research: nonlinear physics. Benefiting from mathematical tools which have become essential, they were able, from the beginning of the 70's, to explore this domain in all physical fields. Since the advent of the laser, new optical effects, depending on the intensity of the light, have been demonstrated. They are grouped under the term "nonlinear optics". In particular, they allow the interaction between light beams through the media they pass through. They allow to imagine realizations of all-optical devices, in particular in the field of telecommunications and signal processing.

I.7.1 The optical solitons

Any impulse or wave packet has a natural tendency to spread out during its propagation in a medium. In optics, a wave localized in space or in time can undergo a spreading, either of its temporal envelope or its spatial dimensions or even of both simultaneously. For a temporal pulse, the spreading is due to chromatic dispersion: the different frequency components, which constitute the pulse, travel at different speeds. Depending on the nature of the dispersion itself (positive or negative), the front of the pulse will therefore travel faster or slower than the back of the pulse, resulting in chromatic spreading. A spatial pulse, preferably called a beam, will undergo spreading under the natural influence of diffraction. An optical soliton [153] is therefore simply the self-induced compensation of these spreads. In a linear medium, various technological processes can be used to remedy the natural dispersion, either temporal or spatial. Spatially, the most common method is the use of waveguides. In such structures, characterized by a local variation of the refractive index, the propagation behavior of a beam is modified by a total internal reflection at the boundary between a region with a high index and one with a lower refractive index. Under certain conditions related to the constructive interference between the different reflections, the trapped beam forms a guided mode. An example

of a waveguide is the planar dielectric guide, which is commonly called a (1+1)-D or 1D guide, because in this case, we consider a propagation axis and a single transverse guiding axis. An optical fiber is therefore a (2+1)-D guide. But, for some materials with nonlinear optical qualities, i.e. whose properties (refractive index or absorption) can be modified by the presence of light, the propagation of optical pulses (in space or in time) can be altered. In particular, if the refractive index of the medium is modified by the light, it is possible under certain conditions to eliminate the broadening temporal or spatial of the pulse. This occurs when the effect of chromatic dispersion or diffraction is counterbalanced by the effect of the self-induced change in the refractive index. We speak then of optical temporal solitons in the case of compensation of chromatic dispersion and optical spatial solitons when the diffraction of the beam is neutralized. Moreover, in linear optics, two beams or pulses can cross each other without interacting. In nonlinear optics, it is quite different because the medium is sensitive to the total intensity of the coupled field and therefore depends on the amplitudes of the different components present. Solitons, although existing in the nonlinear regime, have the extraordinary property of being able to survive a crossing by preserving their energy, their momentum and their shape. This is an essential property of the soliton whose behavior is similar to that of particles. Mathematically, this property is based on the fact that the differential equations to which the propagation obeys are integrable. The integrability in this sense defines an exact analytical solution. Note that in optics, this case is restrictive to scalar Kerr solitons managed mathematically by the one-dimensional Nonlinear Schrödinger (NLS) equation defined by Zakharov and Shabat [154] in 1972. It is therefore necessary to remember that the set of other nonlinear equations which are non-integrable, gathers the class of solitary waves as a solution, representing a much larger family which does not benefit from a corpuscular type of stability, such as the inelastic collision of two entities. The difference between solitary wave and soliton wave is generally made, but we will use the name "soliton" during the whole manuscript to describe a phenomenon which does not undergo a variation of its envelope during its propagation and which benefits from stability properties.

The temporal solitons

In the case of temporal solitons, it is a question of compensating for the natural dispersion of the propagation medium by means of the nonlinear effect : the dispersion is become a way to protect against channel imperfections, because of its insensitivity to small perturbations. On the other hand, this technique creates new problems due, among others, to the coupling with the noise curves (modulation instability) or the polarization instability. Theoretically, the dynamics of the nonlinear propagation of temporal solitons is governed by the NLS equation, which belongs to the remarkable class of integrable nonlinear equations, and which can be solved exactly for an arbitrary initial state by means of the inverse scattering method. The solutions depend on the sign of the dispersion β_2 , that is,

$$\beta_2 = -\frac{1}{v_g^2} \frac{\partial v_g}{\partial \omega} = \frac{2}{c} \frac{\partial n}{\partial \omega} + \frac{\omega}{c} \frac{\partial^2 n}{\partial \omega^2}, \quad (\text{I.29})$$

where v_g is the group velocity, n is the effective index of the mode and ω the frequency of the wave. This coefficient can be either positive (normal dispersion) or negative (abnormal dispersion). In the presence of a Kerr-type nonlinearity (of nonlinear index n_2), a pulse undergoes a nonlinear phase shift $\Delta\varphi = k.n_2.I.L$, after propagation over a length L . This phase shift depends on the light intensity I and is therefore larger at the center than at the front and back of the pulse. By definition, the derivative of this phase shift gives the variation of the instantaneous frequency $\frac{d\Delta\varphi}{dt} = \Delta\omega$, due to the nonlinearity and thus, the frequency shift. It is therefore possible to obtain a soliton pulse if the nonlinear frequency shift exactly compensates for the chromatic dispersion. There are therefore two cases where we can observe temporal solitons. In the anomalous dispersion regime ($\beta_2 < 0$) in the presence of a positive nonlinearity. This is the most common case encountered, in particular, in optical fibers that possess an anomalous dispersion regime, for $\lambda \geq 1.3\mu m$, in the transparency band, thanks to the contribution of modal dispersion. The second combination that yields a temporal soliton corresponds to the combination of a negative nonlinearity and a propagation medium of normal dispersion ($\beta_2 > 0$) [155]. In the other two cases, the nonlinearity only enhances. The linear

dispersion results, in an even larger temporal broadening of the pulse. Figure 7 illustrates the temporal soliton principle in the case of anomalous dispersion. In the linear regime (a), the higher frequencies in the spectrum propagate faster than the lower frequencies so that the pulse arrives distorted after propagation. The nonlinear effect (b) will produce a frequency shift resulting in the slowing down of high frequencies and the acceleration of low frequencies (pulse front). We can see that the nonlinear phase

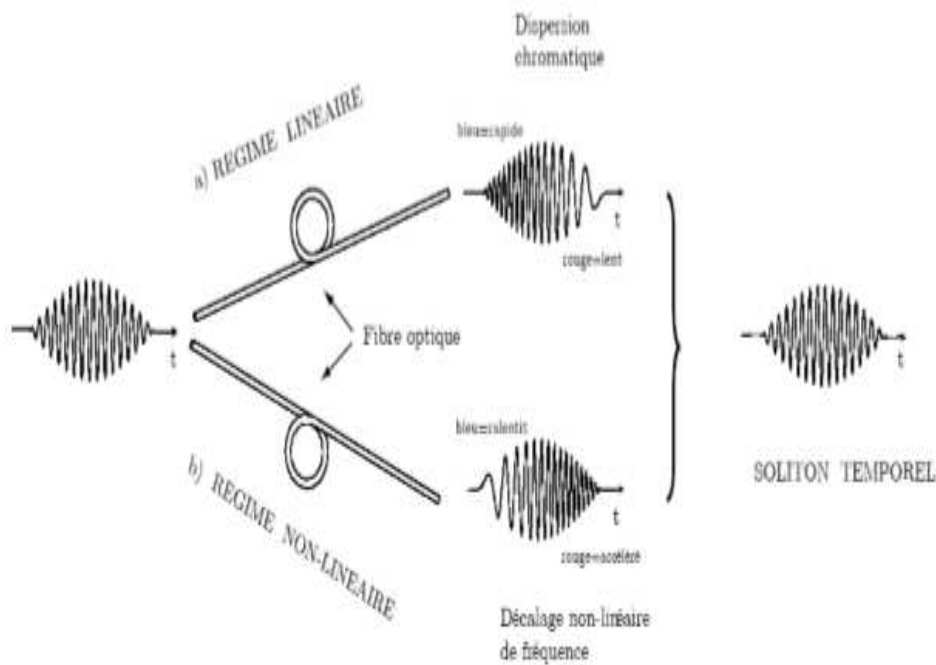


Figure 7: : Schematic diagram of soliton propagation in fibers. The non-linearity of the fiber produces a frequency drift that exactly compensates the one produced by the dispersion. The soliton pulse propagates without deformation

[158].

shift can compensate for the effect of dispersion. It is undoubtedly thanks to guided optics, especially in optical fibers, that this property has not remained a curiosity of academic interest. In spite of a very low nonlinearity, the low propagation losses in optical fibers allow to obtain important cumulative nonlinear phase shifts and thus to explore this field of propagation in the soliton regime. Solitons themselves constitute an information transport vector operating at high rates and over very large distances. Moreover, the signal is no longer a relatively passive vector of information. An exact solution to

NLS equation can be given in the following form:[159]

$$A(z, t) = N\sqrt{P_0} \operatorname{sech}\left(\frac{t}{\delta_0}\right) \exp\left(\frac{iP_0 z}{2\gamma}\right), \quad (\text{I.30})$$

where N is the order of the soliton given by:

$$N^2 = \frac{L_d}{L_{nl}} = \frac{\gamma P_0 \delta_0^2}{|\beta_2|}. \quad (\text{I.31})$$

This dimensionless parameter measures the relative importance of dispersive and non-linear effects. The peak power to generate the fundamental soliton ($N = 1$) is determined by $L_d = L_{nl}$, given by:

$$P_0 = \frac{|\beta_2|}{\gamma \delta_0^2}. \quad (\text{I.32})$$

Only the fundamental temporal soliton ($N = 1$) propagates without deformation. All the other higher-order solitons ($N > 1$) undergo a recurrent deformation motion during their propagation. Therefore, the fundamental temporal soliton is very attractive for the transmission of information in optical communication systems. It can be excited in an optical fiber for very low power levels available with laser diodes. For example, for a dispersion shifted fiber ($|\beta_2| \approx 1 \text{ps/km}$), at wavelength $\lambda_0 = 1.55 \mu\text{m}$, with $\gamma = 3\omega^{-1} \text{km}^{-1}$ and for $\delta_0 = 10 \text{ps}$, we obtain the following peak power $P_0 = 3.3 \text{mW}$. It is worth noting the invariant character of the intensity and the great stability of the solitonic pulse, in particular, its temporal width, during propagation. This invariance of the pulse has made it the ideal candidate for very high speed trans-oceanic transmissions. We are at the heart of the technique of transmission by temporal solitons [161]. Thus, the possibility of self-compensation of the two effects during the namely, propagation, chromatic dispersion and phase self-modulation (a direct consequence of the Kerr effect), will make it possible to escape from the logic specific to the design of these systems, for which propagation is treated as a penalizing but unavoidable phenomenon. The particular temporal soliton impulse guaranteeing this ideal equilibrium is the key.

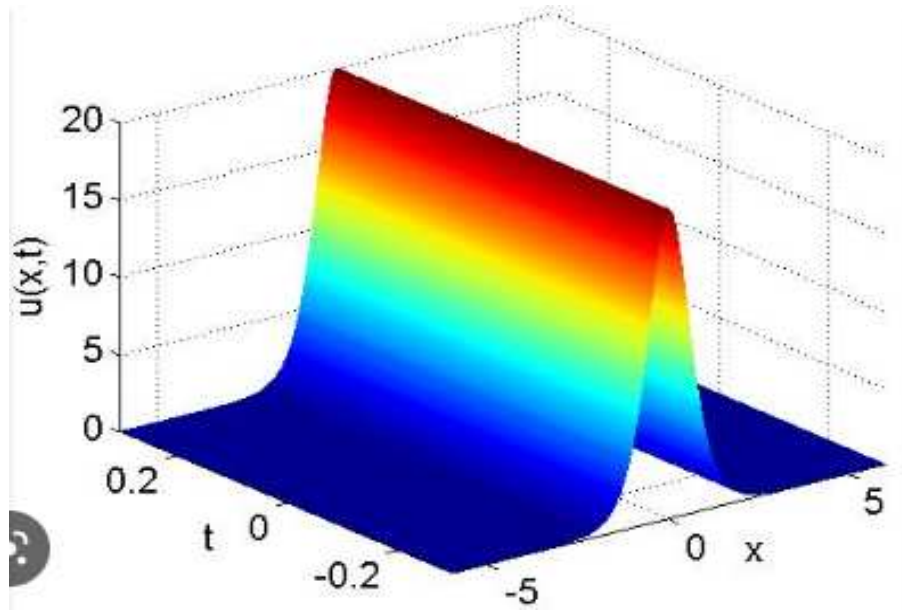


Figure 8: : Modeling of soliton propagation in a nonlinear medium [160].

The spatial solitons

Spatial solitons correspond to optical beams whose natural diffraction has been exactly compensated by the nonlinear effect of the intensity-sensitive propagation medium. The lensing effect, optically induced by the index modification, will allow the beam to self-focus during propagation. When the self-focusing exactly counterbalances the beam broadening due to natural diffraction, observation of a spatial soliton will be possible. Two simple concepts help to understand the formation of a spatial soliton. A geometric model of the self-induced guide: a beam of limited width propagates by obeying the laws of diffraction characterized by the Rayleigh length :

$$L_d \approx r/\theta_D \approx \Pi n_0 r^2 / \lambda, \quad (\text{I.33})$$

where r is the radius of the aperture, n_0 the linear index of refraction and λ , the optical wavelength. This is the propagation length after which the beam diameter has been doubled. In the case where a medium of positive nonlinearity is placed to the right of the aperture, the beam induces an increase in index, proportional to the intensity. The

critical angle of total reflexion between the two media, $\theta_c = \sqrt{2\Delta n/n_0}$, allows one to define a characteristic self-focusing length in the small angle approximation :

$$L_{NL} = r/\theta_c = r/\sqrt{2\Delta n/n_0}. \quad (\text{I.34})$$

A spatial soliton corresponds to a balance between diffraction and self-focusing, i.e., verifying the equality: $L_D = L_{NL}$, leading to $\theta_D = \theta_C$. Compared to temporal solitons, spatial solitons exploit the nonlinearity of massive, or planar, materials over much shorter propagation distances on the order of centimeters. Since the accumulation of nonlinear effect is no longer feasible (compared to the lengths of the optics fibres), high powers from pulsed laser sources were necessary in order to generate the first spatial solitons, namely the Kerr solitons. It is also conceivable to use materials exhibiting a stronger nonlinear response. As such, considerable efforts on material improvement have been made. Since then, the demonstration of photo-refractive space solitons using low power continuous sources and even using white sources (incandescent lamp) has revolutionized this field of research. The physics of spatial solitons remains richer because, due to the difference with temporal solitons, trapping occurs in one or two transverse dimensions and in nonlinear materials of different types. The spatial soliton is all the more fascinating because it has different aspects, which find no equivalent in its temporal counterpart, e.g., the self-focusing in 1D configuration, spirality [181], the existence of optical vortices, the formation of complex patterns or localized structures in cavities, all of which can be observed thanks to stable 2D configurations. These multiple aspects of spatial solitons have greatly stimulated interest in this field of research, as evidenced by the flourishing number of results published over the last decade or so. Briefly, we will describe some key examples from this field of research to illustrate the richness of these phenomena, both in the variety of physics exploited and in the particular configurations thanks to which, it is possible to envisage a large number of applications.

Spatio-temporal solitons

At the cross roads of spatial and temporal solitons, space-time solitons add to the already rich diversity of solitons. The propagation of an intense, focused optical pulse is governed by the interplay between diffraction, group velocity dispersion and the different nonlinear processes present. Under certain conditions, the nonlinearities can be used to compensate for both diffraction and group velocity dispersion, and thus, simultaneously produce a soliton in space and time. A (2+1)-D invariant propagation could thus be conceivable, in a saturating nonlinear medium, with the addition of a time dimension. Beyond their scientific interest, these real "light bullets" constitute a source of potential applications, in particular in all-optical information processing (ultrafast switching, trajectory control, logic operations) in three dimensions [162]. To succeed in meeting such a scientific challenge, i.e., to generate a stable and localized (energy finished) space-time soliton, the following conditions must be met: self-focusing nonlinearity, anomalous dispersion, one or two processes that can prevent a collapse of the pulse (saturating nonlinearity, for example). At this stage of research, some work is directed toward materials with quadratic properties to benefit from saturating nonlinearity. This field of research is in full expansion, since the very first space-time soliton observation was made by Liu et al. [163] in 1999, on a single transverse dimension, exploiting a quadratic process.

I.8 Different types of optical solitons according to their physical origin

The three types of solitons mentioned above (temporal, spatial and spatiotemporal) can be created by various nonlinearities, laser sources and structures. This diversity has generated the creation of different categories of solitons from their physical origin such as: Kerr solitons, solitons in liquid crystals, quadratic solitons, cavity solitons or photorefractive solitons (Bragg solitons).

I.8.1 Kerr solitons

Kerr soliton physics relies on an ideally local (spatial locality) and instantaneous (temporal locality) modification of the refractive index, linearly proportional to the optical intensity, which is reflected by the relation:

$$\Delta n = n_2 I. \quad (\text{I.35})$$

This is referred to as optical Kerr effect by analogy with the traditional electro-optical Kerr effect for which, the refractive index can vary proportionally to the intensity of a static electric field. The microscopic origin of such an effect lies in an induced anisotropy of the polarizability of the medium. It can be electronic (deformation of the peripheral electronic cloud of atoms or molecules), molecular (reorientation of an anisotropic molecule). If we can consider that one of the first observations of solitonic phenomena in optics was that of Garmire et al. [164], its 2D character and the use of a Kerr medium did not allow the stabilization of the propagation, as we have already explained. This is why it was necessary to wait until 1985 and the ingenuity of Barthlemy, Maneuf and Froehly, from the Institute of Research in Optical and Microwave Communications (IRCOM, Limoges), to demonstrate the propagation of a spatial soliton in a Kerr medium. The authors succeeded in fact to be deleted the modulational instability transverse dimension of the 1D soliton - in practice, a laser beam with a strongly elliptical envelope - and thus show its existence despite the absence of frustration of one of the transverse dimensions. To do this, the beam, localized along the soliton dimension (minor axis of the ellipse), was modulated by interference bands along the homogeneous transverse dimension (major axis of the ellipse corresponding to an L_D diffraction length much greater than the length of the medium). By ensuring that the power contained in each bright fringe did not exceed P_{cr} , the modulation instability was inhibited. Following the other dimension, a soliton propagation then became observable over several diffraction lengths, the approximation of a 1D propagation having been realized.

I.8.2 Solitons in liquid crystals

Liquid crystals are also a worthy medium for solitons. The modification of the refractive index, in this type of material, occurs either by molecular reorientation under the effect of an applied electric field, or by thermo-optical effect. The nonlinearity here is nonlocalized and saturating. The experimental observation of a 2D soliton in a liquid crystal was obtained by Karpierz [165]. Soliton interactions in this material have been studied by Chen [166]. The propagation of this kind of soliton over lengths of the order of centimeters was observed by Hutsebaut et al [167].

I.8.3 Solitons in fiber Bragg gratings

Solitons in fiber Bragg gratings (Gap solitons) are optical nonlinear bands, realized by the balance between nonlinearity and dispersion of the FBG, such that the periodicity of the refractive index creates a photonic band gap whose light cannot propagate in this area. In the presence of nonlinear Kerr effect, the intensity of the light waves modifies the nonlinear refractive index to create a shift of the wave toward the forbidden region (into the Gap) and allows the propagation of a pulse, called a gap soliton. Sipe and De Sterke showed that the propagation of these solitons is described by the standard nonlinear Schrödinger (NLS) equation, which can be derived from the coupled-mode equations, supplemented with terms representing the nonlinear contribution to the propagation (self-phase and intermodulation). Bright solitons that propagate without deformation can therefore exist in the normal fiber dispersion regime, since the lattice dispersion overrides the material dispersion [169]. When the nonlinear response of the fiber is taken into account, wave propagation in FBGs is profoundly modified. Soliton solutions can exist at frequencies close to, but outside the band gap. Moreover, solitary wave structures can still propagate in the so-called Gap soliton band gap. In the following sections, we will present these "Gap solitons" as pulse propagation in the band gap then, characterize these soliton waves and finally solve the equation with coupled modes in the band gap and outside this band to find the Bragg solitons [170].

I.9 Conclusion

In this chapter, we have presented a general study on optics fibers and then, we have talked about Bragg gratings and we can say that they are components present in telecommunication systems. They are ideal when used in combination with fiber lasers, fiber amplifiers or laser diodes. In addition, their high flexibility and design make them very interesting for user-specific applications, such as gain equalization or chromatic dispersion compensation. Their high spectral efficiency makes them the almost unique solution for very low channel spacing, and even for future high capacity systems requiring control, such as dispersion . Finally, we have closed this chapter on solitons, whose discovery has been of considerable benefit to the scientific community, in that it has allowed to explain several phenomena that were previously poorly understood. Thus, after several attempts to explain the translation wave that John Scott Russell had to observe, researchers finally discovered that the soliton phenomenon arises from a delicate balance between two effects including nonlinearity and medium dispersion. These effects are essentially the self-phase modulation and the anomalous dispersion. We have seen that the soliton can be either temporal or spatial or both. Indeed, if the refractive index of the medium is modified by the intermediary of the light, it is then possible, in certain circumstances, to suppress the temporal or spatial broadening of the pulse. We speak then of temporal soliton in the case of compensation of chromatic dispersion and spatial soliton in the neutralization of beam diffraction. When we manage to eradicate both dispersion and diffraction, we speak of space-time soliton. Besides the conservative solitons, there are solitons in dissipative systems. In this case, in addition to the balance between dispersion and nonlinearity, the nonlinear losses and gains must be compensated. The study of dissipative time-domain solitons has been of great interest both for fundamental science and for high-speed optical telecommunications.

MODEL AND METHODOLOGY

II.1 Introduction

Over time, we find that most of the work done on the optical fiber uses optical solitons as a transfer wave, preferably nonlinear. This may be due to the fact that the solitons are almost complete waves seen as degree of reliability in the field. Transport of the message from one point to another without change or deformation that is, in a few words, why many researchers have embarked on the study of this wave, but the researchers have not stopped to propagate the wave just in the bands allowed. We realized that there were magnificent results when we propagated the wave in the forbidden bands of light. This is where the term "gap soliton" comes, from which was materialized by the coupled mode equations. The method of solving torque mode equations was first proposed and used by Christodoulides and Joseph [171], in the case where the injected waves exactly satisfy the Bragg condition, that is, when their frequency is at the center of the linear band gap. Aceves and Wabnitz then extended the method to search for solutions corresponding to all frequencies [172] or all wavenumbers [173] within.

In order to improve the previous research, we have considered nonparaxial approximation to the nonlinear coupled mode equations. This model has been illustrated for the first time in this thesis. To derive this model, we have used certain method such as slowly varying envelope approximation, which allowed us to include the parameter of nonparaxiality in the nonlinear coupled mode equation in (2+1)D. Thereafter, we derived this equation using mathematical methods, such as multiple scales and numerical method, namely, the split-step Fourier method, leading to a nonparaxial equation. The MI gain spectrum has been derived in the first part, we present the light pulses in the

FBG. In the second part of our chapter, we review some analytical methods that will be useful in deriving our model equation in nonparaxial regime. Finally, in the third part, we will describe the numerical methods which have made numerical simulations possible.

II.2 The nonlinear nonparaxial coupled mode equation

II.2.1 Propagation of light pulses in fiber Bragg gratings

The propagation of electromagnetic radiation in FBG is governed by the wave equation obtained from Maxwell's equations, which describe the fundamental laws for the electric field \vec{E} , electrical displacement \vec{D} , the magnetic field \vec{H} , and magnetic induction \vec{B} interacting with the environment [174, 176]:

$$\vec{\nabla} \cdot \vec{D} = 0, \quad (\text{II.1})$$

$$\vec{\nabla} \times \vec{E} = -\frac{\partial \vec{B}}{\partial t}, \quad (\text{II.2})$$

$$\vec{\nabla} \cdot \vec{B} = 0, \quad (\text{II.3})$$

$$\vec{\nabla} \times \vec{H} = \frac{\partial \vec{D}}{\partial t}. \quad (\text{II.4})$$

By combining these equations, we obtain, in the time domain:

$$\Delta \vec{E} = \frac{1}{c^2} \frac{\partial^2 \vec{D}}{\partial t^2}, \quad (\text{II.5})$$

Equation Eq.(II.5) can be rewritten as :

$$\frac{\partial^2 \vec{E}}{\partial z^2} + \frac{\partial^2 \vec{E}}{\partial x^2} - \frac{n^2}{c^2} \frac{\partial^2 \vec{E}}{\partial t^2} = \mu_0 \frac{\partial^2 \vec{P}_{NL}}{\partial t^2}. \quad (\text{II.6})$$

The parameter $c = \frac{1}{\sqrt{\mu_0 \epsilon_0}}$ is the speed of light in vacuum with permeability μ_0 and permittivity ϵ_0 . In a waveguide grating, the electrical field \vec{E} is confined in only one transverse direction (y), and it diffracts in the transverse direction (x), with a Bragg resonant periodic structure in the direction of propagation (z). In fact, the linear part $n(x, z)$ of the refractive index is a periodic perturbation in z given by:

$$n^2(x, z) \approx \bar{n}^2(x) + 2\epsilon \bar{n}(x) \Delta n(z) \quad (\text{II.7})$$

with $0 < \epsilon \ll \bar{n}(x)$, where its variation from the average index is assumed to be small. Here, $\bar{n}(x) \approx 1$ is the average and

$$\Delta n(z) = n_1 \cos\left(\frac{2\Pi z}{\Lambda_B}\right), \quad (\text{II.8})$$

is the oscillating part, n_1 being the amplitude of the periodic index modulation for a shallow grating. Λ_B is the spatial period (the Bragg modulation period) of the index grating. As it is well known, strong back reflection occurs at the Bragg resonance condition for which the period of $\Delta n(z)$ is chosen to be half that of the carrying plane waves $e^{i(k_B z - \Omega_B t)}$, where $k_B = \frac{\Pi}{\Lambda_B}$ is the Bragg wavenumber, and Ω_B is the Bragg angular frequency. Therefore, if we consider the propagation of a monochromatic field [177] $\vec{E}(x, z, t)$, at the optical frequency Ω close to the Bragg frequency Ω_B , the electric field distribution inside the FBG can be expressed as a sum of two counter-propagating modulated modes under the two-mode approximation:

$$\vec{E}(x, z, t) = U(y) \left(E_+(x, z, t) \exp[i(k_0 x + k_0 z - \Omega t)] + E_-(x, z, t) \exp[-i(k_0 x + k_0 z - \Omega t)] \right) \vec{x}, \quad (\text{II.9})$$

where the envelope functions $E_+(x, z, t)$ and $E_-(x, z, t)$ describe the electric fields in the forward and backward directions, in the slowly varying envelope approximation, \vec{x} is the polarization direction and $U(y)$ is the transverse mode of the fiber. Intensity-

dependent refractive index changes are described by the nonlinear polarization term:

$$\vec{P}_{NL}(x, z, t) = \epsilon_0 \chi^{(3)} |\vec{E}|^2 \vec{E}, \quad (\text{II.10})$$

where $\chi^{(3)}$ is the third-order nonlinear optical susceptibilities.

II.2.2 Paraxial coupled mode theory

In this case, we will just consider a linear susceptibility, without taking the nonlinear polarization into account anyway, and modeling the refractive index of the Fiber Bragg Grating by the expression:

$$n(z) = \bar{n} + \delta_{n(x,z)} \cos(2k_0x) \cos(2k_0z). \quad (\text{II.11})$$

With $k_0 = \frac{\pi}{\Lambda}$, being the spacial frequency. When we use the relationship between the refractive index $n(x, z)$ and the dielectric function $\epsilon(x, z)$, we obtain:

$$\epsilon(x, z) = n^2(x, z). \quad (\text{II.12})$$

Thus, we find that the dielectric function for a Bragg fibre is given by:

$$\epsilon(x, z) = \bar{n}^2 + 2\bar{n}\delta_n \cos(2k_0x) \cos(2k_0z). \quad (\text{II.13})$$

We neglected the terms of order δn^2 , because, in the FBG, $\delta_n \ll \bar{n}$. The development of the dielectric function by the Fourier series gives :

$$\epsilon(x, z) = \hat{\epsilon}_0 + 2\bar{n}\delta_n \cos(2k_0x) \cos(2k_0z), \quad (\text{II.14})$$

$$\hat{\epsilon}_0 = \bar{n}^2. \quad (\text{II.15})$$

The theory of coupled modes states that if the index modulation δ_n is very small, the solution of the nonlinear wave equation takes the form of Eq.(II.9). Introducing Eq.(II.9)

into Eq.(II.6) leads to

$$\begin{aligned}
& \left(\frac{\partial^2 E_+}{\partial z^2} + ik_0 \frac{\partial E_+}{\partial z} - k_0^2 E_- \right) e^{-i(\Omega t - k_0 x - k_0 z)} + \left(\frac{\partial^2 E_+}{\partial z^2} - ik_0 \frac{\partial E_-}{\partial z^2} - k_0^2 E_+ \right) e^{i(\Omega t - k_0 x - k_0 z)} + \\
& \left(\frac{\partial^2 E_+}{\partial x^2} + ik_0 \frac{\partial E_+}{\partial x} - k_0^2 E_- \right) e^{-i(\Omega t - k_0 x - k_0 z)} + \left(\frac{\partial^2 E_+}{\partial x^2} - ik_0 \frac{\partial E_-}{\partial x} - k_x^2 E_+ \right) e^{i(\Omega t - k_0 x - k_0 z)} \\
& - \frac{\bar{n}^2 - 2\bar{n}\delta_n \cos 2k_0 z}{c^2} \left(\frac{\partial^2 E_+}{\partial t^2} - i\Omega \frac{\partial E_+}{\partial t} - \Omega^2 E_+ \right) e^{-i(\Omega t - k_0 x - k_0 z)} \\
& - \frac{\bar{n}^2 + 2\bar{n}\delta_n \cos 2k_0 z}{c^2} \left(\frac{\partial^2 E_-}{\partial t^2} + i\Omega \frac{\partial E_-}{\partial t} - \Omega^2 E_- \right) e^{i(\Omega t - k_0 x - k_0 z)} \\
& - \frac{\bar{n}^2 - 2\bar{n}\delta_n \cos 2k_0 z}{c^2} \left(\frac{\partial^2 E_+}{\partial t^2} - i\Omega \frac{\partial E_+}{\partial t} - \Omega^2 E_+ \right) e^{-i(\Omega t - k_0 x - k_0 z)} \\
& - \frac{\bar{n}^2 + 2\bar{n}\delta_n \cos 2k_0 z}{c^2} \left(\frac{\partial^2 E_-}{\partial t^2} + i\Omega \frac{\partial E_-}{\partial t} - \Omega^2 E_- \right) e^{i(\Omega t - k_0 x - k_0 z)}
\end{aligned} \tag{II.16}$$

All the terms to the non-derivatives and of factor δ_n will cancel, because they are solutions of the unperturbed wave equation. We will assume that the envelopes (E_+ , E_-) change slowly with time and space and more clearly, we will use the following slowly varying envelope approximation:

$$\begin{aligned}
|ik_0 \frac{\partial E_{\pm}}{\partial x}| &\ll \frac{\partial^2 E_{\pm}}{\partial x^2} \\
|i\Omega \frac{\partial E_{\pm}}{\partial t}| &> \frac{\partial^2 E_{\pm}}{\partial t^2} \\
|ik_0 \frac{\partial E_{\pm}}{\partial z}| &\simeq \frac{\partial^2 E_{\pm}}{\partial z^2}
\end{aligned} \tag{II.17}$$

Here, all second derivatives will be neglected. After some algebraic transformations and certain simplifications, we then obtain:

$$\begin{aligned}
& \left(\frac{\partial^2 E_+}{\partial z^2} + i\left(\frac{\bar{n}}{c} \frac{\partial E_+}{\partial z} + \frac{\partial E_+}{\partial t}\right) + \kappa E_- + \frac{\partial^2 E_+}{\partial x^2} + \kappa E_+ e^{2ik_0 z} \right) e^{-i(\Omega t - k_0 x - k_0 z)} = 0, \\
& \left(\frac{\partial^2 E_-}{\partial z^2} - i\left(\frac{\bar{n}}{c} \frac{\partial E_-}{\partial z} - \frac{\partial E_-}{\partial t}\right) + \kappa E_+ + \frac{\partial^2 E_-}{\partial x^2} - \kappa E_- e^{2ik_0 z} \right) e^{-i(\Omega t + k_0 x + k_0 z)} = 0.
\end{aligned} \tag{II.18}$$

with, $\frac{\bar{n}}{c} = c_g$. The problematic terms are those with $e^{\pm 2ik_0 z}$. These terms, however, can be neglected because they have little effect on $\pm E$. We are interested in light at frequencies around Ω , with the corresponding spatial frequency k_0 . Since we assume that the envelope changes slowly, one can imagine that the effects of the $k_0 = \frac{\pi}{\Lambda}$ spatial fre-

quency terms can be brought out. This kind of approximation is known as the Rotating Wave Approximation (RWA). So, when we neglect these higher frequency terms and use the plane wave orthogonality, we finally obtain the linear coupled mode equations (LCMEs):

$$\begin{aligned} \frac{\partial^2 E_+}{\partial z^2} + i\left(\frac{\partial E_+}{\partial T} + c_g \frac{\partial E_+}{\partial z}\right)(T, x, z) + \frac{\partial^2 E_+}{\partial x^2}(t, x, z) + \kappa E_- &= 0, \\ \frac{\partial^2 E_-}{\partial z^2} + i\left(\frac{\partial E_-}{\partial T} - c_g \frac{\partial E_-}{\partial z}\right)(T, x, z) + \frac{\partial^2 E_-}{\partial x^2}(t, x, z) + \kappa E_+ &= 0. \end{aligned} \quad (\text{II.19})$$

In the spectral domain, the coupled mode equations are written as follows:

$$\begin{aligned} -i\frac{\partial^2 \widetilde{E}_+}{\partial z^2}(x, z, \omega) + \frac{\partial \widetilde{E}_+}{\partial z}(x, z, \omega) + \frac{\partial \widetilde{E}_+}{\partial x}(x, z, \omega) &= iq(\omega)\widetilde{E}_+(x, z, \omega) + i\kappa\widetilde{E}_-(x, z, \omega), \\ -i\frac{\partial^2 \widetilde{E}_-}{\partial z^2}(x, z, \omega) - \frac{\partial \widetilde{E}_-}{\partial z}(x, z, \omega) + \frac{\partial \widetilde{E}_-}{\partial x}(x, z, \omega) &= iq(\omega)\widetilde{E}_-(x, z, \omega) + i\kappa\widetilde{E}_+(x, z, \omega), \end{aligned} \quad (\text{II.20})$$

$$q(\omega) = c_g \Omega = \beta(\omega) - \beta_\beta$$

$$\text{and} \quad (\text{II.21})$$

$$\Omega = \omega - \omega_\beta$$

II.2.3 Relation of linear dispersion

In this paragraph, we will search for continuous solutions of frequency ω to the linear coupled mode Eq.(II.19). For that, we will first of all consider the following equations [178]:

$$\widetilde{E}_+(x, z) = f_1 e^{i(K_z z + K_x x)} + f_2 e^{-i(K_z z + K_x x)}, \quad (\text{II.22})$$

$$\widetilde{E}_-(x, z) = b_1 e^{i(K_z z + K_x x)} + b_2 e^{-i(K_z z + K_x x)}, \quad (\text{II.23})$$

where the constant coefficients f_1, f_2, b_1, b_2 are determined by the initial conditions and where $K(\Omega)$ is the contribution of the network to the propagation constant. Introducing this solution into the coupled Eq.(II.19), we see that the constant coefficients satisfy the

following relations:

$$\begin{aligned}
(K_z + K_x - q)f_1 &= \kappa b_1, \\
(K_z + K_x + q)b_1 &= \kappa f_1, \\
(K_z + K_x - q)f_2 &= \kappa f_2, \\
(K_z + K_x + q)f_2 &= -\kappa b_2.
\end{aligned} \tag{II.24}$$

For the system Eq.(II.19) to have non-trivial solutions, it is necessary that K verifies the following dispersion relation:

$$K_z + K_x = \pm \sqrt{q^2 - \kappa^2} \Rightarrow \Omega(K_z + K_x) = \pm \frac{c}{n} \sqrt{\kappa^2 + K_z^2 + K_x^2}. \tag{II.25}$$

The shape of this relation is shown in Figure (9). Obviously, this equation has only one band gap at which is centered at $\Omega = 0$, and its width is given by $\Delta\Omega = 2\kappa \frac{c}{n} = \frac{\Pi\delta_n c}{n^2\Lambda}$ (see figure 9). In the particular case where only the traveling wave propagates initially in the grating, we can easily calculate the solution in the time domain by inverse Fourier transform of the solution Eq.(II.24) and Eq.(9). On the basis of the relations Eq.(II.26) and the following relations Eq.(II.27)

$$\begin{aligned}
E_+(x, z, t) &= f_1 e^{i(k_z + k_x - \Omega t)}, \\
E_-(x, z, t) &= r(K) f_1 e^{i(k_z + k_x - \Omega t)}.
\end{aligned} \tag{II.26}$$

Then, $|r(K)|^2$ which expresses the amount of energy that is transferred from the progressive wave to the regressive wave, reflected by the Bragg grating, is given by

$$r(K) = \frac{K - q}{k} = -\frac{k}{K + q}. \tag{II.27}$$

In Figure (10), we present, as an illustration, the reflection characteristic of a FBG, which has become a standard fiber component in fiber optic telecommunication systems. This function is obtained by solving the linear coupled equations in the frequency domain

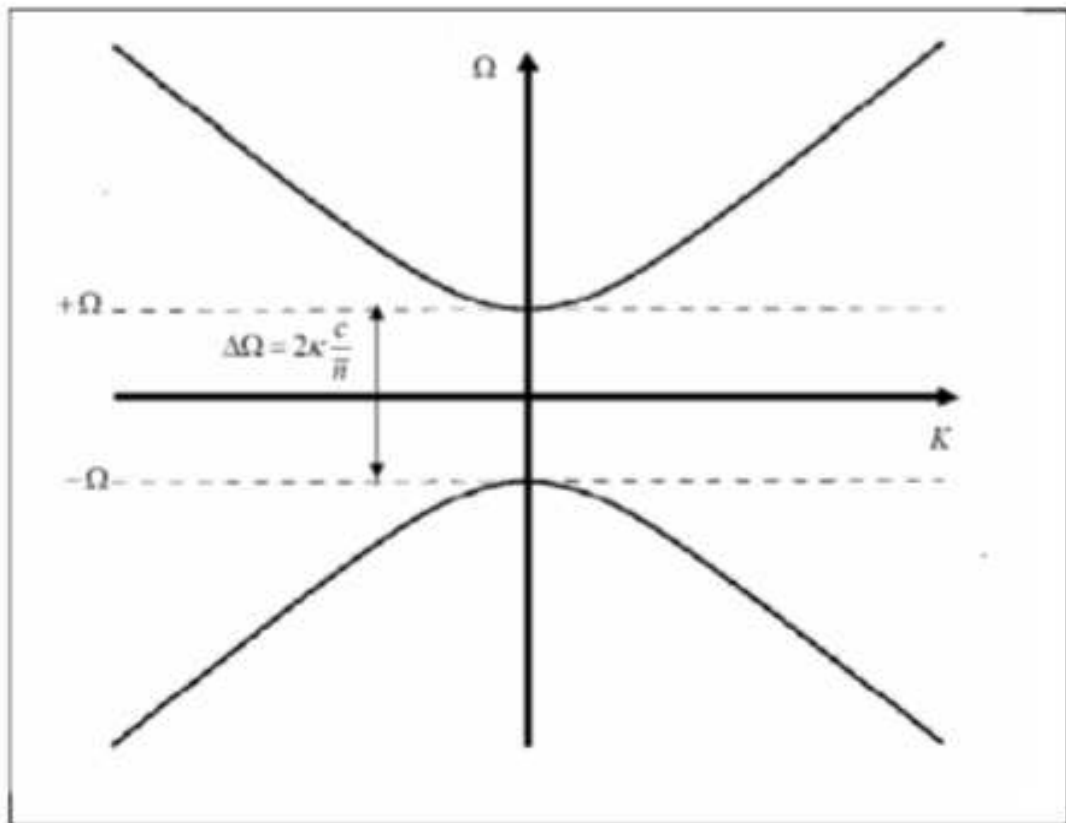


Figure 9: Dispersion relationship showing a periodic Bragg grating band [179].

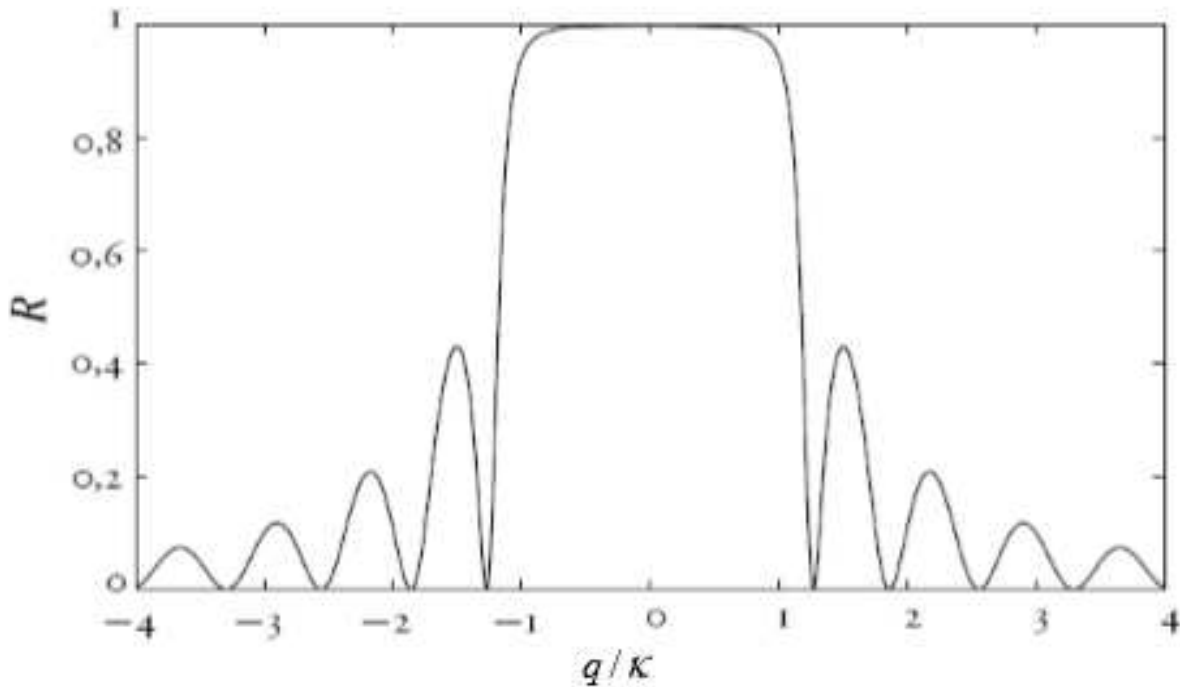


Figure 10: Intensity reflectivity of a fibered Bragg grating, whose parameters are: length $L = 8\text{mm}$ and $\kappa = 5\text{cm}^{-1}$ or $\delta_n \approx 10^{-6}$ if the length of Bragg $\lambda_\beta = 1550\text{nm}$. The maximum reflectivity $\max R$ can reach values higher than 95, when $\kappa L \geq 2$, and is ≈ 100 ($\kappa L = 4$) [180].

from appropriate initial conditions [181]. We observe that the reflection of a finite grating is very large and relatively uniform over a range of reduced frequencies 2κ , corresponding to the width of the band gap. The waves, at the wavelength Λ_β , but also at neighboring wavelengths undergo the Bragg reflection. The global reflectivity R of the FBG is all the higher that the length L of the network or the variation of index δ_n is big. Moreover, it can be shown that the range of wavelengths (or frequencies) affected by the grating, which is proportional to κ , widens when the modulation depth δ_n increases. δ_n thus appears to be a measure of the efficiency of the FBG to reflect the energy of a wave injected into it, i.e. to transmit the energy of a progressive wave towards a regressive wave. The description of the properties of FBGs has so far been limited to the linear effects of light-matter interaction. When the nonlinear response of the fiber is taken into account, the wave propagation in FBGs is deeply modified.

II.2.4 Theory of nonlinear coupled modes

The theory of coupled modes has the simplicity that it can easily be extended for nonlinear systems. We start from the nonlinear propagation Eq. (II.6) knowing that \vec{E} and \vec{P} are odd vectors under inversion symmetry. The second degree coefficient $\chi^{(2)}$, must vanish in any material, because the second order microscopic susceptibility tensors are randomly directed and mean-compensating, which cancels the macroscopic susceptibility tensor $\chi^{(2)}$. We further assume a weak nonlinearity. So, we consider only the main nonlinear term of order 3, that is, $\chi^{(3)}$. With this assumption, the nonlinear polarization will be simplified as given in the first paragraph of this chapter. Using this nonlinear polarization, we arrive at the nonlinear wave equation:

$$\frac{\partial^2 \vec{E}(x, z, t)}{\partial x^2} + \frac{\partial^2 \vec{E}(x, z, t)}{\partial z^2} - \frac{\epsilon(z, x)}{c^2} \frac{\partial^2 \vec{E}(x, z, t)}{\partial t^2} = \frac{\chi^{(3)}}{c^2} \frac{\partial^2 \vec{E}^3(x, z, t)}{\partial t^2}. \quad (\text{II.28})$$

The second member of this equation can be put in the following form:

$$\frac{\chi^{(3)}}{c^2} \frac{\partial^2 \vec{E}^3(x, z, t)}{\partial t^2} = \frac{\chi^{(3)}}{c^2} \left(\vec{E}^2 \frac{\partial^2 \vec{E}(x, z, t)}{\partial t^2} + 2 \vec{E}(x, z, t) \left(\frac{\partial \vec{E}(x, z, t)}{\partial t} \right)^2 \right). \quad (\text{II.29})$$

Inserting the ansatz Eq.(II.9) into the Eq.(II.28) yields many terms, but since we assume the weak nonlinearity and the approximation of the slowly varying the slowly varying envelope Eq.(II.29), we obtain the equation:

$$\frac{3\chi^{(3)}\omega_0^2}{c^2} [(|E_+|^2 E_+ + |E_-|^2 E_+) e^{-(\Omega t - k_x z - k_0 x)} + (2|E_+|^2 E_- + |E_-|^2 E_-) e^{-(\Omega t + k_0 z + k_0 x)}]. \quad (\text{II.30})$$

By putting together the two equations, Eq.(II.30) and Eq.(II.19), finally, we find the nonlinear equations of coupled modes:

$$\begin{aligned} \frac{\partial^2 \vec{E}_+}{\partial z^2} + i \left(\frac{\partial}{\partial T} + c_g \frac{\partial}{\partial z} \right) E_+(T, x, z) + \kappa E_- + \frac{\partial^2 \vec{E}_+}{\partial x^2} + \Gamma (|E_+|^2 + 2|E_-|^2) E_+ &= 0, \\ \frac{\partial^2 \vec{E}_-}{\partial z^2} + i \left(\frac{\partial}{\partial T} - c_g \frac{\partial}{\partial z} \right) E_-(T, x, z) + \kappa E_+ + \frac{\partial^2 \vec{E}_-}{\partial x^2} + \Gamma (|E_-|^2 + 2|E_+|^2) E_- &= 0, \end{aligned} \quad (\text{II.31})$$

with the nonlinear coupling coefficient $\Gamma = \frac{3\chi^{(3)}\omega_0^2}{c^2}$ and $\kappa = \frac{\omega_0 \delta n}{2c}$. The nonlinear terms with 2 in front of them is called cross-phase Modulation and the other is called auto-phase modulation.

II.2.5 On the Townes soliton

We consider the following NLS equation:

$$i\psi_\tau(\tau, x, y) + \Delta y + |\psi|^2 \psi = 0, \quad (\text{II.32})$$

we will take;

$$\psi(\tau, r) = \exp^{i\tau} R(r), \quad (\text{II.33})$$

when we replace Eq.(II.33) in Eq.(II.32) we obtain:

$$i \frac{\partial \exp^{i\tau}}{\partial \tau} R(r) + \Delta \exp^{i\tau} R(r) + \exp^{i\tau} |R|^{2\sigma} R = 0. \quad (\text{II.34})$$

Translating the Laplacian into a spherical coordinate we obtain :

$$i \times i R(r) + \left(\frac{\partial^2}{\partial r^2} + \frac{1}{r^2} \frac{\partial^2}{\partial \theta^2} + \frac{1}{r^2} \frac{\partial}{\partial r} \right) R(r) + \exp^{i\tau} |R|^{2\sigma} R = 0, \quad (\text{II.35})$$

with $\Rightarrow \sigma = 1$ we arrive at

$$-R(r) + \left(\frac{\partial^2}{\partial r^2} + \frac{1}{r} \frac{\partial}{\partial r} \right) R(r) + R^3 = 0, \quad (\text{II.36})$$

this equation, can still be written :

$$\Delta R - R + R^3 = 0. \quad (\text{II.37})$$

The reader can see the sketch of the behavior of the Townes soliton on the figures below; [183], in the first proposition when $\epsilon/k \ll 1$, the self-focusing of the lowest term is reduced to :

$$L_{\tau\tau}(\tau) = -\frac{\beta}{L^3}, \quad (\text{II.38})$$

$$\beta_{\tau}(\tau) = -\frac{\epsilon}{k} CG_S \frac{N_c}{2M} \left(\frac{1}{L^2} \right)_{\tau}, \quad (\text{II.39})$$

$$N_c = \int R^2 r dr \approx 1, 86, \quad (\text{II.40})$$

$$M = \frac{1}{4} \int r^2 R^2 r dr \approx 0, 55. \quad (\text{II.41})$$

II.3 Analytical method

In this section, we will illustrate the different methods analytical used for the solution of our nonlinear non-paraxial coupled equation. So, we will first start with the multiple space and time method that which will allow us to reduce the nonlinear non paraxial

coupled mode equation to a 2D NLS. In a second step, we will study the modulational instability (MI) of plane waves on this equation.

II.3.1 The Method of Multiple Scales

Any asymptotic expansion of must equations simultaneously describe the decreasing and oscillatory behavior of the solution, in order to be uniformly valid in $t = O(1/\epsilon^\kappa)$. The Poincaré-Lindstedt method is a method that is close to this one, but it cannot provide better results than the multiple time and space method. The Poincaré-Lindstedt method provides a way to construct asymptotic approximations of periodic solutions, but it cannot be used to obtain solutions that evolve aperiodically on a slow time scale. The multiple scale method is a more general approach that involves two key tricks. The first is the idea of introducing scaled spatial and temporal coordinates to capture the slow modulation of the pattern, and treating them as separate variables in addition to the original variables that must be retained to describe the state of the pattern itself. This is essentially the idea of multiple scales. The second is the use of what are called solvability conditions in the formal derivation. We note from the analytical solution, that the functional dependence of x on t and ϵ is not disjoint, because x depends on the combination of ϵt as well as on individual t and ϵ . Thus, instead of $x = x(t; \epsilon)$, we write $x = \widehat{x}(t, \epsilon t, \epsilon)$. We return to the regular expansion and rewrite it as $x(t) = \cos t + \epsilon \sin t - \epsilon t \cos t$ [184]. As in the case of analytical solution, regular expansion also shows that x depends on the combination of ϵt as well as on the individual t and ϵ . The trouble with the naive regular expansion is that the small damping changes both the amplitude of the oscillation on a time scale ϵ^{-1} and the phase of the oscillation on a time scale ϵ^{-2} by the slow accumulation of small effects. Thus, the oscillator has three processes acting on their on time scales. First, there is the basic oscillation on the time scale of 1 from the inertia causing the restoring force to overshoot the equilibrium position. Then, there is a small drift in the amplitude on the time scale of ϵ^{-1} and finally, a very small drift in the phase on the time scale of ϵ^{-2} due to the small friction. We recognize

these three time scales by introducing three time variables: $T_0 = t$ is the fast time of the oscillation. $T_1 = \epsilon t$ is the slower time of the amplitude drift. $T_2 = \epsilon^2 t$ is even slower time of the phase drift. The rapidly changing features will then be combined into factors which are functions of T_0 , while the slowly changing features will then be combined into factors which are functions of T_1 and T_2 . Thus, we look for a solution of the form $x(t; \epsilon) = x(T_0, T_1, T_2; \epsilon)$. In general, if we choose n time scales for the expansion, we look for a solution of the form $x(t; \epsilon) = x(T_0, T_1, T_2 \dots T_n; \epsilon)$, where the time scales are defined as $T_0 = t, T_1 = \epsilon t, T_2 = \epsilon^2 t \dots, T_n = \epsilon^n t$. Thus, instead of determining x as a function of t , we determine x as a function of T_0, T_1, \dots, T_n . Note that as real time t increases, the fast time T_0 increases at the same rate, while the slower time T_i increase slowly. Using the chain rule, we have

$$\begin{aligned} \frac{d}{dt} &= \frac{\partial}{\partial T_0} \frac{\partial T_0}{\partial t} + \frac{\partial}{\partial T_1} \frac{\partial T_1}{\partial t} + \frac{\partial}{\partial T_2} \frac{\partial T_2}{\partial t} + \dots \\ &= \frac{\partial}{\partial T_0} + \epsilon \frac{\partial}{\partial T_1} + \epsilon^2 \frac{\partial}{\partial T_2} + \dots \end{aligned} \quad (\text{II.42})$$

$$\frac{d^2}{dt^2} = \frac{\partial^2}{\partial T_0^2} + 2\epsilon \frac{\partial^2}{\partial T_0 \partial T_1} + \epsilon^2 \left(\frac{\partial^2}{\partial T_0 \partial T_2} + \frac{\partial^2}{\partial T_1^2} \right) + \dots \quad (\text{II.43})$$

Hence, becomes

$$\frac{\partial^2 x}{\partial T_0^2} + 2\epsilon \frac{\partial^2 x}{\partial T_0 \partial T_1} + \epsilon^2 \left(\frac{\partial^2 x}{\partial T_0 \partial T_2} + \frac{\partial^2 x}{\partial T_1^2} \right) + 2\epsilon \left(\frac{\partial x}{\partial T_0} + \epsilon \frac{\partial x}{\partial T_1} + \epsilon^2 \frac{\partial x}{\partial T_2} \right) + x + \dots = 0 \quad (\text{II.44})$$

$$x = 1,$$

$$\frac{\partial x}{\partial T_0} + \epsilon \frac{\partial x}{\partial T_1} + \epsilon^2 \frac{\partial x}{\partial T_2} + \dots = 0, \quad (\text{II.45})$$

for

$$T_0 = T_1 = T_2 \dots = 0.$$

We note that when $t = 0$, all T_0, T_1 , etc. are zero. The benefits of introducing the multiple time variables are not yet apparent. In fact, it appears that we have made the problem harder since the original ordinary differential equation has been turned into a partial differential equation. This is true, but experience with this method has shown that the

disadvantages of including this complication are far outweighed by the advantages. It should be pointed out that the solution of [184] is not unique and that we need to impose more conditions for uniqueness on the solution. This freedom will enable us to prevent secular terms from appearing in the expansion (at least over the time scales we are using). We now seek an asymptotic approximation for x of the form:

$$x(t) = x(T_0, T_1, \dots, T_n; \epsilon) \sim x_0(T_0, T_1, \dots, T_n) + \epsilon x_1(T_0, T_1, \dots, T_n) + \epsilon^2 x_2(T_0, T_1, \dots, T_n) + \dots \quad (\text{II.46})$$

It must be understood that there are actually only two independent variables, t and ϵ , in Eq.(II.46); T_i are functions of these two, and so is not independent. Nevertheless, the principal steps in finding the coefficients x_n are carried out as though T_0, T_1, \dots, T_n and ϵ were independent variables. This is one reason why these steps cannot be justified rigorously in advance, but are merely heuristic. Secondly, it must Eq.(II.45) enters both through the gauges (which are just the powers of ϵ) and also through the coefficients x_n by way of T_i . Although there is no general theorem allowing the differentiation of a generalized asymptotic expansion term by term, it is nevertheless reasonable to construct the coefficients on the assumption that such differentiation is possible, and then to justify the resulting series by direct error estimation afterwards.

II.3.2 Modulational instability phenomenon

Modulation instability (MI) implies that an intense CW beam can be converted into a train of pulses as it passes through a fiber array. Experimental observation of this phenomenon is difficult when a CW beam is used because the input power required is too large to be realistic. MI is a ubiquitous phenomenon in physics, corresponding to the growth of a weakly modulated continuous wave in a nonlinear medium and leading to the generation of a periodic wave train of large amplitude. In space, it transforms weakly modulated plane waves into spatially periodic patterns. In the frequency domain, MI is the result of energy transfer from a strong single spectral component to

sidebands. While the linear stability analysis predicts a limited band of unstable modulation frequencies, recent developments, based on nonlinear theory, have revealed the existence of MI beyond this limited frequency range. These experimental studies are the first experimental demonstrations of the "extraordinary" phenomenon of MI. Realized at the same time in optics and in hydrodynamics, they clearly underline the interdisciplinarity of this process. For the illustration, we consider the non-paraxial equation

$$\frac{\partial A}{\partial \xi} = \frac{i}{2} \frac{\partial^2 A}{\partial S^2} + ia \frac{\partial^2 A}{\partial \xi^2} + i|A|^2 A, \quad (\text{II.47})$$

where s and ξ (x and z) stand for the scaled (unscaled) transverse and longitudinal coordinates, respectively; $\xi = \frac{z}{kx_0^2}$, $s = \sqrt{2} \frac{x}{x_0}$, $A = kx_0 \frac{n_2}{n_0} \phi$. Here, x_0 is arbitrary space width, ϕ is unscaled field envelope, n_2 is Kerr coefficient and a is non-paraxial parameter given by

$$a = \frac{1}{(kx_0)^2}. \quad (\text{II.48})$$

The following study on the propagation stability of non-paraxial beams is based on the linear stability approach. The steady-state solution of Eq.(II.47) is given by:

$$A(s, \Phi) = \sqrt{p_0} \exp(i\Phi_{nl}), \quad (\text{II.49})$$

where the nonlinear phase shift Φ_{nl} is related to the incident power p_0 as

$$\Phi_{nl} = (p_0 - ap^{2_0})\xi. \quad (\text{II.50})$$

To study whether the steady-state solution is stable against small perturbations, we introduce the perturbed field of the form

$$A(s, \xi) = [\sqrt{p_0} + \xi A_1(s, \xi)] \exp[i(p_0 - ap_0^2)\xi] \quad (\text{II.51})$$

where a is a small quantity. By substituting Eq.(II.51) into Eq.(II.47), and neglecting higher-order terms of, we get the linearized equation

$$\begin{aligned} \frac{\partial A_1}{\partial \xi} &= \frac{i}{2} \frac{\partial^2 A_1}{\partial s^2} + ip_0(A_1 + A^*), \\ -\frac{ia}{4} \frac{\partial^4 A_1}{\partial s^4} - i2ap_0 \frac{\partial^2 A_1}{\partial s^2} - i2ap^{2_0}(A_1 + A^*), \end{aligned} \quad (\text{II.52})$$

where $*$ denotes complex conjugate. We assume a general solution of the form:

$$A_1(\xi, s) = c \cos(K\xi - \Omega s) + id \sin(K\xi - \Omega s), \quad (\text{II.53})$$

where K and Ω are the wave number and the frequency of perturbation. Inserting Eq.(II.53) into Eq.(II.52) and separating real and complex parts, we obtain a set of two homogeneous equations for c and d . From the solutions of the dispersion relation, we investigate the stability of the steady-state solutions by determining the MI gain. MI occurs only when at least one of the eigenvalues of the linearized equation possesses a nonzero and negative imaginary part, which results in an exponential growth of the amplitude with the perturbation. MI is measured by the power gain and is defined as

$$G_{\pm} = 2\text{Im}(\Omega_{\pm}) > 0, \quad (\text{II.54})$$

where $\text{Im}(\Omega_{\pm})$ denotes the imaginary part of Ω_{\pm} .

II.4 Numerical method

As the non-paraxial nonlinear Schrödinger equation is generally not easy to solve, with the help of analytical methods, some numerical methods used in this thesis are presented in this section.

II.4.1 Split-step Fourier method

In numerical analysis, the split-step Fourier method is a pseudo-spectral numerical method used to solve nonlinear partial differential equations like the NLS equation. The name arises for two reasons. First, the method relies on computing the solution in small steps, and treating the linear and the nonlinear steps separately (see below). Second, it is necessary to Fourier transform back and forth, because the linear step is made in the frequency domain, while the nonlinear step is made in the time domain. An example of usage of this method is in the field of light pulse propagation in optical fibers, where the interaction of linear and nonlinear mechanisms makes it difficult to find general analytical solutions. However, the split-step method provides a numerical solution to the problem. Another application of the split-step method that has been gaining a lot of attention since the 2010s is the numerical simulation of Kerr frequency comb dynamics in optical microresonators [185]. The relative ease of implementation of the Lugiato-Lefever equation with reasonable numerical cost, along with its success in reproducing experimental spectra as well as predicting soliton behavior in these microresonators has made the method very popular. Consider, for example, the NLS equation:

$$\frac{\partial A}{\partial z} = -\frac{i\beta_2}{2} \frac{\partial^2 A}{\partial t^2} + i\gamma|A|^2 A = [\hat{D} + \hat{N}]A, \quad (\text{II.55})$$

where $A(t, z)$ describes the pulse envelope in time t , at the spatial position z . The equation can be split into a linear part,

$$\frac{\partial A_D}{\partial z} = \frac{i\beta_2}{2} \frac{\partial^2 A}{\partial t^2} = \hat{D}A, \quad (\text{II.56})$$

and a nonlinear part,

$$\frac{\partial A_N}{\partial z} = i\gamma|A|^2 A = \hat{N}A. \quad (\text{II.57})$$

Both the linear and the nonlinear parts have analytical solutions. However, if only a small step h is taken along z , then, the two parts can be treated separately with only a

small numerical error. One can, therefore, first take a small nonlinear step,

$$A_N(t, z + h) = \exp[i\gamma|A|^2h]A(t, z), \quad (\text{II.58})$$

using the analytical solution. The dispersion step has an analytical solution in the frequency domain, so it is first necessary to Fourier transform AD using

$$\widetilde{A}_D(\omega, z) = \int_{-\infty}^{+\infty} A_D(t, z) \exp[i(\omega - \omega_0)t] dt, \quad (\text{II.59})$$

where ω_0 is the center frequency of the pulse. It can be shown that using the above definition of the Fourier transform, the analytical solution to the linear step is

$$\widetilde{A}_D(\omega, z + h) = \exp[i\frac{\beta}{2}(\omega - \omega_0)^2h]A_D(\omega, z). \quad (\text{II.60})$$

By taking the inverse Fourier transform of $\widetilde{A}_D(\omega, z + h)$, one obtains $A_D(t, z + h)$; the pulse has thus been propagated a small step h . By repeating the above N times, the pulse can be propagated over a length of Nh .

The above shows how to use the method to propagate a solution forward in space. However, many physics applications, such as studying the evolution of a wave packet describing a particle, require one to propagate the solution forward in time rather than in space. The nonlinear Schrödinger equation, when used to govern the time evolution of a wave function, takes the form

$$i\frac{\partial\psi}{\partial t} = -\frac{\hbar^2}{2m}\frac{\partial^2\psi}{\partial x^2} + \gamma|\psi|^2\psi = [\widehat{D} + \widehat{N}]A, \quad (\text{II.61})$$

where $\widehat{D} = -\frac{\hbar^2}{2m}\frac{\partial^2\psi}{\partial x^2}$, and $\widehat{N} = \gamma|\psi|^2\psi$, and that, m is the mass of the particle and \hbar is Planck's constant.

The formal solution to this equation is a complex exponential

$$\psi(x, t) = e^{it(\widehat{D} + \widehat{N})\psi(x, 0)}. \quad (\text{II.62})$$

Since \hat{D} and \hat{N} are operators, they do not in general commute.

$$\exp(h\hat{D})\exp(h\hat{N}), \quad (\text{II.63})$$

and

$$\exp(h\hat{N})\exp(h\hat{D}), \quad (\text{II.64})$$

and Strang's formulas :

$$\exp(h\hat{D}/2)\exp(h\hat{N})\exp(h\hat{D}/2), \quad (\text{II.65})$$

and

$$\exp(h\hat{N}/2)\exp(h\hat{D})\exp(h\hat{N}/2). \quad (\text{II.66})$$

Of Lie formulas, follows the Fourier Split-Step method, in which a formal solution is given

$$\begin{aligned} \psi(z+h, t) &= \exp(h(\hat{D} + \hat{N}))\psi(z, t), \\ &\approx \exp(h\hat{D})\exp(h\hat{N})\psi(z, t). \end{aligned} \quad (\text{II.67})$$

The symmetrical Fourier Split-Step method is one of the most widely used pseudo-spectral methods for studying the propagation of pulses in nonlinear and dispersive media [186]. In this method, the propagation length is subdivided into intervals of lengths h . If the value of h is sufficiently low, we can approximate the solution by assuming that along each interval, the operators of dispersion \hat{D} and nonlinear \hat{N} act independently.

From the Strangs formula Eq.(II.65) and Eq.(II.66), the dispersion effects act continuously on the two parts of the length segment h : $[z, z + h/2[$ and $]z + h/2, z + h]$; while the nonlinear effects are inserted at the point $z + h/2$ in the middle of the segment. In this way, the variations of the nonlinear operator \hat{N} in the meantime $[z + h]$ can be overlooked. The formal solution of the amplitude of the variable field $\psi(z + h, t)$ as a function of $\psi(z, t)$, is given by the equation:

$$\psi(z + h, t) = \exp\left(\frac{h\hat{D}}{2}\right) \exp(h\hat{N}) \exp\left(\frac{h\hat{D}}{2}\right) \psi(z, t). \quad (\text{II.68})$$

The dispersion operator, comprising partial time derivatives Eq.(II.67) will be calculated in the spectral domain using the Fourier transforms. The differential operator $\frac{\partial}{\partial t}$ is replaced by $i\omega$ and we calculate each partial derivative of order n as follows: $\frac{\partial^n}{\partial t^n} \xleftrightarrow{F} (i\omega)^n$, where F denotes the Fourier transform. The same calculation principle is applied to the last two terms of the nonlinear operator Eq.(II.68), which represents the Raman effect and which also have time derivatives. However, since N depends on z through $\psi(z, t)$, it is then replaced, along a segment, by its integral which can be approximated using the trapezoid method:

$$\int_z^{z+h} \hat{N}(z') dz' \approx \frac{h}{2} [\hat{N}(z) + \hat{N}(z+h)]. \quad (\text{II.69})$$

Note that $\psi(z + h, h)$ is not known when we want to calculate $\hat{N}(z)$. We must therefore proceed by iterations in order to estimate $\hat{N}(z + h)$ and we have several possibilities for choosing the initial value. This is what will bring us to the proposition and to the study of two implementations. Further, an algorithm based on split-step Fourier method-S is developed for solving NLS equation and the soliton switching is studied in the fiber.

II.4.2 Fourth-order Runge-Kutta method

Runge-Kutta method is a numerical technique used to solve ordinary differential equation of the form:

$$\frac{dy}{dx} = f(x, y), \quad (\text{II.70})$$

with $y(x_0) = y_0$.

Runge-Kutta 4th was first developed to solve first-order ordinary differential equa-

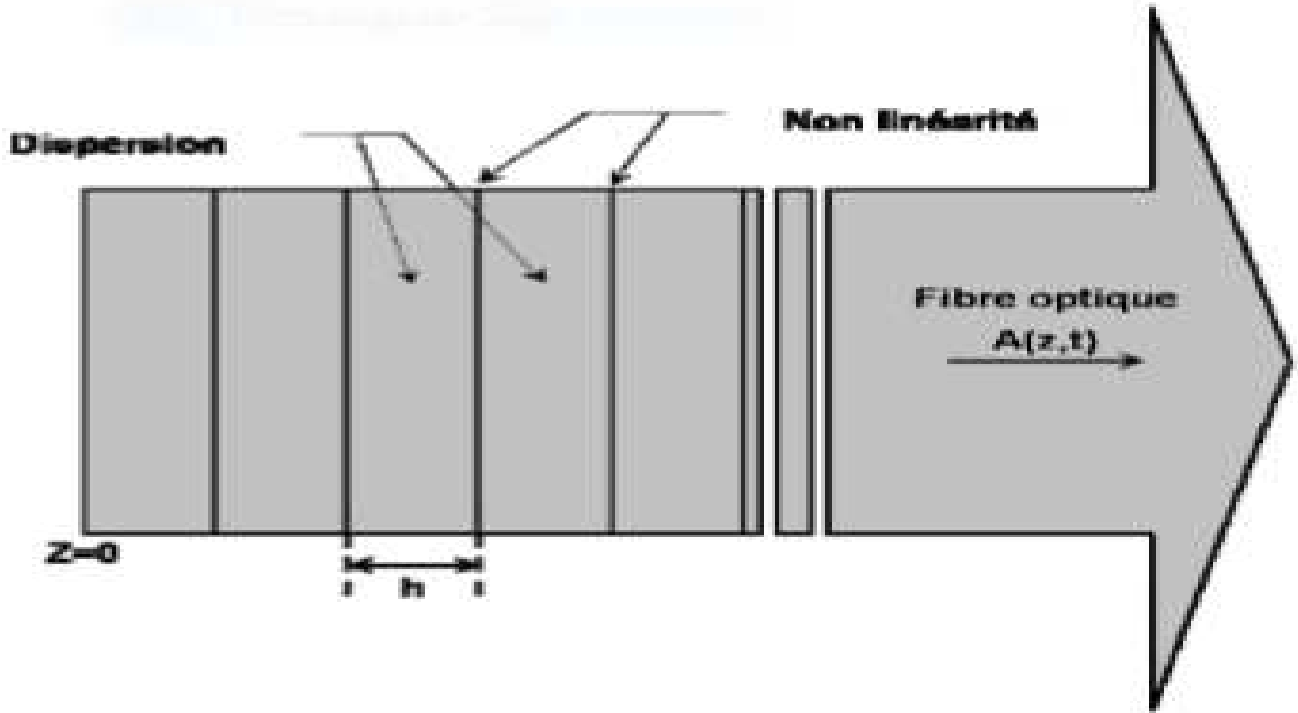


Figure 11: Schematic illustration of the split-step Fourier method [187]

tion. Later, it was adapted to solve higher-order ordinary differential equations or coupled (simultaneous) differential equations. It is based on the following

$$y_{i+1} = y_i + (a_1k_1 + a_2k_2 + a_3k_3 + a_4k_4), \tag{II.71}$$

where knowing the value of $y = y_i$ at x_i , we can find the value of $y = y_{i+1}$ at x_{i+1} , and $h = x_{i+1} - x_i$.

Equation Eq.(II.70) is equivalent to the first five terms of Taylor series

$$\begin{aligned} \frac{dy}{dx} = y_i + \frac{dy}{dx} \Big|_{x_i, y_i} (x_{i+1} - x_i) + \frac{1}{2!} \frac{d^2y}{dx^2} \Big|_{x_i, y_i} (x_{i+1} - x_i)^2 + \frac{1}{3!} \frac{d^3y}{dx^3} \Big|_{x_i, y_i} (x_{i+1} - x_i)^3 \\ + \frac{1}{4!} \frac{d^4y}{dx^4} \Big|_{x_i, y_i} (x_{i+1} - x_i)^4 \end{aligned} \tag{II.72}$$

Knowing that $\frac{dy}{dx} = f(x, y)$ and $h = x_{i+1} - x_i$,

$$y_{i+1} = y_i + hf(x_i, y_i) + \frac{h^2}{2!} f'(x_i, y_i) + \frac{h^3}{3!} f''(x_i, y_i) + \frac{h^4}{4!} f'''(x_i, y_i) \dots \tag{II.73}$$

Based on equating Eq.(II.72) and Eq.(II.73), the solutions are obtained such as

$$y_{i+1} = y_i + \frac{h}{6}(k_1 + 2k_2 + 2k_3 + k_4), \quad (\text{II.74})$$

where

$$k_1 = f(x_i, y_i), \quad (\text{II.75a})$$

$$k_2 = f\left(x_i + \frac{h}{2}, y_i + \frac{hk_1}{2}\right), \quad (\text{II.75b})$$

$$k_3 = f\left(x_i + \frac{h}{2}, y_i + \frac{hk_2}{2}\right), \quad (\text{II.75c})$$

$$k_4 = f(x_i + h, y_i + hk_3). \quad (\text{II.75d})$$

The RK4 method makes four estimates of $f(x, y)$ per segment, each estimate is refined by the previous one; the first at the starting point x , the second and the third at the point $x + h/2$, from the middle of the segment and the last at the end point $x + h$.

II.5 Conclusion

In this chapter, we have presented the coupled linear and nonlinear mode equations with a nonparaxiality terms that appear in the nonparaxial regime, leading to the presence of the second derivative with respect to 2 in the nonlinear wave equation. Thanks to the multiple scale and time method, we will be able to reduce it to a new 2D NLS equation. Then, using standard linear stability analysis, the instability criteria for MI has been proposed. Some numerical method, Runge-kutta method of order 4, have been presented and to the use in the next chapter

RESULTS AND DISCUSSIONS

III.1 Introduction

In this chapter, we study the propagation of gap-soliton bullets in nonlinear periodic waveguides, at frequencies close to the Bragg gap reflection, beyond the paraxial approximation. Using a multi-scale analysis, we derive a (2D) NLS equation with higher-order correction terms that consider non-paraxial regimes in the slowly varying envelope approximation. In addition, a fully numerical simulation of the newly derived model equation demonstrates that mutual balancing between Kerr, dimensionality, higher-order dispersions and non-paraxiality allows wave propagation, while retaining the shape of the gap-soliton bullets in a lattice waveguide. Subsequently, we will study the modulational instability (MI) of the CW in the model equation. For a normal dispersion, we find a finite threshold instability. The role of non-paraxiality between layers of the FBG in the MI is identified.

III.2 Derivation a 2D NLS equation with higher-order correction terms in the nonparaxial regimes.

Difficulty in describing the nonparaxial propagation of an electromagnetic field using a parabolic wave equation arises whenever the beam waist and the diffraction length become comparable [186], or when the spectral width of a pulse is much smaller than the pulse central frequency [187]. As is well-known, implementing the non-paraxial interference modeling under arbitrary spatial correlation is mathematically hard challenging. In addition, the local and non-local kernel features have physical implications

on the spatial behavior of the optical waves and quantum particles in the setup volume, that the paraxial approached models cannot account for. It has been shown that the propagation equation of the first order for non-paraxial beams and ultra-short pulses is equivalent to a generalized uncertainty principle deformed free particle Schrödinger equation [188, 189]. Furthermore, by using the mathematical analogy between a non-paraxial optical system and the generalized Schrödinger equation deformed by the existence a minimal measurable length, the Feynman path integral method for nonparaxial optics has been constructed and the ultrafocused optical pulses can be used as an optical analog of quantum gravity [190]. In the context of nonlinear optical devices, a non-paraxial NLS equation has been derived to describe spatial solitons in 2D Kerr media that includes ultra-narrow soliton beams. Here, the nonparaxiality arises from linear 2D diffraction [191]. The non-paraxial theory of self-focusing and self-trapping of the Hermite cosh-Gaussian laser beam in a rippled density plasma with relativistic nonlinearity has been analyzed, where the variation of beam width parameter with the distance of propagation has been studied by solving coupled second-order nonlinear differential equation for different modes with varying parameters [192]. The standard scalar paraxial parabolic (Fock-Leontovich) propagation equation has been generalized to include all-order non-paraxial corrections in the smallness parameter in a tensorial refractive-index perturbation on a homogeneous isotropic background [193, 194]. A 2D NLS equation that includes the combined effect of small-time dispersion and nonparaxiality on self-focusing has been derived and the regimes in which each mechanism dominates have been identified [195]. Most of the problems related to beam propagation in optics are treated in the so-called paraxial approximation which is only valid for light rays very close to the optical axis. Within this framework, the evolution of the beam in the presence of a small refractive index variation is described by the parabolic (or Fock-Leontovich) wave equation. This equation is valid if we use the slowly varying approximation and if one neglects the polarization-scrambling term [196, 197], and the validity of the paraxial approximation has been questioned by numerous authors previously [198], and even with respect to optical vortices interacting with atoms [199]. However,

devices at micro and nano scales are currently developed in optical and quantum technology. At these scales, non-paraxial propagation of waves and particles as well as effects due to the two-point correlation are unavoidable. So, the nonparaxial description is required because of the short propagation distances, significantly shorter than the limit distance that assures the validity of the paraxial approach. For the theoretical interpretation of the experimental results, nonparaxial optics is an interesting branch of research, which is a generalization of the standard paraxial optics, with applications for the generation of subwavelength anti-diffracting beams to obtain super-resolved microscopy [200, 201]. The energy, momentum, and propagation of the Laguerre-Gaussian (cylindrical coordinates) beam modes, Hermite-Gaussian (Cartesian coordinates) beam modes and Ince-Gaussian (elliptical coordinates) beam modes of the paraxial wave equation in an apertured nonparaxial regime have been investigated [202]. The filamentation of a laser beam and modifications of the plasma density profile in the plane transverse to the beam axis as well as the propagation characteristics of the wave propagating in a hot collisionless plasma in the non-paraxial region has been studied [203]. It has been shown that the microscopic interaction of the spin-orbit of the two-component Bose-Einstein condensate with the nonparaxial Laguerre-Gaussian beams will not only provide enhanced Rabi frequencies due to increased intensity but also will generate different channels of transitions along with their external control mechanism [204]. In particles carrying orbital angular momentum, when the beams are focused to a spot with a size comparable to a characteristic scale of a problem, more realistic wave-packet treatment beyond the paraxial approximation is needed, in particular, for proper study of the spin-orbit phenomena and scattering problems in atomic and high-energy physics, especially when the quantum interference and coherence play a notable role [205, 206]. The optimal focal distance of a planar-convex lens has been determined beyond the paraxial approximation within the context of geometrical optics [207]. Three-dimensional nonparaxial accelerating fields have been generated by suitably shaped mirrors [208, 209]. Very recently, 3D nonparaxial accelerating beams associated with different coordinate systems have been experimentally realized [210].

III.3 Asymptotic study of the dynamics of gap-soliton bullet in the nonparaxial regime

The existence of Bragg solitons, near (but outside) the band gap results from the compensation of the grating dispersion by the nonlinearity of the fiber, where the Bragg grating is inscribed [212, 214]. Sipe and de Sterke have shown that the propagation of these solitons is described by a standard NLS equation, which can be derived from the coupled mode equations, supplemented by terms representing the nonlinear contribution to the propagation. Bragg solitons have been observed experimentally in FBGs [216] and in semiconductor guides. Their main characteristic is that they can propagate at speeds much lower than the speed of light in the fiber in the absence of the grating. We will present the asymptotic study of the dynamics of Gap-soliton bullet in the FBGs. We will use the multiple scale analysis method to reduce the system of coupled nonlinear nonparaxial equations to an equation called the perturbed nonparaxial 2D NLS equation, which describes the nonlinear nonparaxial propagation of the pulses at the edges of the photonic band gap. We consider the following nonparaxial nonlinear coupled mode equations:

$$\begin{aligned} \frac{\partial^2 E_+}{\partial z^2} + i\left(\frac{\partial}{\partial t} + c_g \frac{\partial}{\partial z}\right)E_+ + \kappa E_- + \frac{\partial^2 E_+}{\partial x^2} + \Gamma(|E_+|^2 + 2|E_-|^2)E_+ &= 0, \\ \frac{\partial^2 E_-}{\partial z^2} + i\left(\frac{\partial}{\partial t} - c_g \frac{\partial}{\partial z}\right)E_- + \kappa E_+ + \frac{\partial^2 E_-}{\partial x^2} + \Gamma(|E_-|^2 + 2|E_+|^2)E_- &= 0, \end{aligned} \quad (\text{III.1})$$

This Fig. 12 illustrate the Gap soliton in 3D this solitons refer to intense nonlinear pulse propagation in periodic variation fiber. We have shown the gap in this figure so that in the continuation of the work we can advance by making propagate the ballets of light in this zone of gap in nonparaxial regime

with the nonlinear coupling coefficient being $\Gamma = 3\chi^{(3)}\Omega^2/c^2$, and $\kappa = \Omega\delta_n/2c$. $(|E_+|^2 + 2|E_-|^2)E_+$. The expressions $(|E_-|^2 + 2|E_+|^2)E_-$ are coupling terms that include cross-

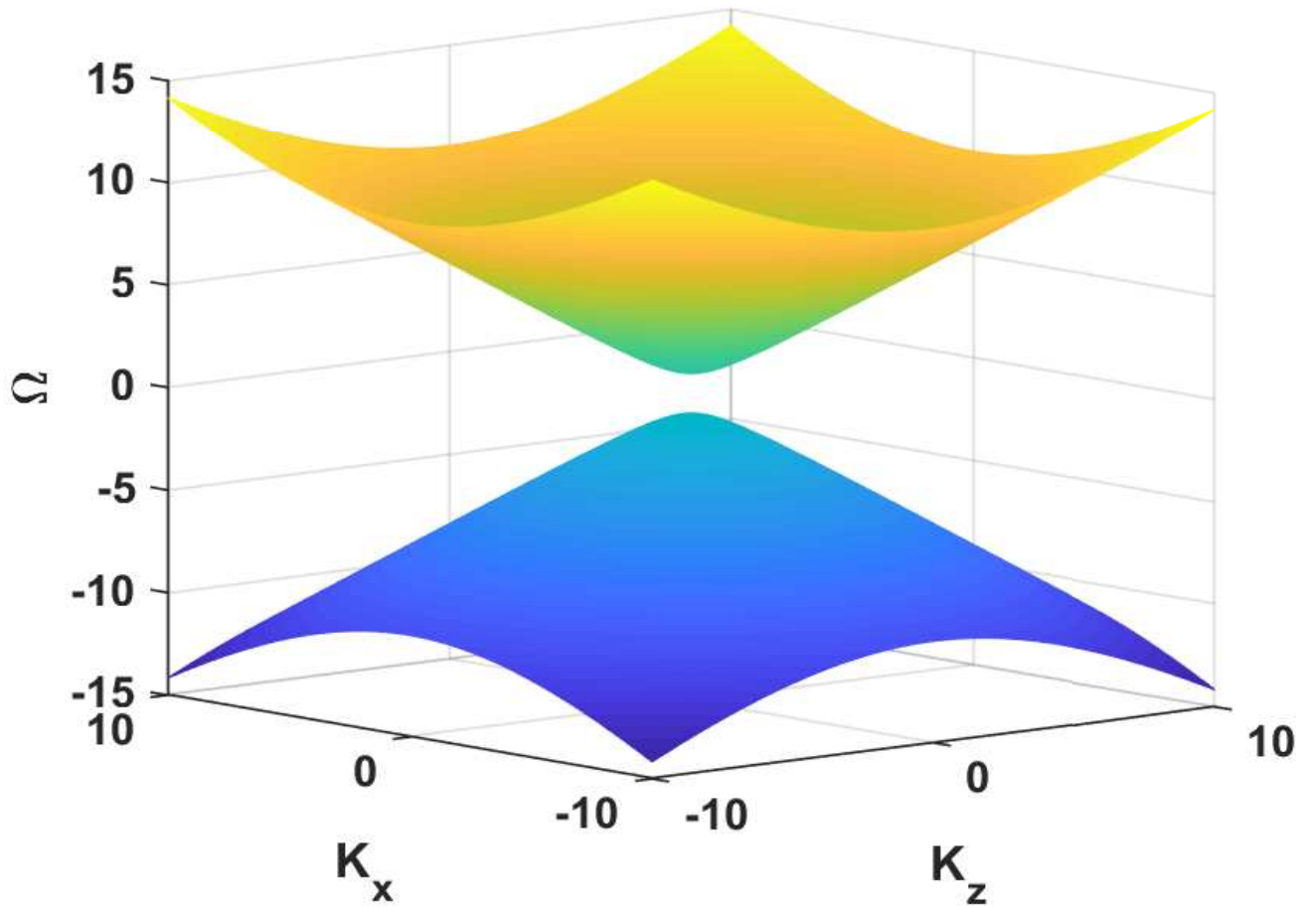


Figure 12: Dispersion relationship showing a periodic Bragg grating band

phase modulation (multiplied by 2) and auto-phase modulation (with any coefficient).

In the linear case, i.e., $\Gamma = 0$, solutions for system of Eq. (III.1) are taken to be

$$\begin{pmatrix} E_+ \\ E_- \end{pmatrix} = \begin{pmatrix} U_+ \\ U_- \end{pmatrix} e^{i(\Omega t - k_z z - k_x x)} + c.c. \quad (\text{III.2})$$

with Ω, k_z, k_x satisfying the dispersion relation $(\Omega^2 - (k_x^2 + k_z^2))^2 = c_g k_z^2 + \kappa^2 - 2\epsilon k_x^2 k_z^2$. In the particular case where $\Omega = \kappa$ and $k_x = k_z = 0$, solutions (III.2) reduce to

$$\begin{pmatrix} E_+ \\ E_- \end{pmatrix} = c \begin{pmatrix} 1 \\ -1 \end{pmatrix} e^{-i\kappa T} + c.c. \quad (\text{III.3})$$

We should note that solution (III.3) satisfy $L \begin{pmatrix} E_+ \\ E_- \end{pmatrix} = 0$, where L is an operator given by:

$$L = \begin{bmatrix} i\frac{\partial}{\partial t} & \kappa \\ \kappa & i\frac{\partial}{\partial t} \end{bmatrix}$$

In the nonlinear equations of coupled modes, we find the solution of the above equation in the linear case and then present the nonparaxial nonlinearity in the coupled mode equations. Therefore, using the method of analysis at multiple scales method, we look for solutions of the form:

$$\begin{pmatrix} E_+ \\ E_- \end{pmatrix} = \epsilon^{1/2} A(\tau_1, \tau_2, X, Z) \begin{pmatrix} 1 \\ -1 \end{pmatrix} e^{-i\kappa T} + \epsilon U_1 + \epsilon^{3/2} U_2 + \epsilon^3 U_3 + \dots, \quad (\text{III.4})$$

where $\tau_1 = \epsilon t, \tau_2 = \epsilon^2 t, X = \epsilon^{1/2} x$, and $Z = \epsilon^{1/2} z$. We now solve for $\begin{pmatrix} E_+ \\ E_- \end{pmatrix}$ in successive orders of ϵ , where the expansion as a function of term of $O(\epsilon)$ leads to the set of

equations:

$$LU_1 = -c_g \frac{\partial A}{\partial z} \begin{pmatrix} 1 \\ 1 \end{pmatrix} e^{-i\kappa T}. \quad (\text{III.5})$$

We notice that the solution to the above is linear and is obtained in the following form:

$$U_1 = -\frac{c_g}{2\kappa} \frac{\partial A}{\partial z} \begin{pmatrix} 1 \\ 1 \end{pmatrix} e^{-i\kappa T}. \quad (\text{III.6})$$

In order to go to higher orders, we first need a careful calculation of nonlinear limits.

The development will be done in order $\theta(\varepsilon^{3/2})$:

$$\begin{aligned} \left| \varepsilon^{1/2} A - i\varepsilon \frac{c_g}{2k} \cdot \frac{\partial A}{\partial z} \right|^2 &= \left(\varepsilon^{1/2} A - i\varepsilon \frac{c_g}{2k} \cdot \frac{\partial A}{\partial z} \right) \left(\varepsilon^{1/2} A^* - i\varepsilon \frac{c_g}{2k} \cdot \frac{\partial A^*}{\partial z} \right) \\ &= \varepsilon |A|^2 + \varepsilon^{3/2} \frac{c_g}{2k} \left(A \frac{\partial A^*}{\partial z} - A^* \frac{\partial A}{\partial z} \right) \end{aligned} \quad (\text{III.7})$$

.

Expanding the square modulus terms gives

$$\begin{aligned} 2 \left| \varepsilon^{1/2} A + i\varepsilon \frac{c_g}{2k} \frac{\partial A}{\partial z} \right|^2 &= 2 \left(\varepsilon^{1/2} A + i\varepsilon \frac{c_g}{2k} \frac{\partial A}{\partial z} \right) \left(\varepsilon^{1/2} A^* + i\varepsilon \frac{c_g}{2k} \frac{\partial A^*}{\partial z} \right) \\ &= 2 \left(\varepsilon |A|^2 + i\varepsilon^{3/2} \frac{c_g}{2k} \left(A \frac{\partial A^*}{\partial z} - A^* \frac{\partial A}{\partial z} \right) + \varepsilon^2 \frac{c_g^2}{4k^2} \frac{\partial A}{\partial z} \frac{\partial A^*}{\partial z} \right) \end{aligned} \quad (\text{III.8})$$

.

The nonlinear terms are

$$\begin{aligned} (|E_+|^2 + 2|E_-|^2) E_+ &= \left(3\varepsilon |A|^2 + i\varepsilon^{3/2} \frac{c_g}{2k} \left(A^* \frac{\partial A}{\partial z} - A \frac{\partial A^*}{\partial z} \right) + 3\varepsilon^2 \frac{c_g^2}{4k^2} \frac{\partial A}{\partial z} \frac{\partial A^*}{\partial z} \right) \\ &\times \left(\varepsilon^{1/2} A - i\varepsilon \frac{c_g}{2k} \frac{\partial A}{\partial z} \right) e^{-i\kappa T} + c.c. \end{aligned} \quad (\text{III.9})$$

$$= \left(\begin{aligned} &3\varepsilon |A|^2 A - i\varepsilon^2 \frac{c_g}{2k} \left(2|A|^2 \frac{\partial A}{\partial z} + A^2 \frac{\partial A^*}{\partial z} \right) \\ &+ \varepsilon^{5/2} \left(\frac{c_g^2}{2k^2} A \frac{\partial A}{\partial z} \frac{\partial A^*}{\partial z} + \frac{c_g^2}{4k^2} A^* \left(\frac{\partial A}{\partial z} \right)^2 \right) - i\varepsilon^3 \frac{3c_g^3}{8k^3} \left(\frac{\partial A}{\partial z} \right)^2 \left(\frac{\partial A^*}{\partial z} \right) \end{aligned} \right) e^{-i\kappa T} \quad (\text{III.10})$$

+c.c.

Similarly,

$$\begin{aligned} (|E_+|^2 + 2|E_-|^2) E_- = - \left(\begin{array}{l} 3\varepsilon^{3/2} |A|^2 A - i\varepsilon^2 \frac{c_g}{2k} (2|A|^2 \frac{\partial A}{\partial z} + A^2 \frac{\partial A^*}{\partial z}) \\ + \varepsilon^{5/2} (\frac{c_g^2}{2k^2} A \frac{\partial A}{\partial z} \frac{\partial A^*}{\partial z} + \frac{c_g^2}{4k^2} A^* (\frac{\partial A}{\partial z})^2) + i\varepsilon^3 \frac{3c_g^3}{8k^3} (\frac{\partial A}{\partial z})^2 (\frac{\partial A^*}{\partial z}) \end{array} \right) e^{-i\kappa T} \\ + c.c. \end{aligned} \quad (\text{III.11})$$

Then, we continue the computation for high correction orders of (E_+, E_-) . The expansion of the order $\theta(\varepsilon^{3/2})$ gives:

$$LU_2 = - \left(i \frac{\partial A}{\partial \tau_1} + \frac{\partial^2 A}{\partial z^2} + \frac{c_g}{2\kappa} \frac{\partial^3 A}{\partial z^3} + \frac{c_g^2}{2\kappa} \frac{\partial^2 A}{\partial z^2} + \frac{\partial^2 A}{\partial^2 x^2} + 3\Gamma |A|^2 A \right) \begin{pmatrix} 1 \\ -1 \end{pmatrix} e^{-i\kappa T} + c.c. \quad (\text{III.12})$$

We should specify that the slow variation of the terms around $U_1 = -\frac{c_g}{2\kappa} \begin{pmatrix} 1 \\ -1 \end{pmatrix} e^{-i\kappa T}$

is zero in space L . The physical condition will be given by

$$i \frac{\partial A}{\partial \tau_1} + \frac{\partial^2 A}{\partial z^2} + \frac{c_g}{2\kappa} \frac{\partial^3 A}{\partial z^3} + \frac{c_g^2}{2\kappa} \frac{\partial^2 A}{\partial z^2} + \frac{\partial^2 A}{\partial^2 x^2} + 3\Gamma |A|^2 A = 0. \quad (\text{III.13})$$

For higher-order effects, we continue the expansion at order $0(\varepsilon^2)$, and make the rescaling $\tau_2 = \varepsilon^2 t$, so that:

$$LU_3 = - \left[\begin{array}{l} (i \frac{c_g}{2\kappa} \Gamma(4|A|^2 \frac{\partial A}{\partial z} + 2A^2 \frac{\partial A^*}{\partial z}) + \frac{c_g^3}{4\kappa^2} \frac{\partial^3 A}{\partial z^3} + \frac{c_g^3}{4\kappa^2} \frac{\partial^4 A}{\partial z^4}) \\ + \frac{c_g}{2\kappa} \Gamma(2|A|^2 \frac{\partial^2 A}{\partial z^2} + A^2 \frac{\partial^2 A^*}{\partial z^2}) + \frac{c_g}{2\kappa^2} \frac{\partial^4 A}{\partial z^4} + \frac{c_g}{2\kappa} \frac{\partial^5 A}{\partial z^5} \end{array} \right] \begin{pmatrix} 1 \\ -1 \end{pmatrix} e^{-i\kappa T} + c.c. \quad (\text{III.14})$$

The solution to the above equation is found in the form

$$U_3 = - \left(\begin{array}{l} i \frac{c_g}{4\kappa^2} \left[\Gamma(4|A|^2 \frac{\partial A}{\partial z} + 2A^2 \frac{\partial A^*}{\partial z}) + \frac{c_g^2}{2\kappa} \frac{\partial^3 A}{\partial z^3} + \frac{c_g^2}{2\kappa} \frac{\partial^4 A}{\partial z^4} \right] \\ + \frac{c_g}{4\kappa^2} \left[\Gamma(2|A|^2 \frac{\partial^2 A}{\partial z^2} + A^2 \frac{\partial^2 A^*}{\partial z^2}) + \frac{c_g^2}{2\kappa} \frac{\partial^4 A}{\partial z^4} + \frac{\partial^5 A}{\partial z^5} \right] \end{array} \right) \begin{pmatrix} 1 \\ -1 \end{pmatrix} e^{-i\kappa T} + c.c. \quad (\text{III.15})$$

Calculation can be extended up to the order $O(\varepsilon^5/2)$ which leads to

$$LU_4 = - \left[\begin{array}{l} i \frac{\partial A}{\partial \tau_2} + \frac{c_g^2}{4\kappa^2} (\Gamma 4 \frac{\partial |A|^2}{\partial z} \frac{\partial A}{\partial z} + 2A^2 \frac{\partial A^*}{\partial z}) + \frac{c_g^4}{8\kappa^3} \frac{\partial^4 A}{\partial z^4} + \frac{c_g^4}{8\kappa^3} \frac{\partial^5 A}{\partial z^5} \\ + \frac{c_g^2 \Gamma}{4\kappa^2} 2A \frac{\partial^3 |A|^2}{\partial z^3} + A^* (\frac{\partial A}{\partial z})^2 + \frac{c_g^5}{8\kappa^3} \frac{\partial^5 A}{\partial z^5} + \frac{c_g^3}{4\kappa^2} \frac{\partial^6 A}{\partial z^6} \\ + \frac{c_g^2}{4\kappa^2} (\Gamma 4 \frac{\partial^2 |A|^2}{\partial z^2} \frac{\partial A}{\partial z} + 2 \frac{\partial^2 A^2}{\partial z^2} \frac{\partial A^*}{\partial z}) + \frac{c_g^3}{8\kappa^3} \frac{\partial^5 A}{\partial z^5} + \frac{c_g^3}{8\kappa^3} \frac{\partial^6 A}{\partial z^6} \\ + \frac{c_g^2 \Gamma}{4\kappa^2} 2A \frac{\partial^4 |A|^2}{\partial z^4} + \frac{\partial^2 A^2}{\partial z^2} \frac{\partial^2 A^*}{\partial z^2} + \frac{c_g^3}{8\kappa^3} \frac{\partial^6 A}{\partial z^6} + \frac{c_g}{4\kappa^2} \frac{\partial^7 A}{\partial z^7} \end{array} \right] \begin{pmatrix} 1 \\ -1 \end{pmatrix} e^{-i\kappa T} + c.c. \quad (III.16)$$

In general, when we consider higher-order effects, nonlinear perturbed terms are added to the classical NLS equations. This is termed as the nonparaxial NLS equation. Summing up all the steps and defining the slow time $\tau_1 + \tau_2 = t$, one obtains the following 2D equation:

$$i \frac{\partial A}{\partial \tau} + \frac{\partial^2 A}{\partial z^2} + \frac{\partial^2 A}{\partial x^2} + \frac{c_g^2}{2k} \frac{\partial^2 A}{\partial z^2} + 3\Gamma |A|^2 A = -\varepsilon F(A), \quad (III.17)$$

with

$$\begin{aligned} F(A) = & \Gamma \frac{c_g^2}{4k^2} \left(5A^* (\frac{\partial A}{\partial z})^2 + 10A \frac{\partial A}{\partial z} \frac{\partial A^*}{\partial z} + 4|A|^2 \frac{\partial^2 A}{\partial z^2} + 2A^2 \frac{\partial^2 A^*}{\partial z^2} \right) \\ & + \Gamma \frac{c_g^2}{4k^2} \left(5 \frac{\partial^2 A^*}{\partial z^2} (\frac{\partial A}{\partial z})^2 + 10 \frac{\partial^2 A}{\partial z^2} \frac{\partial A}{\partial z} \frac{\partial A^*}{\partial z} + 4|A|^2 \frac{\partial^3 A}{\partial z^3} + 2A^2 \frac{\partial^3 A^*}{\partial z^3} \right) \\ & + \frac{c_g^4}{8k^3} \frac{\partial^4 A}{\partial z^4} + \frac{c_g^{11}}{8k^3} \frac{\partial^5 A}{\partial z^5} + (\frac{c_g^3}{4k^2} + \frac{c_g^6}{8k^3}) \frac{\partial^6 A}{\partial z^6} + \frac{c_g}{4k^2} \frac{\partial^7 A}{\partial z^7} \end{aligned} \quad (III.18)$$

The above equation describes the nonparaxial nonlinear propagation of the pulses in a periodic medium (Bragg grating) with higher-order effects outside the forbidden band. Such higher-order effects include dispersion terms up to the seventh-order and nonlinear derivative terms, while Aceves et al. [218] obtained a 2D NLS equation that was including terms up to the fourth-order dispersion.

III.3.1 Numerical gap-soliton bullet stability under nonparaxiality effects

In the previous section, we derived the perturbed 2D NLS Eq.(III.17) in the slowly-varying envelope approximation from the coupled-mode equations. A natural question is whether its solutions can remain stable over propagation. Otherwise, what are the values of the involved parameters and coefficients for its solutions to remain stable? In

order to proceed with the answer to such a concern, we first need to make the change of variables $y = \frac{\sqrt{2\kappa}}{c_g} z$, $\psi = \sqrt{3\Gamma} A$ [197], which leads to the nondimensional equation

$$\begin{aligned} \frac{2\kappa}{c_g^2} \frac{\partial^2 \psi}{\partial y^2} + i \frac{\partial \psi}{\partial \tau} + \Delta_{\perp} \psi + |\psi|^2 \psi = -\frac{\epsilon}{12} \left(5\psi^* \frac{\partial \psi^2}{\partial y} + 10\psi \left| \frac{\partial \psi}{\partial y} \right|^2 + 4|\psi|^2 \frac{\partial^2 \psi}{\partial y^2} + 2\psi^2 \frac{\partial^2 \psi^*}{\partial y^2} + \frac{1}{2} \frac{\partial^4 \psi}{\partial y^4} \right) \\ - \frac{\epsilon}{12} \cdot \frac{2\sqrt{\kappa}}{c_g} \left(\begin{aligned} &5\sqrt{2\kappa} \psi^* \frac{\partial^3 \psi^2}{\partial y^3} + 10 \frac{2\kappa}{c_g} \frac{\partial^2 \psi}{\partial y^2} \left| \frac{\partial \psi}{\partial y} \right|^2 + 4|\psi|^2 \frac{\partial^3 \psi}{\partial y^3} + 2 \frac{\partial^2 \psi^2}{\partial y^2} \frac{\partial^3 \psi^*}{\partial y^3} \\ &+ 3 \frac{c_g^8}{\sqrt{2\kappa}} \frac{\partial^5 \psi}{\partial y^5} + 3 \frac{c_g^4}{2\kappa \sqrt{2\kappa}} \frac{\partial^6 \psi}{\partial y^6} + \frac{12\kappa}{c_g^5} \frac{\partial^7 \psi}{\partial y^7} \end{aligned} \right) \end{aligned} \quad (\text{III.19})$$

where $\Delta_{\perp} = \partial_{xx} + \partial_{yy}$. Once more, it should be noted that when the coefficient $\frac{\epsilon}{12} \cdot \frac{2\sqrt{\kappa}}{c_g} \rightarrow 0$, the nonparaxiality effect is switched off and the remaining terms belong to the NLS equation proposed in Ref. [217, 218, 219, 220]. Additionally, if $\epsilon \rightarrow 0$, one recovers the equation proposed by Fibich [221, 222, 223, 224], who initially introduced nonparaxiality in the Bragg grating to study the implications of such an effect on the beam width and self-focusing. It should be noticed from the above that the terms contributing to paraxiality and nonparaxiality have in common the small parameter ϵ , the parameter κ , the group velocity c_g that can be tuned for a suitable balance between dispersion and nonlinearity, which is necessary for the Townes soliton to be stable. Moreover, we solve Eq.(III.19) using the split-step Fourier method, with the initial condition being a Townes soliton. To start, we display the propagation of the initial condition in the medium in Fig.(13), for $\epsilon = 0.01$, $\kappa = -1$ and $c_g = 0.5$. Obviously, for this combination of parameters, the propagation gives rise to a broad range of phenomena that characterize the instability of the soliton. However, this instability gives rise to composite solitons, made of several peaks, with a persisting background of the initial condition. Compared to this previous case, the values $\epsilon = 0.025$, $\kappa = -1.2$ and $c_g = 0.55$ lead to a solitonic structure that delocalized during propagation and split into several objects as time increases. To remind, rows from top to bottom, respectively, correspond to instants $t = 2$, $t = 3$, $t = 4$ and $t = 5$. When values of parameters change to $\epsilon = 0.032$, $\kappa = -2.3$, and $c_g = 0.64$, the initial condition rapidly evolves into asymmetric bullets, whose the heart becomes symmetric as time increases and recombine to get the initial state background [see Fig.(15)]. However, like in the previous case of Fig.(14), the structures de-

localize as time increases, which supports its propagation during disintegration and recombination. Additionally, the first instant of the structures in Fig.(16), shows that this state is unstable as the original symmetry is spontaneously broken. Nevertheless, with the chosen values of the system parameters, the recombination process as time evolves causes the intensity to increase, leading to the quasi-original form of the gap-soliton bullet obtained in Fig. 16(c1). This last combination of parameters shows that it is possible to get suitable parameters for which stable objects can be obtained from the above system. Beyond such an objective, one should also be interested in the generated composite solitons, which to some extent may enrich the family of useful solitons in optics and materials. However, one of the facts that should be of interest here is the splitting-recombination phenomenon that can be useful in securing information during transportation, as solitonic waves have drawn considerable attention in that direction.

In general, the increase of the dispersion strength reveals some hidden phenomena of the system that did not appear when we were at lower orders. This can best be understood either by showing the system's stability or instability, which can later lead to collapse. In this paper, we describe the phenomenon of division recombination which appears thanks to the presence of the higher-degree terms due to nonparaxiality. This process leads to an increase in the intensity of the incident light power to produce shorter pulses. Additional nonlinear and higher-order scattering effects come into play essentially altering the physical characteristics and stability of the optical soliton propagating in the nonlinear non-paraxial medium. The system's dynamics is described as part of a non-paraxial nonlinear equation that includes higher-order dispersion terms. To better illustrate the presence of higher-order terms in this contribution, unlike those of Aceves, et al. [224, 225, 226, 227], whose Fig.(13) shows that the system remains stable throughout its evolution, we cannot talk about collapse. On the other hand, Fig.(16) of the present thesis rather an unstable state and a spontaneous rupture of the system, which could be translated into a collapse corresponding to the radical divisions of the solitons as they propagate in the optical fiber. In addition, we observe an increase in their intensity due to modification of system parameters related to nonparaxiality and

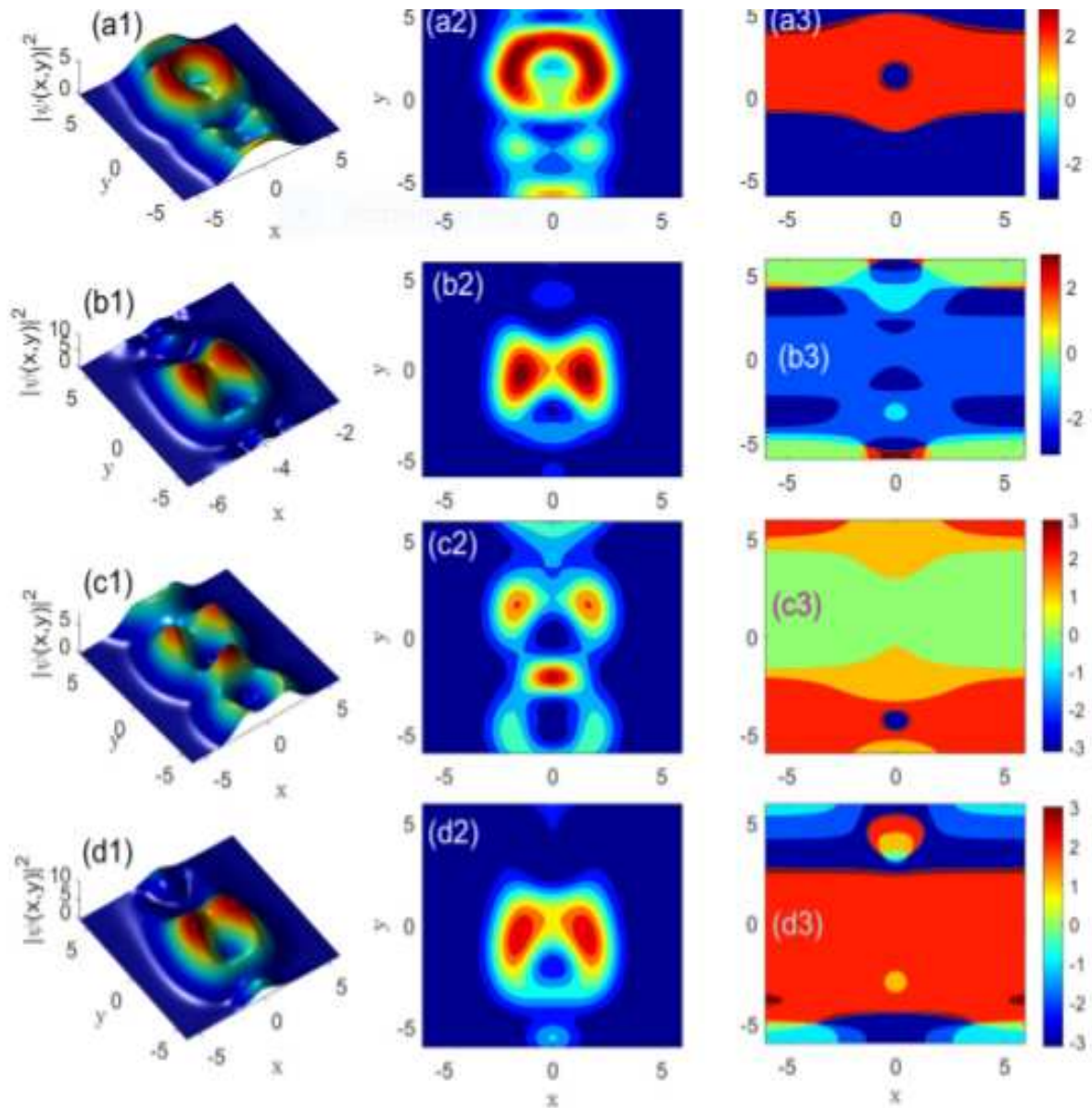


Figure 13: Panels (a1), (b1), (c1) and (d1) show the intensity profiles for the propagation of the initial gap-soliton bullet at the respective instants $t=0$, $t=2$, $t=3$, $t=4$ and $t=5$, with panels (a2), (b2), (c2) and (d2) corresponding to their contour plots. The third column, with index 3, from left displays the phase distribution at the respective instants, with the other parameters being $\epsilon = 0.01$, $\kappa = -1$ and $c_g = 0.5$.

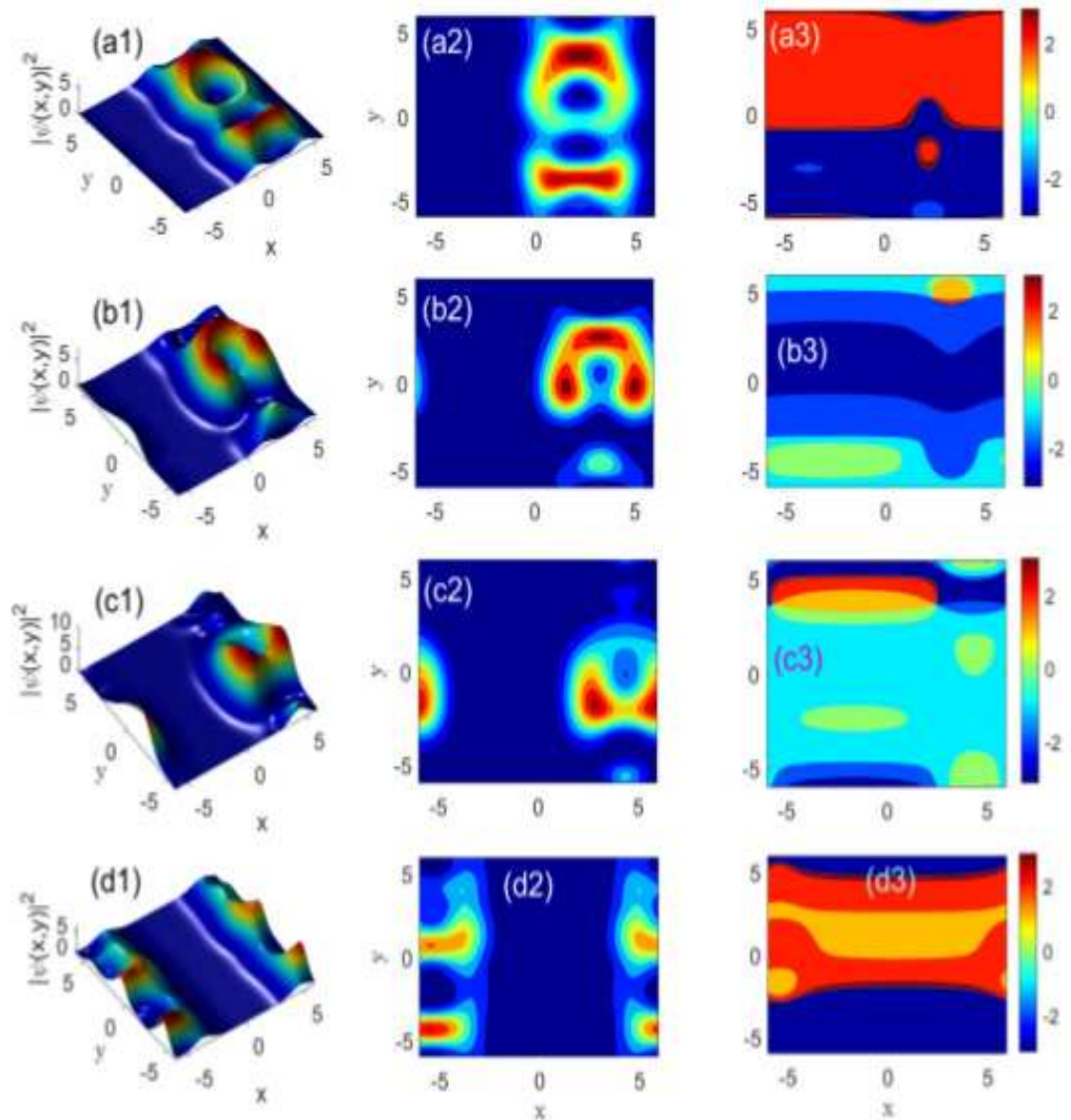


Figure 14: Panels (a1), (b1), (c1) and (d1) show the intensity profiles for the propagation of the initial gap-soliton bullet at the respective instants $t=0$, $t=2$, $t=3$, $t=4$ and $t=5$, with panels (a2), (b2), (c2) and (d2) corresponding to their contour plots. The third column, with index 3, from left displays the phase distribution at the respective instants, with the other parameters being $\epsilon = 0.01$, $\kappa = -1$ and $c_g = 0.5$.

the group speed. However, the terms of higher-order have allowed us to highlight the phenomenon of division-recombination and observation of a collapse at precise times and with certain values directly linked to our system. Subsequently, this collapse ended up being reconstituted, with the soliton regaining its normal shape. This can then be explained by the presence of nonparaxiality which, at higher orders, maintains the system stable even though it goes through several changes transient modes. More importantly, previous works do not support system collapsing [228, 229, 230, 231], which to some extent may be responsible for the generation of new states, with interesting features and undeniable practical implications. The phenomena described in the present paper bring forth the effectivity and efficiency of nonparaxiality, especially when solitons and their stability are involved in coupled nonlinear systems. The stability can be affected by such effects, with a strong impact on their intrinsic structure and width. This, however, does not prevent us from confirming the stability of the structures generated here, partly due to the enhanced modeling features, in comparison to the work of Aceves et al [232, 233, 234, 235]. Of course, such a confirmation may appear obsolete, which requires further studies, which is not the aim of the present work.

III.4 Modulational instability growth rates in a 2D NLS equation in nonparaxial regime

The starting point is based on the nonparaxial 2D NLSE equation.(III.19) [236, 237, 238]. In this subsection, we will show how the system becomes unstable and how the nonparaxial parameters influence the dynamics of the system [239, 240, 241].

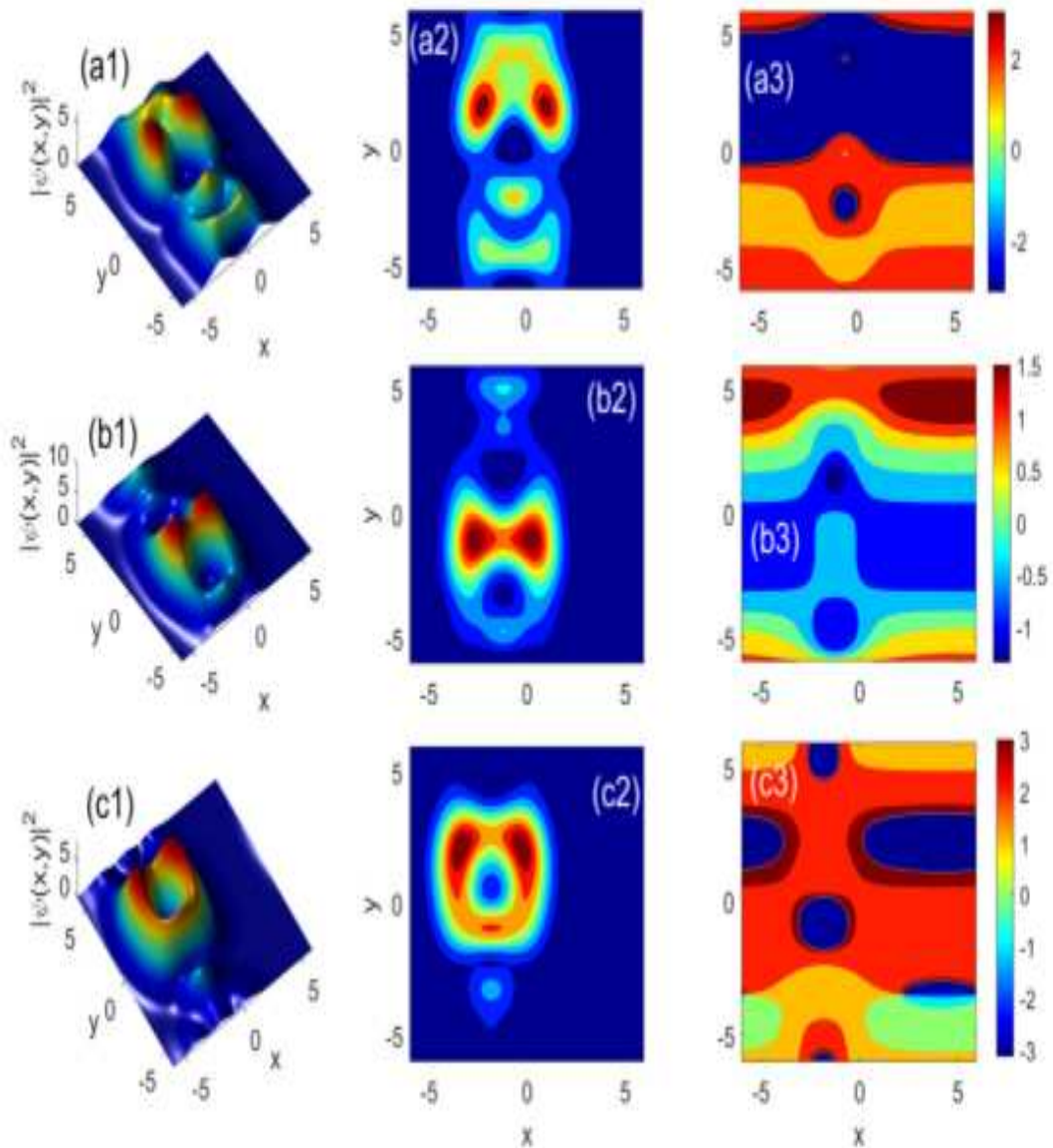


Figure 15: Panels (a1), (b1) and (c1) show the intensity profiles for the propagation of the initial light bullet at the respective instants $t=0$, $t = 2$, $t = 3$, and $t = 5$, with panels (a2), (b2) and (c2) corresponding to their contour plots. The third column, with index 3, from left displays the phase distribution at the respective instants, with the other parameters being $\epsilon = 0.032$, $\kappa = -2.3$, and $c_g = 0.64$.

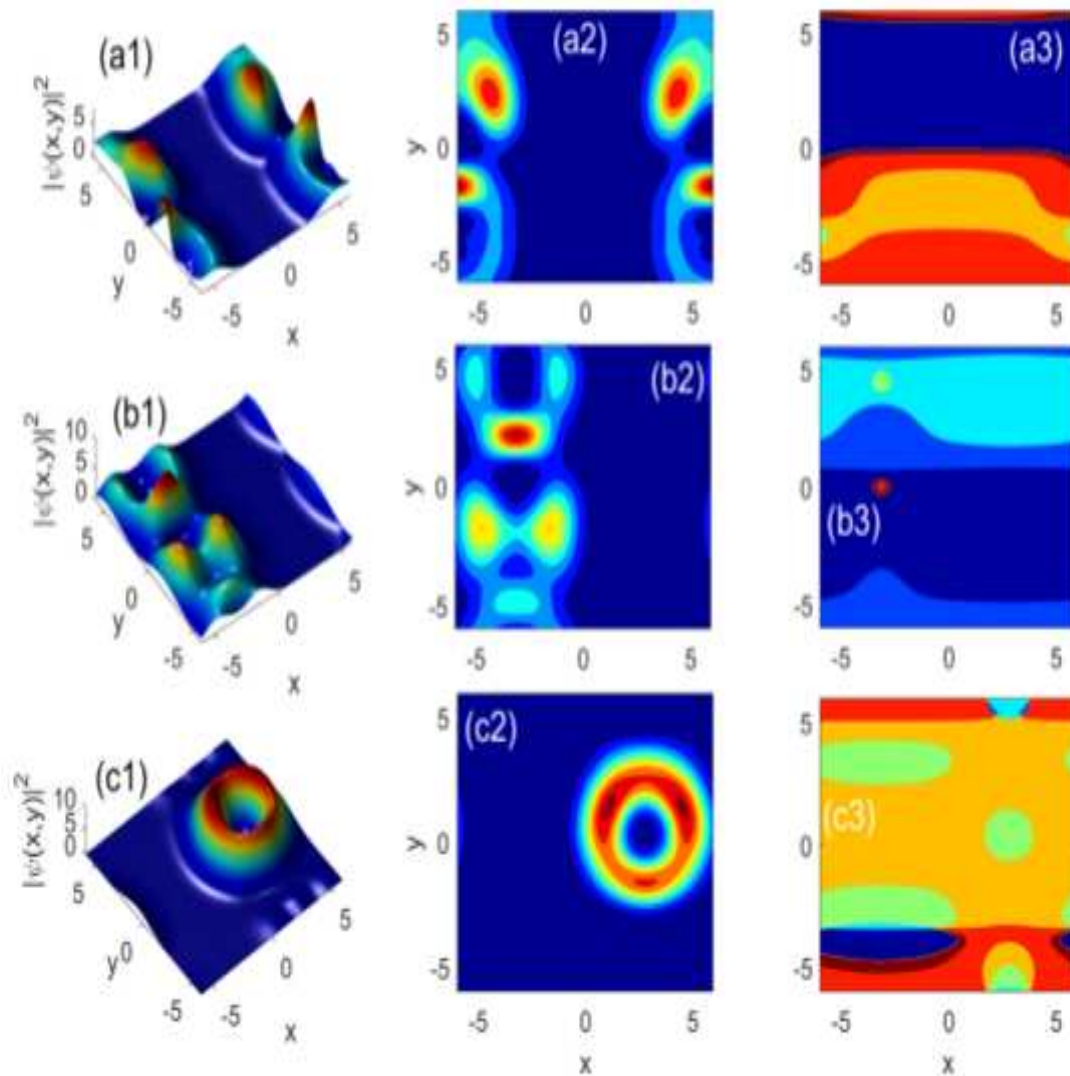


Figure 16: Panels (a1), (b1) and (c1) show the intensity profiles for the propagation of the initial light bullet at the respective instants $t=0$, $t = 2$, $t = 3$, and $t = 5$, with panels (a2), (b2) and (c2) corresponding to their contour plots. The third column, with index 3, from left displays the phase distribution at the respective instants, with the other parameters being $\epsilon = 0.04$, $\kappa = -2.9$, and $c_g = 0.69$.

III.4.1 The study of the linear stability analysis

Study of the instability of nonlinear, nonparaxial solitons is based on the linear stability analysis of the model. The steady state solution of Eq.(III.19) is

$$\psi(y, x, \tau) = \sqrt{p_0} \exp(iQ_{nl}), \quad (\text{III.20})$$

where the nonlinear phase shift Q_{nl} is related to the forward power p_0 as:

$$Q_{nl} = p_0\tau. \quad (\text{III.21})$$

To investigate the modulation stability of this solution, let us perturb the stationary result of Eq.(III.19) in the following way:

$$\psi(y, x, \tau) = [\sqrt{p_0} + \epsilon\psi_1(y, x, \tau)] \exp(ip_0\tau), \quad (\text{III.22})$$

where $\psi_1(y, x, \tau)$ is an arbitrary small perturbation. When Eq.(III.22) is substituted into Eq.(III.19) with higher-order terms in ψ_1 dropped, we obtain the evolution equation

$$\begin{aligned} a_1 \frac{\partial^2 \psi_1}{\partial y^2} + i \frac{\partial \psi_1}{\partial \tau} + p_0(\psi_1 + \psi_1^*) + \Delta_{\perp} \psi_1 = 10bp_0 \frac{\partial \psi_1}{\partial y} + 4bp_0 \frac{\partial^2 \psi_1}{\partial y^2} + \\ 2b_1p_0 \frac{\partial^2 \psi_1^*}{\partial y^2} + \frac{b_1}{2} \frac{\partial^4 \psi_1}{\partial y^4} + 2cdp_0 \frac{\partial^3 \psi_1}{\partial y^3} + 4cp_0 \frac{\partial^3 \psi_1}{\partial y^3} + cf \frac{\partial^5 \psi_1}{\partial y^5} + cg \frac{\partial^6 \psi_1}{\partial y^6} + \\ ch \frac{\partial^7 \psi_1}{\partial y^7}. \end{aligned} \quad (\text{III.23})$$

The different coefficient of the equation are given by: $a_1 = \frac{2\kappa}{c_g^2}$; $b_1 = \frac{\epsilon}{12}$; $c = -\frac{\epsilon}{12} \frac{2\sqrt{\kappa}}{c_g}$; $d = 5\sqrt{2\kappa}$; $e = 10\frac{2\kappa}{c_g}$; $f = \frac{3c_g^8}{2\sqrt{\kappa}}$; $g = \frac{3c_g^4}{2\kappa\sqrt{2\kappa}}$; $h = \frac{12\kappa}{c_g}$.

We now assume that the spatial perturbation $\psi_1(y, x, \tau)$ takes the form:

$$\psi_1 = ae^{i(k_x x + k_y y - \Omega \tau)} + be^{-i(k_x x + k_y y - \Omega \tau)} \quad (\text{III.24})$$

where K and ω are the wave number and spatial frequency of the perturbation wave, respectively. Insert Eq.(III.24) into Eq.(III.23), we obtain a square matrix in cosine and

sine as follows

$$\begin{pmatrix} -k + a_{11} & a_{12} \\ a_{21} & k + a_{22} \end{pmatrix} \begin{pmatrix} a \\ b \end{pmatrix} = \begin{pmatrix} 0 \\ 0 \end{pmatrix}, \quad (\text{III.25})$$

where

$$a_{11} = (a_1 - 4b_1p_0 + 1)k_y^2 - p_0 + k_x^2 + 10ib_1p_0k_y + 2ip_0(-cd - 2c)k_y^3 + \frac{b_1}{2}k_y^4 + icfk_y^5 - cgk_y^6 - ichk_y^7,$$

$$a_{12} = -p_0 - 2b_1p_0k_y, \quad (\text{III.26})$$

$$a_{21} = -p_0 - 2b_1p_0k_y,$$

$$a_{22} = (a_1 - 4b_1p_0 + 1)k_y^2 - p_0 - k_x^2 - 10ib_1p_0k_y + 2ip_0(cd + 2c)k_y^3 + \frac{b_1}{2}k_y^4 - icfk_y^5 - cgk_y^6 + ichk_y^7$$

The condition for the existence of nontrivial solution for the system Eq.(III.25) gives rise to a second-order polynomial equation for the wave number K that represents the dispersion law for the perturbation, i.e.,

$$K^2 + sK + p = 0, \quad (\text{III.27})$$

in which $s = a_{22} - a_{11}$, and $p = a_{21}a_{12} - a_{11}a_{22}$. To investigate the modulational instability process, we must study of the imaginary part of the roots of the dispersion equation Eq.(III.27). Whenever K approaches non-zero imaginary part number, then the steady-state solution becomes unstable. The dispersion equation has two roots given as follows:

$$K_{1,2} = \frac{1}{2}(-s \pm \sqrt{s^2 - 4p}). \quad (\text{III.28})$$

The steady-state solution becomes unstable only when K has a non-zero imaginary part, then the perturbation grows exponentially and the modulational instability occurs.

When the above conditions are satisfied, with the contribution of the non-paraxial approximation we find that the propagation of solitons takes place but with different values of the nonparaxiality parameters that strongly affect the system, the presence of the perturbation in this case will reveal us Growth rates. The general expressions of the growth rates of the MI or the gain spectrum are defined as follows

$$G = \text{Im} [K_{1,2}] \quad (\text{III.29})$$

III.4.2 Numerical solution of the 2D NLS equation in nonparaxial regime

It is interesting to follow the evolution of the growth rate of MI with variation of system parameters, in particular the variation of the parameters of non-paraxiality ϵ , and coupling coefficient κ . To elucidate the role of non-paraxiality parameters and wavenumber K , in the expansion of the MI region. We focus first on the influence of the κ parameter on MI gains G_+ , respectively. Fig.(17), shows the evolution of modulation instability gains for different values: $c_g = 5$, $eps = 1.3$, $p_0 = 5.2$, $Ky = .1$ gain G_+ decreases with increasing the coupling coefficient $\kappa = 1 \times 10^5$. While there is no significant influence on the width and amplitude of the G_+ gain profile. Have found that the maximum gains vary considerably according to the frequency variations, for Fig. 17(a) we can notice that for the frequency $Kx = -0.01$. We have an evolution curve which becomes constant as the frequency increases up to $K_x = 0.95$. We have a linear line which means that there is no variation of the system the soliton normally propagates in the fiber of bragg, the MI does not affect the propagation of said soliton with this frequency. We can also notify that here the gain reached is max, when we go further with very high frequencies $K_x = 4.8$. We have no remarkable influence, further the frequencies drop considerably up to $K_x = -0.13$. The gain is very low have observed not much at all the soliton is flat. For the Fig. 17(b) we discuss according to the values of the coupling coefficient itself κ , and we note that we have several zones of instability. Initially G_+ presents three windows of instability according to K_x , for the value $\kappa = -3 \times 10^{-6}$. The soliton thus

moves in three zones of instability without any time oscillate, secondly G_+ presents a window of instability according to K_x , for the value $\kappa = -4.2 \times 10^{-7}$. The soliton propagates in a zone of instability with oscillation. Thirdly G_+ does not present any window of instability according to K_x for $\kappa = -3.81 \times 10^{-8}$. There is no zone of instability. Finally, G_+ presents two windows of instability according to K_x for $\kappa = 1.52 \times 10^{-5}$. We have two zones of instability in which the soliton propagates without oscillation. For Fig. 17(c), we have the gain G_+ as a function of K_x for $\kappa \times 10^5$. We have five windows, therefore five areas of instability, where the soliton can propagate freely. Figure (18), we have investigate the impact of the nonparaxiality parameter ϵ according to the following values: $c_g = 5, p_0 = 5.2, \kappa = 1 \times 10^{-4}, \epsilon = 1.3$. In Fig.18(a), we have the top view of K_x as a function of K_y , where the shape changes completely. In Fig. 18(b), we have a representation of the gain G_+ as a function of K_x , for different values of frequencies K_y . We have several curves which refer to different interpretations. For the red curve, we have $K_y = -0.0025$. We can see that there are two lobes which cancel at zero, when we leave the first lobe for the second. For the pink curve, we have $K_y = -0.3$. We also have two lobes but they do not cancel at zero. For the blue curve, we have $K_y = 0.2$. We also have two lobes that do not cancel at zero. Finally, the black curve are plotted for $K_y = 0.35$. We have three lobes that do not cancel at zero. In Fig. 18(c), we have a representation of the gain G_+ as a function of K_y , according to the different values of the frequencies K_x . For the black curve the value is $K_x = -0.01$. We have three peaks that cancel at zero after the second peak. For the red curve, we have one peak that does not cancel. For the green curve the value is $K_x = -3.6$. We have two peaks, but we notice that after the first peak, it tends to cancel at zero before reconstituting itself, meaning that, at a certain point, this soliton is determined at a certain value of the frequency. When we reach higher values, this soliton reconstitutes itself. This reconstitution is due to the non paraxiality effect on the NLS equation with a higher-order dispersion. Finally on the blue line we have use $K_x = 2.4$. We have obtained three vortices among which, the first and the third which tend to merge at the black line, where the solitons propagate, but the second vortex does not join the green one in this case, the soliton is in an unstable state or sometimes,

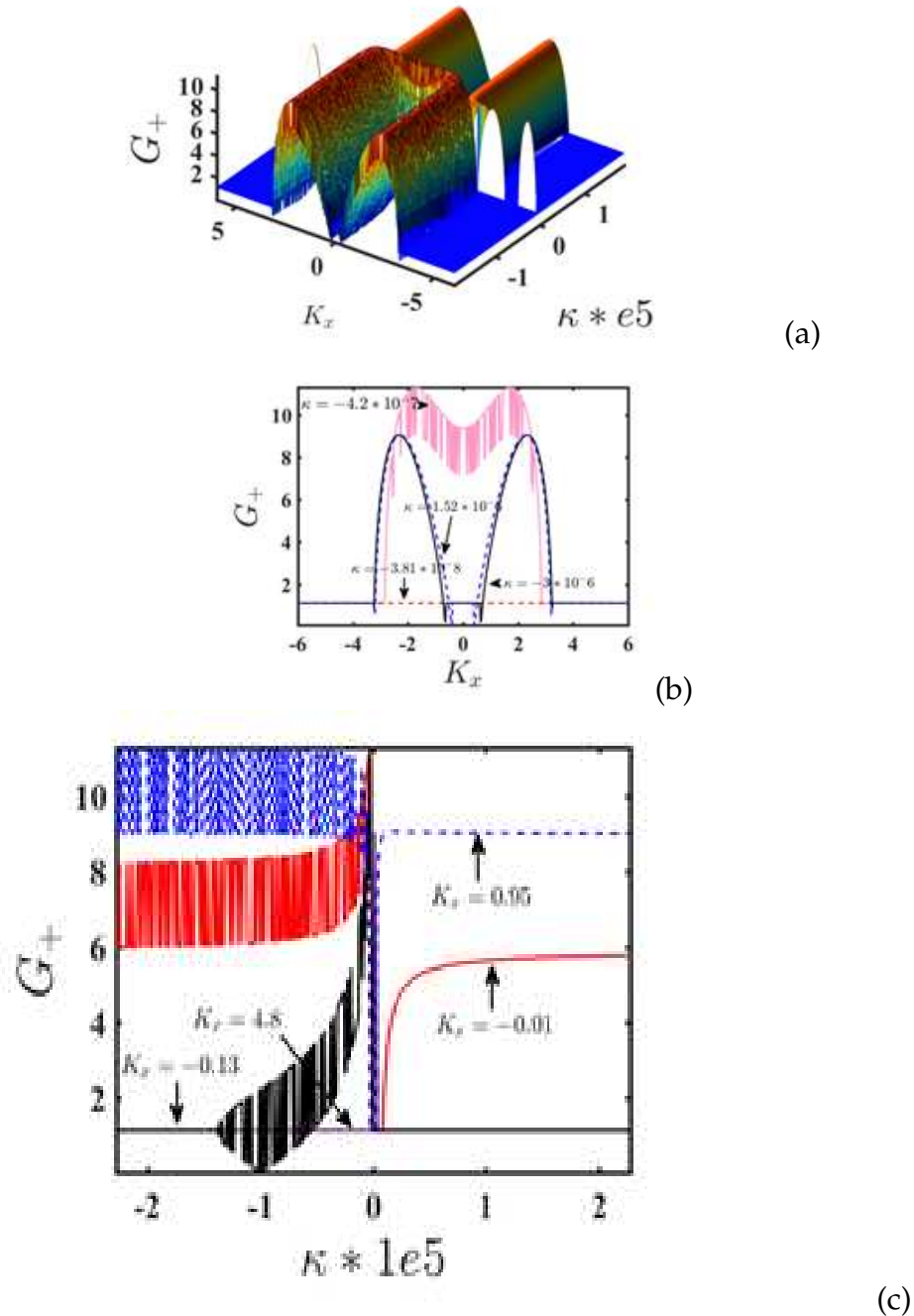


Figure 17: Growth rate of the modulational instability associated with solutions G_+ of Eq (III.29). Graph (a) shows the 3D representation of the gain G_+ as functions of K_x and $\kappa * 10^5$. Graph (b) shows the MI gain for different values of G_+ as a function of K_x in 2D. Graph (c) shows the 2D representation of the gain G_+ as a function of $\kappa = 1 \times 10^5$. The other parameters used are: $c_g = 5$, $\epsilon = 1.3$, $P_0 = 5.2$, $K_y = 0.1$. It is obvious that by increasing the value of kappa, the instability zone expands; this means that the nonparaxiality parameter increases the MI in the FBG. It is shown that the growth rate of instability G_+ can be dramatically affected by the nonparaxiality parameter κ .

can lead to the appearance of the last blue peak. In Fig.(19), we have taken the negative

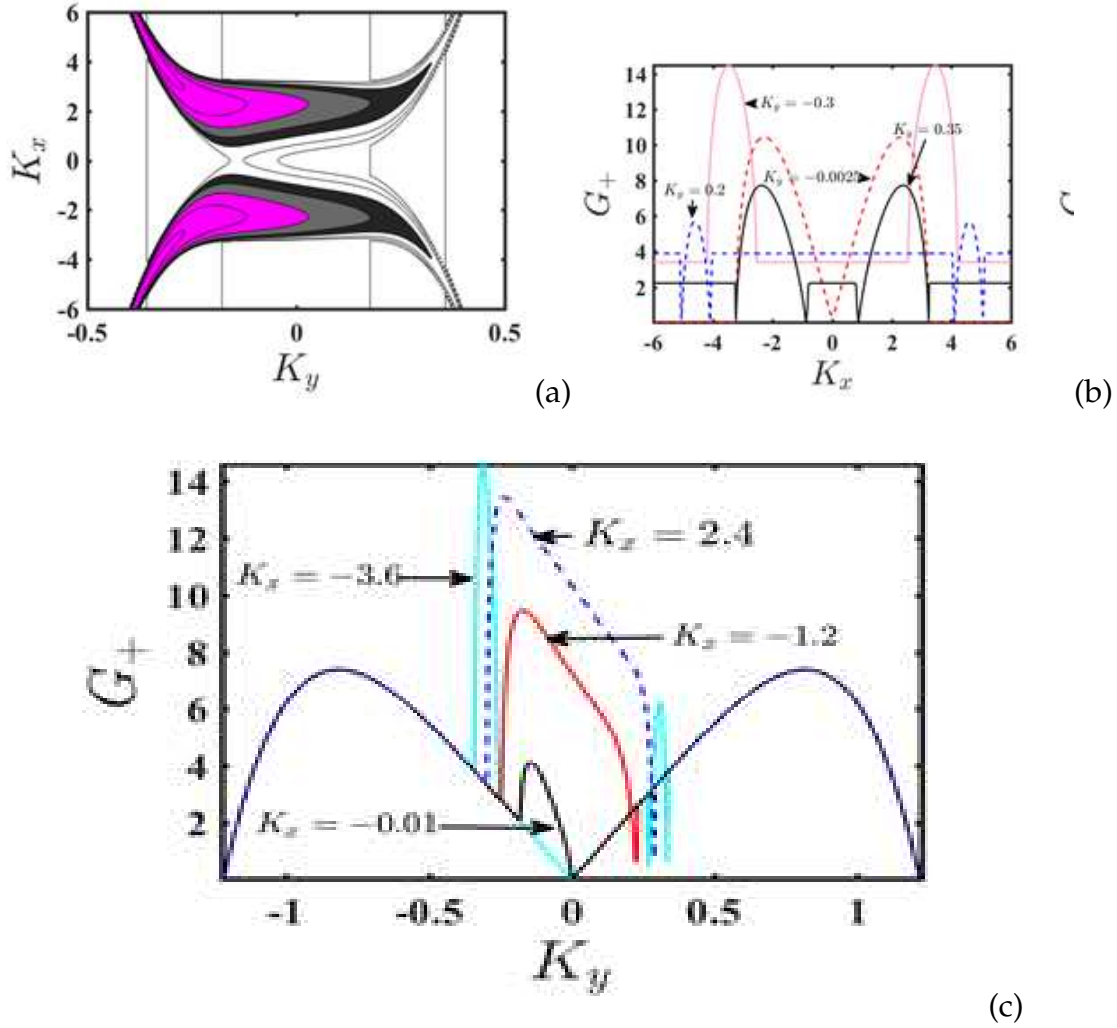


Figure 18: Modulational instability gain associated with solutions G_+ of Eq. (III.29). Graph (a) shows k_x as a function of K_y , and Graph (b) shows the gain spectrum G_+ as a function of K_x . Graph (c) shows the gain spectrum G_+ as a function of K_y , for a fixed $\epsilon = -1.3$ value. The other parameters used are: $c_g = 5$, $p_0 = 5.2$, $\kappa = 1 \times \epsilon^{-4}$.

value of $\epsilon = -1.3$. In Fig. 19(a), we observe the representation of the top view of the gain of G_+ as a function of K_y . In Fig.19(b), we have the representation of the gain G_+ as a function of K_x , for different values of frequencies K_y . For $K_y = -0.0025$, we have the red curve that reveals two lobes that cancel at zero. For $K_y = -0.3$, the pink curve reveals only one lobe, which cancels at two points between $[-1.8; 1.8]$. For $K_y = 0.2$. For $K_y = 0.35$, we have two lobes that do not cancel out anywhere but oscillate. In Fig. 19(c), we have the representation of the gain G_+ as a function of K_y . Here, we discuss the different frequency values among which $\Omega_x = -0.01$, $\Omega_x = -1.2$, $\Omega_x = -3.6$, and

$\Omega_x = 2.4$, respectively. We have several peaks that do not necessarily cancel each other. We just have the black curve which cancels before zero and after zero, then the pink curve which joins this one at zero. So, we can say that for low values frequency solitons tend to be unstable before regaining their stability. For high frequency values, the soliton propagates by remaining stable during its movement in the FBG. In the Fig.(19), we

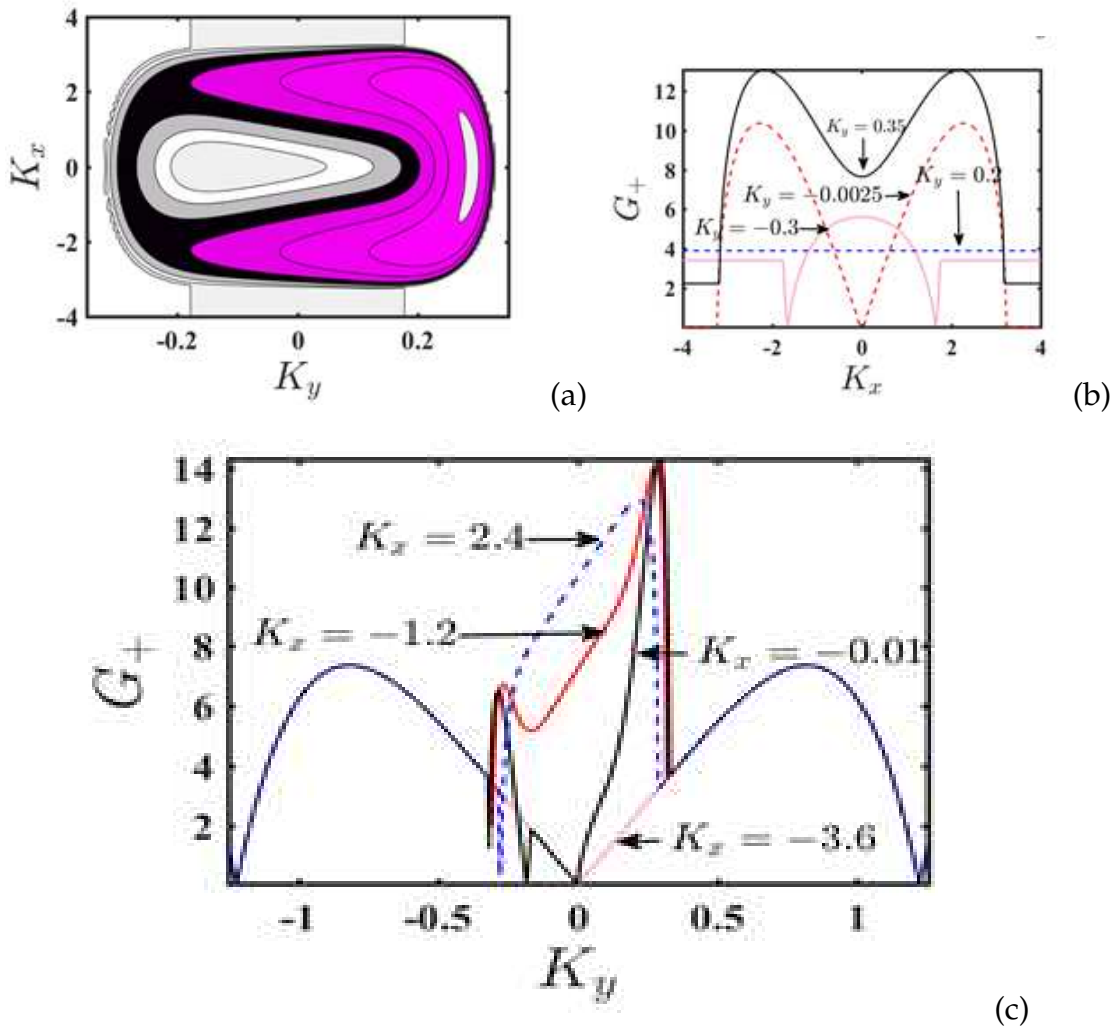


Figure 19: Modulational instability gain associated with solutions G_+ , of Eq. (III.29). Graph (a) shows K_x as a function of K_y , Graph (b) shows the gain spectrum G_+ as a function of K_x . Graph (c) shows the gain spectrum G_+ as a function of K_y , for a fixed $\epsilon = -1.3$ value . The other parameters used are: $c_g = 5, p_0 = 5.2, \kappa = 1 \times \epsilon^{-4}$.

have plotted K_x versus p_0 , because we are looking for the effect of p_0 on the dynamics of soliton. We can say that increases the propagation width but the amplitude remains constant. In the Fig.(20), we have plotted X versus Y for the behavior of solitons dur-

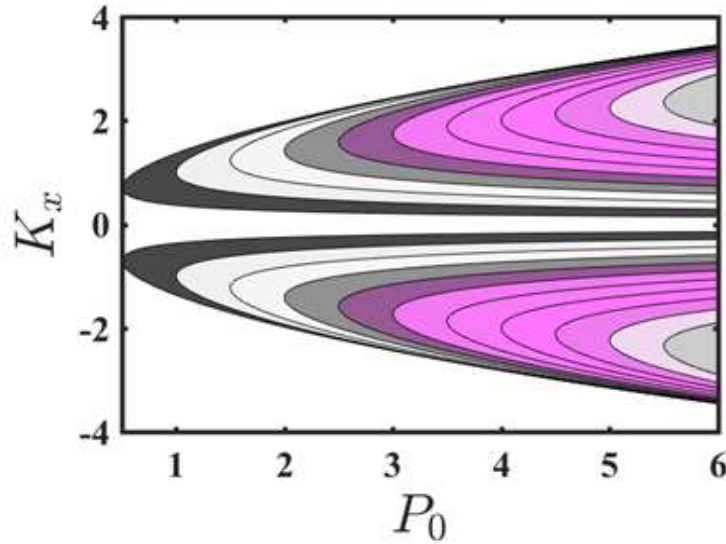


Figure 20: Effect of p_0 on the gain of modulational instability. Here, p_0 takes high values. The graph shows a curve of K_x versus p_0 . The other parameters used are: $c_g = 5$, $p_0 = 6$, $\kappa = 1 \times \epsilon^{-4}$.

ing of propagation according to different values of the propagation distance Z between 0 and 30. We observe that the peaks tend to decrease which means that the more the propagation distance increases, the less peaks are observed along the Y axis. So this one affects considerably the soliton during the propagation. In the Fig.(21) and Fig.(22), For higher values of the propagation distance $Z = 30$ at 48 , we can see that the peaks disappear completely. We just have parallel lines that form along the Y axis, which proves that the soliton is perfectly unstable.

III.5 Conclusion

Throughout this chapter, we can say that it was about deriving the analytical model of the 2D NLS equation. We found the appearance of higher-order dispersion terms caused by the effect of nonparaxiality. Then, we made a numerical study which led us to interesting results concerning the stability of the gap-soliton bullet. We were able to illustrate different graphs as a function of some important parameters of the system such as the group velocity, the coupling coefficient κ , and the parameter of nonparaxiality ϵ .

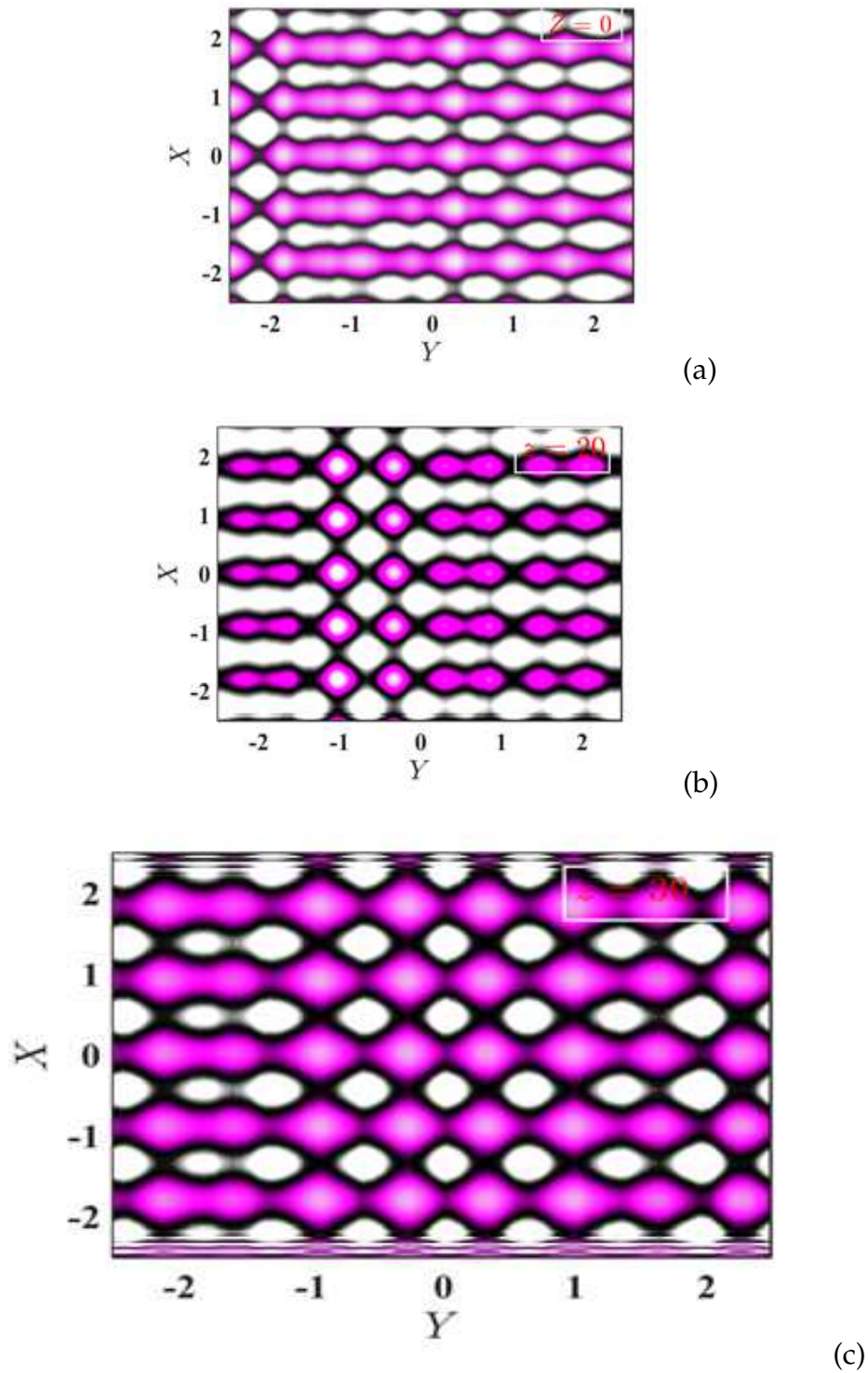


Figure 21: 2D representation of the evolution of solitons in an instability medium in the nonparaxial regime. $Z=0$ in Fig. 20(a), $Z=20$ in Fig.20(b), and $Z=30$ in Fig. 20(c). Other parameters are: $p_0 = 1.0, k = -1, c_g = 5, v_g = 5, \epsilon = 1.3, \epsilon = -1.3, \kappa = 2 \times 10^{-4}$, Initial: input is $U = \sqrt{p_0}(1 + 10^{-4}(\cos(1.1 \times 2\pi x) + \cos(1.5 \times 2.p_0 y)))$.

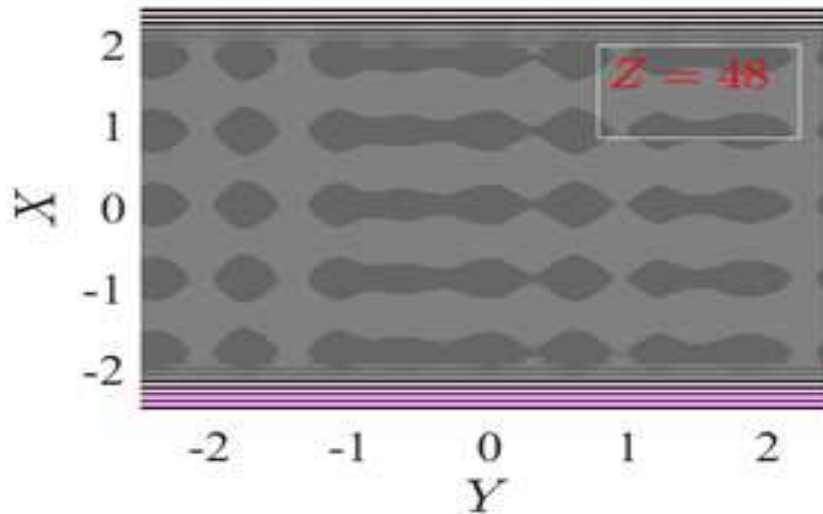


Figure 22: 2D representation of the evolution of solitons in an instability medium in the non-paraxial regime for $Z=48$, Z is considered here as a counter.

Finally, we have studied the modulational instability of our model, presenting the gain of stability as a function of certain parameters such as the coupling coefficient κ , and the nonparaxial parameter ϵ . We look into account the variation a function of other parameter such as the wave number K_x and K_y , the group velocity c_g , and the incident power p_0 . We observe some instability zone when the coupling coefficient κ and the wave number K vary considerably. This leads to formation of different lobes in the course of the soliton propagation in the FBG, where the nonparaxiality has a great effect on the propagation of solitons via the modulational instability.

General Conclusion and Perspectives

In this present thesis, after giving a general overview on FBGs, we have used the multiple scales method combine with coupled wave equations model to derive a new version of nonlinear nonparaxial wave equation, that we have named, a 2D NLS equation that includes nonparaxial correction terms. A complete numerical investigation of gap-soliton bullets, using a Townes bullet soliton as the initial condition, has been carried out. The impact of the nonparaxiality terms on the stability of the Townes soliton has been addressed using different combinations of system parameters known as the group velocity, the coupling coefficient κ , and the nonlinearity parameter ϵ . Beyond such stability, granted by some values of such parameters, other classes of solitons were debated along with the recombination capacity of the initial state upon propagation in the nonparaxial medium. Composite solitons with interesting dynamical features have been described. This reveals the richness of the derived model, which may give rise to more exotic patterns if suitable detection methods are used. Therefore, one of the general methods that support soliton generation in most of the physical systems in nature is modulational instability. The latter takes place when nonlinearity and dispersion are well-balanced. we have studied the propagation of a nonparaxial beam in a nonlinear Kerr medium using the linear stability method. The expression of the MI gain spectrum for the non-paraxial beam has been derived. The linear stability analysis of the plane waves, solutions of the amplitude equation, revealed the existence of instability regions strongly influenced by the coupling parameters and the nonparaxiality parameters. We have therefore constructed a typical dependence of the MI gain on the perturbation wavenumbers and the system parameters. By solving the second order polynomial, with nonlinearity in the nonparaxial approximation, obtained from

the non-trivial solution condition, we have drawn MI gain regions. The results were confirmed by numerical simulations, where the effects of the coupling coefficients on the evolution of the MI gain have been studied in depth. On the other hand, the MI growth rate and the instability region are sensitive to the coupling parameters. A judicious choice of all these coupling parameters gives us the freedom to control of the MI growth rate of instability. Moreover, we have also proved that the propagation distance affects the gap-soliton bullet considerably during its propagation. The higher the value of Z , the less peaks there are, and so on, until they tend to disappear to form lines that do not tell us much about the propagation of the soliton. The future works are as follows:

- We will consider wave propagation in materials with a saturable refractive index.
- More accurate models should include vectorial effects and backscattering.
- We will consider Gap solitons in Bragg gratings with dispersive reflectivity.
- Construct the bright and dark Bragg solitons in the upper and lower branches of the dispersion curve, of our new model equation using the coupled amplitude-phase method.
- We will also investigate the link between parametric gap solitons to chaos by means of second-harmonic generation in Bragg grating.
- We will investigate, in the vicinity of the parity-time symmetric periodic structure band gap, the interaction of forward and backward propagating waves.

Bibliography

- [1] A. Hasegawa and F. Tappert, *Appl. Phys. Lett.* **23**, 142 (1973).
- [2] A. Hasegawa and F. Tappert, *Appl.* **23**, 171 (1973).
- [3] L. F. Mollenauer, R. H. Stolen and J.P. Gordon, *Phys. Rev. Lett.* **45**, 1095 (1980).
- [4] R.H. Stolen, L. F. Mollenauer and W. J. Tomlinson, *Opt. Lett.* **8**, 186 (1983).
- [5] L. F. Mollenauer, R. H. Stolen, J.P. Gordon and W. J. Tomlinson, *Opt. Lett.* **8**, 289 (1983).
- [6] T. C. Kofan, B. Michaux and M. Remoissenet, *J. State. Phys.* **21**, 1395 (1988).
- [7] G. P. Agrawal, *Applications of nonlinear fiber optics.* New York: Academic Press. (2003).
- [8] A. Hasegawa and Y. Kodama, *Solitons in optical communications.* Oxford: Clarendon Press. (1995).
- [9] L. P. Pitaevskii and S. Stringari, *Bose-Einstein condensation.* Oxford: Clarendon Press. (2003).
- [10] F. Dalfovo, S. Giorgini, L. P. Pitaevskii and S. Stringari, *Rev. Mod. Phys.* **71**, 463 (1999).
- [11] T. B. Benjamin and J. E. Feir. *Fluid. Mech.* **27**, 417 (1967).
- [12] L. Berg. *Phys. Rep.* **303**, 260 (1998).
- [13] M. Peyrard and A. R. Bishop. *Phys. Rev. Lett.* **62**, 2755 (1989).

- [14] C. B. Tabi, A. Mohamadou and T. C. Kofan, *J. Phys. Condens. Matter.* **21** 335101 (2009).
- [15] M. Abemgnigni Njifon, C. B. Tabi and T. C. Kofan, *J. Opt. Soc. Am. B.* **37** A331 (2020).
- [16] L. T. Megne, C. B. Tabi and T. C. Kofan, *Phys. Rev. E.* **102**, 042207 (2020).
- [17] Y. S. Kivshar and G. P. Agrawal. *Optical solitons: from fibers to photonic crystals.* San Diego: Academic; (2003).
- [18] K. O. Hill, Y. Fujii, D. C. Johnson and B. S. Kawasaki. *Appl. Phys. Lett.* **32**, 647 (1978).
- [19] B. S. Kawasaki, K. O. Hill, D. C. Johnson and Y. Fujii. *Opt. Lett.* **3**, 66 (1978).
- [20] G. Meltz, W. W. Morey and W. H. Glenn. *Opt. Lett*, **14**, 823 (1989).
- [21] R. Kashyap. *Fiber Bragg gratings.* San Diego:Academic Press (1999).
- [22] A. Othonos and K. Kalli. *Fiber Bragg gratings:fundamentals and applications in telecommunications and sensing.*Boston, London: *Artech. House* (1999).
- [23] A. B. Aceves and S. Wabnitz.*Phys. Lett. A.* **141**, 37 (1989).
- [24] B. J. Eggleton, R. E. Slusher, C. M. De Sterke, P. A. Krug and J. E. Sipe. *Phys. Rev. Lett.* **76**, 1627 (1996).
- [25] B. A. Malomed. *Soliton management in periodic systems.* New York: *Springer* (2006).
- [26] P. St and J. Russell. *J. Mod. Opt.* **38**, 1599 (1991).
- [27] C. M. De Sterke and J. E. Sipe. *Prog Opt.* **33** 203 (1994).
- [28] S. Helsby, C. Corbari, M. Ibsen, P. Horak and P. Kazansky. *Phys. Rev. A.***75**, 013618 (2007).

- [29] P. Di Trapani, D. Caironi, G. Valiulis, A. Dubielis, R. Dalielius and A. Piskarskas. *Phys. Rev. Lett.* **81**, 570 (1998).
- [30] X. Liu, L. J. Qian and F. W. Wise. *Phys. Rev. Lett.* **82**, 4631 (1999).
- [31] K. W. Chow, I. M. Merhasin, B. A. Malomed, K. Nakkeeran, K. Senthilnathan and P. K. A. Wai. *Phys RevE.* **77**, 026602 (2008).
- [32] B. J. Eggleton, C. M. De Sterke and R. E. Slusher. *J. Opt. Soc. Am. B.* **16**, 587 (1999).
- [33] K. LeeR and Y. Lai. *Phys. Rev. A.* **69**, 021801 (R) (2004).
- [34] N. G. R. Broderick, D. Taverner, D. J. Richardson, M. Ibsen and R. I. Laming. *Phys. Rev. Lett.* **79**, 4566 (1997).
- [35] W. C. K. Mak, B. A. Malomed and P. L. Chu. *Phys. Rev. E.* **67**, 026608 (2003).
- [36] N. K. Efremidis, N. S. Nye and D. N. Christodoulides. *Phys. Rev. A.* **96**, 043820 (2017).
- [37] M. J. Steel and C. M. De Sterke. *Phys. Rev. E.* **54**, 4272 (1996).
- [38] H. Sakaguchi and B. A. Malomed. *Phys. Rev. E.* **77**, 056606 (2008).
- [39] Y. P. Shapira and M. Horowitz. *Phys. Rev. A.* **83**, 053803 (2011).
- [40] F. Le Kien and K. Hakuta. *Phys. Rev. A.* **81**, 023812 (2010).
- [41] F. Le Kien and K. Hakuta. *Phys. Rev. A.* **81**, 063808 (2010).
- [42] S. Longhi. *Phys. Rev. E.* **72** 056614 (2005).
- [43] B. Kalithasan, K. Porsezian, K. Senthilnathan and P. Tchofo Dinda. *Phys. Rev. A.* **81** 053802 (2010).
- [44] V. E. Perlin and H. G. Winful. *Phys. Rev. A.* **64**, 043804 (2001).
- [45] S. V. Raja, A. Govindarajan, A. Mahalingam and M. Lakshmanan. *Phys. Rev. A.* **100** 033838 (2019).

- [46] Y. J. Tsofe and B. A. Malomed. *Phys. Rev.E.* **75**, 056603 (2007).
- [47] P. Y. P. Chen, B. A. Malomed and P. L. Chu. *Phys. Rev.E.* **71**, 066601 (2005).
- [48] S. V. Raja, A. Govindarajan, A. Mahalingam and M. Lakshmanan. *Phys. Rev. A.* **102** 013515 (2020).
- [49] J. Atai and B. A. Malomed. *Phys. Rev. E.* **62** 8713 (2000).
- [50] J. Atai and B. A. Malomed. *Phys. Rev. E.* **64**, 066617 (2001).
- [51] S. Dasanayaka and J. Atai. *Phys. Lett. A.* **375**, 225 (2010).
- [52] S. Dasanayaka and J. Atai. *Phys. Rev. E.* **84**, 026613 (2011).
- [53] T. Ahmed and J. Atai. *Phys. Rev. E.* **96** 032222 (2017).
- [54] T. Dohnal and A. B. Aceves. *Stud. Appl. Math.* **115**, 209 (2005).
- [55] C. Sulem and P. L. Sulem. *Springer-Verlag* (1999).
- [56] K. D. Moll, A. L. Gaeta and G. Fibich. *Phys. Rev. Lett.* **90**, 203902 (2003).
- [57] L. Berge, V. K. Mezentsev, J. J. Rasmussen, P. L. Christiansen and Y. B. Gaididei. *Opt Lett.* **25**, 1037 (2000).
- [58] I. Towers and B. A. Malomed. *J. Opt. Soc. Am. B.* **19**, 537 (2002).
- [59] H. Saito and M. Ueda. *Phys. Rev. Lett.* **90**, 040403 (2003).
- [60] F. K. Abdullaev, J. G. Caputo, R. A. Kraenkel and B. A. Malomed. *Phys. Rev. A.* **67**, 013605 (2003).
- [61] G. D. Montesinos, V. M. Prez-Garca and P. Torres. *Phys. D.* **191**, 193 (2004).
- [62] F. K. Abdullaev and R. A. Kraenkel. *Phys. Lett. A.* **272**, 395 (2000).
- [63] A. Itin, T. Morishita and S. Watanabe. *Phys. Rev. A.* **74**, 033613 (2006).

- [64] M. I. Rodas-Verde, G. D. Montesinos, H. Michinel and V. M. Prez-Garca. *J. Opt. Soc. Am. B.* **23**, 56 (2006).
- [65] V. Zharnitsky, E. Grenier, C. K. R. T. Jones CKRT and S. K. Turitsyn. *Phys. D.* **152**, 794 (2001).
- [66] F. K. Abdullaev, B. B. Baizakov and M. Salerno. *Phys. Rev. E.* **68**, 066605 (2003).
- [67] G. D. Montesinos, V. M. Prez-Garca and H. Michinel. *Phys. Rev. Lett.* **92**, 133901 (2004).
- [68] R. H. Enns and S. S. Rangnekar. *Phys. Rev. A.* **45**, 3354 (1992).
- [69] A. Desyatnikov, A. Maimistov and B. A. Malomed. *Phys. Rev. E.* **61**, 3107 (2000).
- [70] D. Mihalache, D. Mazilu, L. C. Crasovan B. A. Malomed and F. Lederer. *Phys. Rev. E.* **61**, 7142 (2000).
- [71] D. Mihalache, D. Mazilu, L. C. Crasovan, I. Towers, A. V. Buryak and B. A. Malomed. *Phys. Rev. Lett.* **88**, 073902 (2002).
- [72] K. Senthilnathan, Q. Li, K. Nakkeeran and P. K. A. Wai. *Phys. Rev. A.* **78**, 033835 (2008).
- [73] M. Djoko and T. C. Kofane. *Commun. Nonlin. Sci. Numer. Simulat.* **48**, 179 (2017).
- [74] M. Djoko and T. C. Kofane. *Commun. Nonlin. Sci. Numer. Simulat.* **68**, 169 (2019).
- [75] M. Djoko and T. C. Kofane. *Opt. Commun.* **416**, 190 (2018).
- [76] M. Djoko, C. B. Tabi and T. C. Kofane. *Phys. Scr.* **94**, 075501 (2019).
- [77] B. A. Malomed, P. Drummond, H. He, A. Berntson, D. Anderson and M. Lisak. *Phys. Rev. E.* **56**, 4725 (1997).
- [78] X. Liu, K. Beckwitt and F. Wise. *Phys. Rev. E.* **62**, 1328 (2000).

- [79] D. Mihalache, D. Mazilu, L. C. Crasovan, L. Torner, B. A. Malomed and F. Lederer. *Phys. Rev. E.* **62**, 7340 (2000).
- [80] M. Blaauboer, G. Kurizki and B. A. Malomed. *Phys. Rev. E.* **62**, R57 (2000).
- [81] M. Blaauboer, B. A. Malomed and G. Kurizki. *Phys. Rev. Lett.* **84**, 1906 (2000).
- [82] R. El-Ganainy, D. N. Christodoulides, C. Rotschild and M. Segev. *Opt. Express.* **15**, 10207 (2007).
- [83] L. D. Carr and C. W. Clark. *Phys. Rev. Lett.* **97**, 010403 (2006).
- [84] G. Burlak and B. A. Malomed. *Phys. Rev. A.* **77**, 053606 (2008).
- [85] B. J. leMesurier, P. L. Christiansen, . Y. B. Gaididei and J. J. Rasmussen. *PhysRevE.* 2004 **70** 046614.
- [86] Chen X-Y, Chuang Y-L, Lin C-Y, Wu C-M, Li Y, Malomed BA, Lee R-K. *Phys Rev A.* **96**, 043631 (2017).
- [87] P. Pedri and L. Santos. *Phys. Rev. Lett.* **95**, 200404 (2005).
- [88] I. Tikhonenkov, B. A. Malomed and A. Vardi. *Phys. Rev. Lett.* **100** 090406 (2008).
- [89] H. Saito and M. Ueda. *Phys. Rev. A.* **74**, 023602 (2006).
- [90] M. A. Porras, M. Carvalho, H. Leblond and B. A. Malomed. *Phys. Rev. A.* **94**, 053810 (2016).
- [91] Y. V. Kartashov and V. V. Konotop. *Phys. Rev. Lett.* **125**, 054101 (2020).
- [92] E. Shamriz, Z. Chen and B. A. Malomed. *Phys. Rev. A.* **101** 063628 (2020).
- [93] Y. Linzon, K. A. Rutkowska, B. A. Malomed and R. Morandotti. *Phys. Rev. Lett.* **103** 053902 (2009).
- [94] A.S. Desyatnikov, D. Buccoliero, M. R. Dennis and Y. S. Kivshar. *Phys. Rev. Lett.* **104**, 053902 (2010).

- [95] C. Rotschild, O. Cohen, O. Manela, M. Segev and T. Carmon. *Phys. Rev. Lett.* **95**, 213904 (2005).
- [96] Y. Lamhot, A. Barak, O. Peleg and M. Segev. *Phys. Rev. Lett.* **105** 163906 (2010).
- [97] G. Chi and Q. Guo. *Opt. Lett.* **20**, 1598 (1995).
- [98] M. Gross. *Travels to the Nanoworld Perseus, New York* (, 1999).
- [99] B. D. Josephson, *Phys. Lett.* **1**, 251 (1962).
- [100] G. J. Panayotis, C. Maraver, G. K. Panayotis, F. Williams, *Springer* (2014).
- [101] G. Barone, and A. Paterno, *Physics and Applications of the Josephson Effect, Wiley, New York* (1982).
- [102] K. K. Likharev, *Gordon and Breach, New York* (1986).
- [103] M. Ivanchenko and L. A. Zil'berman, *Zh. Eksp. Teor. Phys.* **55**, 2395; (1968).
- [104] V. Ambegaokar and B.I. Halperin, *Phys. Rev. Lett.* **22**, 1364 (1969).
- [105] M. P. Stephen, *Phys. Rev. Lett.* **21**, 1629 (1968); M. P. Stephen, *Phys. Rev.* **186**, 393 (1969).
- [106] M. Simmonds and W. H. Parker, *Phys. Rev. Lett.* **24**, 876 (1970).
- [107] P. K. Hansma and G. I. Rochlin, *J. Appl. Phys.* **43**, 4721 (1972).
- [108] A. V. Buryak, V. V. Steblina and R. A. Sammut. *Opt Lett.* **24**, 1859(1999) .
- [109] G. Fibich. *Phys. Rev. Lett.* **76**, 4356 (1996).
- [110] A. P. Sheppard and M. Haelterman. *Opt Lett.* **23**, 1820 (1998).
- [111] P. Chamorro-Posada, G. S. McDonald and G. H. C. New. *J. Mod. Opt.* **45** 1111 (1998).
- [112] G. Baruch, G. Fibich and S. Tsynkov. *Opt. Express.* **16**, 13323 (2008).

- [113] J. M. Christian, G. S. McDonald and P. Chamorro-Posada. *J. Opt. Soc. Am. B.* **26**, 2323 (2009).
- [114] S. I. Fewo, H. Moussambi and T. C. Kofan. *Phys. Scr.* **84**, 035002 (2011).
- [115] S. Blair. *Chaos.* **10**, 570 (2000).
- [116] v. Chamorro-Posada, G. S. McDonald and G. New. *J. Opt. Soc. Am. B.* **19**, 1216 (2002).
- [117] P. Chamorro-Posada and G. S. McDonald. *Opt. Lett.* **28**, 825 (2003).
- [118] J. M. Christian, G. S. McDonald and P. Chamorro-Posada. *Phys. Rev. E.* **74**, 066612 (2006).
- [119] J. M. Christian, G. S. McDonald, P. Chamorro-Posada. *J. Phys. A.* **40**, 1545 (2007).
- [120] J. M. Christian, G. S. McDonald and P. Chamorro-Posada. *Phys. Rev. A.* **76**, 033833 (2007).
- [121] D. D. E. Temgoua and T. C. Kofane. *Phys. Rev. E.* **91**, 063201 (2015).
- [122] D. D. E. Temgoua and T. C. Kofane. *Phys. Rev. E.* **93**, 062223 (2016).
- [123] D. D. E. Temgoua and T. C. Kofane. *Phys. Rev. E.* **97**, 042205 (2018).
- [124] J. Sanchez-Curto, P. Chamorro-Posada and G. S. McDonald. *J. Opt. A. Pure. Appl. Opt.* **11**, 054015 (2009).
- [125] A. B. Aceves, G. Fibich and B. Ilan. *Phys. D.* **189**, 277 (2004).
- [126] A. Ciattoni, P. D. Porto, B. Crosignani and A. Yariv. *J. Opt. Soc. Am. B.* **17**, 809 (2000).
- [127] G. P. Agrawal. *New York: Academic Press* p. 195211(2006.).
- [128] C. Conti. *Phys. Rev. A.* **89**, 061801 (2014).
- [129] M. C. Braidotti, Z. H. Musslimani and C. Conti. *Phys. D.* **338**, 34 (2017).

- [130] M. C. Braidotti, i C. Cont, M. Faiza, S. Dey, L. Alasfar, S. Alsaleh and A. Ashour. *E. P. L.* **124**, 44001 (2018).
- [131] P. Chamorro-Posada, G. S. McDonald and G. H. C. New. *J. Mod. Opt.* **45**, 1111 (1998).
- [132] N. Pathak, M. Kaur, S. Kaur and T. S. Gill. *Contrib. Plasma. Phys.* **59**, e201900026 (2019).
- [133] B. Crosignani, v. Di Porto and A. Yariv. *Opt. Lett.* **22**, 778 (1997).
- [134] A. Ciattoni, P. Di Porto, B. Crosignani and A. Yariv. *J. Opt. Soc. Am. B.* **17**, 809 (2000).
- [135] G. Fibich and G. C. Papanicolaou. *Opt. Lett.* **22**, 1379 (1997).
- [136] C. G. Chen, P. T. Konkola, J. Ferrera, R. K. Heilmann and M. L. Schattenburg. *J. Opt. Soc. Am. A.* **19**, 404 (2002).
- [137] G. F. Quinteiro, F. Schmidt-Kaler and C. T. Schmiegelow. *Phys. Rev. Lett.* **119**, 253203 (2017).
- [138] T. A. Klar and S. W. Hell. *Opt. Lett.* **24**, 954 (1999).
- [139] E. DelRe, F. DiMei, J. Parravicini, G. Parravicini, A. J. Agranat, C. Conti. *Nat. Photon.* **9**, 228 (2015).
- [140] A. B. Stilgoe, T. A. Nieminen and H. Rubinsztein-Dunlop. *J. Opt.* **17**, 125601 (2015).
- [141] P. K. Chauhan, G. Purohit and R. P. Sharma. *J. Phys. Conf. Ser.* **208**, 012094 (2010).
- [142] A. Bhowmik and S. Majumder. *J. Phys. Commun.* **2**, 125001 (2018).
- [143] L. Sarkadi, I. Fabre, F. Navarrete and R. O. Barrachina. *Phys. Rev. A.* **93**, 032702 (2016).
- [144] M. Schulz. *Adv. At. Mol. Opt. Phys.* **66**, 507 (2017).

- [145] D. V. Karlovets and V. G. Serbo. *Phys. Rev. Lett.* **119**, 173601 (2017).
- [146] P. Carpena and A. V. Coronado. *Eur. J. Phys.* **27**, 231 (2006).
- [147] M. A. Bandres, M. A. Alonso, I. Kaminer and M. Segev. *Opt. Express.* **21**, 13921 (2013).
- [148] M. A. Alonso and M. A. Bandres. *Opt. Express.* **22**, 14738 (2014).
- [149] L. Li, Y. Jiang, P. Jiang, X. Li, Y. Qiu, P. Jia, Z. Pi, Y. Hu, Z. Chen and J. Xu. *Opt. Express.* **28**, (2020).
- [150] T. Erdogan, Fiber Grating Spectrah. *J. L. T.* **15 (8)**, 12771294(1997).
- [151] K.O. Hill, Y. Fujii, D.C. Johnson and B.S. Kawasaki. *Appl. Phys. Lett*, **10**, 647649 (1978)
- [152] L.Brilland. *These de doctorat de l'Universite des Sciences et Technologies de Lille*, 215 (2000).
- [153] G.Meltz, W.W.Morey ,W.H.Glenn. *Opt. Lett*,**14**, 823825, (1989).
- [154] K.O.Hill, B.Malo, .Bilodeau, D.C.Johnson , J.Albert. *Appl.Phys. Lett.* **62**,1035(1993).
- [155] J.Martin , F.Ouellette. *Electron.Lett*, **30**, 81 (1994).
- [156] A. Othonos.h. *Rev.Sci*, **68** 4309(1997) .
- [157] R. KASHYAP.h. *Academic. press*,**35**, 450 (1999).
- [158] Z.H.Wang , G.D.Peng, P.L.Chu. *Optics communications*, **177**, 245 (2000).
- [159] A.Rosenthal, M.Horowitz. *IEEE Journal of quantum electronics*, **39**, 1018 (2003).
- [160] Y.Ma and L. D. Marks. *Acta Cryst*, **45**, 174 (1989).
- [161] D. Marcuse, h. *Bell Syst. Tech. J.* **50**, 1791 (1971).
- [162] A. W. Snyder.h. *J. Opt.Soc. Amer*, **62**, 1267 (1972).

- [163] A. Yariv, *h. IEEE J. Quantum Electron*, **9**,919 (1973).
- [164] H. Kogelnik, *h. Bell . Tech J.*, **48**, 2909 (1969).
- [165] J. E. Sipe et al. *Opt. Soc. Am.*, **11**, 1307 (1994).
- [166] J. Skaar, *Norwegian University of Science and Technology*, **65**, 562 (2000).
- [167] J.Skaar, L.Wang, and T.Erdogan. *h. IEEE. J.Quant. Electron*, **37**, 165 (2001).
- [168] J. S. Russell. *the british association for advancement of science, Londres* **311**, 1511(1844).
- [169] Janssen. *Shinfield Park (England)*, **62**, 286 (2002).
- [170] F. Benjamin. *Journal of Fluid Mechanics* **27**, 417 (1967).
- [171] C. Wieman, Moriconi. *Phys. Rev. B*, **64**, 875(2002).
- [172] Ketterle. *Review of Modern Physics*, **74**, 1131 (2002).
- [173] S. Trillo, W.E. Torruellas, Saffman, and Skryabin. *Coupled propagation of light and matter waves,Berlin* **433**, 448(2001).
- [174] D.Adame and Al. *Phys. Rev. E* **52** 2183 (1995).
- [175] Cuenda , Sanchez. *UC3M. (barcelona)*, **15**, 185 (2004).
- [176] Arai and Al. *Phys. Lett. B*, **556**, 192 (2003).
- [177] Ichinose. *Quantum Grav*, **18**, 5239(2001) .
- [178] These Doctorat, Bourgogne, France (2004).
- [179] Korteweg and Vries , *Philosophical Magazine*, **39**, 422 (1895).
- [180] N. J. Zabusky and M.D. Kruskal. *Physical Review Letters*, **15**, 240(1965).
- [181] B. and Caudrey. *Acta. Applicandae Mathematica*, **39**, 193(1995).
- [182] A.Segev. *Optics and Photonics News*, **13**, 27 (2002).

- [183] Agrawal. *San Diego*, **135**,202(2001).
- [184] D. Johnson. *Cambridge university press*, **122**, 212 (1983).
- [185] Zakharov, and Shabat. *Phys. JETP*, **34**, 62(1972).
- [186] Hasegawa, and Tappert. *Appl. Phys. Lett*, **23**, 142(1973).
- [187] Hasegawa, and Tappert. *Appl. Phys. Lett*, **23**, 171(1973).
- [188] Dumais and Al. *Opt. Lett*, **21**, 260(1996).
- [189] Blow and Al. *Opt. Lett*, **12**, 202(1987).
- [190] Mollenauer and Al. *Phys. Rev. Lett*, **45**, 1095 (1980).
- [191] S. Segev. *Optical spatial solitons and their interactions: Universality and diversity, Science*, **286**, 1518 (1999).
- [192] Buryak and al. *Phy. Rev. Lett*, **82**, 81 (1999).
- [193] Wise, D. Trapani. *Optics and Photonics. News Special*, **13**, 28(2002).
- [194] M.c. Leod and Al. *Phys. Rev. A*, **52**, 3254 (1995).
- [195] Liu and al. *Phys. Rev. Lett*, **82**, 4632 (1999).
- [196] A. D. Boardman. and Al. *Opt. Commun*, **55**, 201 (1985).
- [197] M. Ibens and Al. *Journal of Optics*, **17**, 139 (1986).
- [198] N. Akhmediev, A. Ankiewicz. *Lect. Notes. Phys*, **661**, 268 (2005).
- [199] E. GARMIRE and Al. *op. cit*, **46**, 362 (1966).
- [200] V.E. ZAKHAROV , A.M. RUBENCHIK. *op. cit*, **122**, 451 (1974).
- [201] G. P. Agrawal, J. Wiley. *Sons. Inc*, **44**, 862 (2002).
- [202] G. P. Agrawal. *Appl. Phys. Lett*, **112**, 365 (2001).

- [203] S. MANEUF and Al. *Opt. Commun*, **65**, 193 (1988).
- [204] J.S. AITCHISON and Al. *Opt. Lett*, **15**, 471 (1990).
- [205] J.S. AITCHISON and al. *Electron.Lett*, **28**, 1879 (1992).
- [206] U. BARTUCH and al. *Opt. Commun*, **134**, 49 (1997).
- [207] J.S. AITCHISON and Al. *IEEE J. Quantum Electron*, **33**, 341 (1997).
- [208] S. SPALTER and Al. *Opt. Lett*, **27**, 363 (2002).
- [209] A.D. Boardman and A.P. Sukhorukov Dordrecht. *Opt. Lett*, **41**, 312 (2001).
- [210] Bajdecki , A.D. Boardman and A.P. Sukhorukov Dordrecht. *Opt. Lett*, **48**,258 (2001).
- [211] Hutsebaut et a., *JNOG22, A02HUT11*, **25**, 455 (2003).
- [212] G.Nicolis, and I. Prigogine. *New York*, **63**, 169 (1977).
- [213] Y. Kuramoto. *Springerverlag, Berlin*, **45**, 135 (1984).
- [214] J. D. Moores. *Opt. Commun*, **96**, 65 (1993).
- [215] W. Chen and D. L. Mills. *Phys. Rev. Lett*, **58**,160 (1987).
- [216] J. E. Sipe and H. G.Winful. *Opt. Lett*, **13**, 134 (1988).
- [217] D. N. Christodoulides and R. I. Joseph. *Phys. Rev. Lett*, **62**,1746 (1989).
- [218] A. B. Aceves and S. Wabnitz. *Phys. Lett. A*, **141**, 42 (1989).
- [219] H. G.Winful, J. H. Marburger, and E. Gamire. *Appl. Phys. Lett*, **35**,379 (1979).
- [220] B. J. Eggleton, R. E. Slusher, C.M. de Sterke, P. A. Krug,and J. E. Sipe.*Phys. Rev. Lett*, **76**, 1627 (1996).
- [221] B. J. Eggleton, C. M. de Sterke, and R. E. Slusher. *Opt. Soc. Amer. B*, **14**, 2980 (1997).

- [222] D. Taverner, N. G. R. Broderick, D. J. Richardson, M. Ibsen, and R. I. Laming. *Opt. Lett*, **23**, 259 (1998).
- [223] D. Taverner, N. G. R. Broderick, D. J. Richardson, R. I. Laming, and M. Ibsen. *Opt. Lett*, **23**, 328 (1998).
- [224] N. G. R. Broderick, D. Taverner, and D. J. Richardson. *Opt. Express*, **13**, 447 (1998).
- [225] N. G. R. Broderick, D. Taverner, D. J. Richardson, M. Ibsen, and R. I. Laming. *Phys. Rev. Lett*, **79**, 4566 (1997).
- [226] N. G. R. Broderick, D. Taverner, D. J. Richardson, M. Ibsen, and R. I. Laming. *Opt. Lett*, **22**, 1837, (1997).
- [227] D. E. Pelinovsky, L. Brzozowski, and E. H. *Phys. Rev. E*, **62**, 4536, (2000).
- [228] G. P. Agrawal. *Academic Press, Optics and Photonics, New York*, **25**, 89, (2001).
- [229] R. KASHYAP. *Academic. press*, **58**, 255, (1999).
- [230] R.H. Chiao, E. Garmire. *Phys. Rev. Lett*, **13**, 479, (1964).
- [231] D. Anderson, M. Bonnedal. *Phys, Fluids*, **22**, 105, (1979).
- [232] M.F. Feit, J.A. Fleck. *J. Opt. Soc. Am*, **3**, 633, (1998).
- [233] P. Chamorro-Posada , G.S. McDonald. *J. of Mod. Opt*, **45**, 1111, (1998).
- [234] N. Akhmediev , A. Ankiewicz. *J.M. Soto-Crespo, Opt.Lett*, **18**, 411, (1993).
- [235] P. Chamorro-Posada, G.C. McDonald. *Opt. Comm*, **12**, 1886, (2001).
- [236] S. Blair, K. Wanger. *Opt. Quantum. Electron*, **30**, 738, (1998).
- [237] P. Chamorro-Posada , G.S. McDonald. *G.H.C. New, Opt. Comm*, **92**, 192, (2001).
- [238] G.P Agrawal. *Academic. Press, London*, **11**, 90, (2001).
- [239] W.S. Chun, F.D. Yuan. *Acta. Phys. Sin*, **49**, 460, (2000).

[240] B. Crosignani, P. Di Porto P, and A. Yariv. *Opt. Lett*, **22**, 1820, (1997).

[241] A.P. Sheppard, M.Haelterman. *Opt. Lett*, **23**, 1820-1822, (1998)

List of Publications

1- J. A. AMBASSA OTSOBO, L. Tiam Megne, C.B. Tabi and T. C. Kofane. *Stability of nonparaxial gap-soliton bullets in waveguide gratings*. *ELSEVIER: Chaos, Solitons and Fractals* **158**, 112034 (2022).